



De Kergariou, C. M. Y., Demoly, F., Perriman, A. W., Le Duigou, A., & Scarpa, F. (2022). The Design of 4D-Printed Hygromorphs: State-of-the-Art and Future Challenges. *Advanced Functional Materials*, [2210353]. <https://doi.org/10.1002/adfm.202210353>

Publisher's PDF, also known as Version of record

License (if available):
CC BY

Link to published version (if available):
[10.1002/adfm.202210353](https://doi.org/10.1002/adfm.202210353)

[Link to publication record in Explore Bristol Research](#)
PDF-document

This is the final published version of the article (version of record). It first appeared online via Wiley at <https://doi.org/10.1002/adfm.202210353>. Please refer to any applicable terms of use of the publisher.

University of Bristol - Explore Bristol Research

General rights

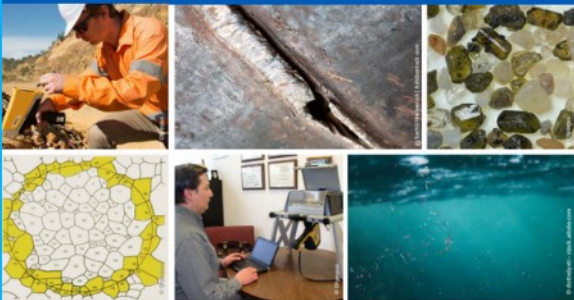
This document is made available in accordance with publisher policies. Please cite only the published version using the reference above. Full terms of use are available: <http://www.bristol.ac.uk/red/research-policy/pure/user-guides/ebr-terms/>



2nd Advanced Optical Metrology Compendium

Advanced Optical Metrology

Geoscience | Corrosion | Particles | Additive Manufacturing: Metallurgy, Cut Analysis & Porosity



EVIDENT
OLYMPUS

WILEY

The latest eBook from **Advanced Optical Metrology**.
Download for free.

This compendium includes a collection of optical metrology papers, a repository of teaching materials, and instructions on how to publish scientific achievements.

With the aim of improving communication between fundamental research and industrial applications in the field of optical metrology we have collected and organized existing information and made it more accessible and useful for researchers and practitioners.

EVIDENT
OLYMPUS

WILEY

The Design of 4D-Printed Hygromorphs: State-of-the-Art and Future Challenges

Charles de Kergariou,* Frédéric Demoly, Adam Perriman, Antoine Le Duigou, and Fabrizio Scarpa

In recent years, 4D printing has allowed the rapid development of new concepts of multifunctional/adaptive structures. The 4D printing technology makes it possible to generate new shapes and/or property-changing capabilities by combining smart materials, multiphysics stimuli, and additive manufacturing. Hygromorphs constitute a specific class of new smart materials where their properties and morphing capabilities are dependent on the surrounding humidity, which drives actuation. Although multiple efforts have been made to fabricate hygromorph demonstrators, a comprehensive design process to produce hygromorphs by multiple 4D printing techniques is not yet available. The broad aim of this review and concept paper is to i) highlight existing scientific and technology gaps in the field of 4D-printed hygromorphs, ii) identify tools existing in other research fields for filling those gaps, and iii) discuss a series of guidelines for tackling future challenges and opportunities to develop 4D-printed composite hygromorph materials and related manufacturing processes. Accordingly, this review describes the materials and additive manufacturing techniques used for hygromorph composite fabrication. Moreover, the relevant parameters that control actuation, the models selection and performance, the design methods and the actuation measurements for customized 4D-printed hygromorph materials, are discussed.

many materials such as composites. The present review focuses on printed adaptive macroscale composite materials, i.e., materials made of not miscible phases, the latter being at the macro and meso scales. Adding time as the fourth dimension in 3D printing leads to the generation of structures capable of deforming on their own, when subjected to an external stimulus. Dimassi et al.^[1] conducted an ontological study about 4D printing, describing the connections and interactions between all the aspects of this research field. 4D printed materials is a large research domain and the present study limits its investigation to three main themes such as shown in **Figure 1**. Only multi-phases environmentally stimulated 4D-printed structures are considered in the present review.

The term “4D printing” sometimes refers to other functionalities, for instance, energy storage^[2] or color-changing.^[3] The study focuses exclusively on coupled geometric/physical/mechanical deformations with composite materials triggered by humidity (also called “hygromorphs”)

at macroscale. Therefore, the actuation is built from the difference of expansion between at least two materials. Outside of composite materials-based structures, shape memory polymers are extensively implemented to achieve similar shape changes.^[4] Such active materials are for the most part ignored in the present study. They will be only discussed when


1. Introduction

1.1. Scope of the Study

3D printers are highly versatile in producing parts layer by layer, and also allow further exploration of the design space of

C. de Kergariou, F. Scarpa
Bristol Composites Institute
School of Civil
Aerospace and Mechanical Engineering
University of Bristol
University Walk
Bristol BS8 1TR, UK
E-mail: hl18503@bristol.ac.uk

F. Demoly
ICB UMR 6303 CNRS – University Bourgogne Franche-Comté
UTBM
Belfort 90010, France
A. Perriman
School of Cellular and Molecular Medicine
University of Bristol
University Walk
Bristol BS8 1TD, UK
A. Le Duigou
University Bretagne Sud, IRDL
Polymer and Composites
UMR CNRS 6027, Lorient 56100, France

 The ORCID identification number(s) for the author(s) of this article can be found under <https://doi.org/10.1002/adfm.202210353>.

© 2022 The Authors. Advanced Functional Materials published by Wiley-VCH GmbH. This is an open access article under the terms of the Creative Commons Attribution License, which permits use, distribution and reproduction in any medium, provided the original work is properly cited.

DOI: 10.1002/adfm.202210353

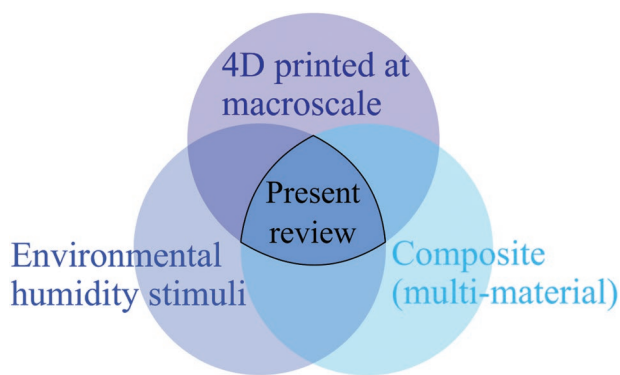


Figure 1. Main topics considered in the present review.

combined with another material to create composite or multi-material structures. Among the multiple stimuli available to actuate such structure (heat,^[5] pH,^[6] electricity,^[7–9] magnetic field^[10]) only a limited amount of studies have been conducted on humidity-based actuation. Consequently, studies related to combined humidity and temperature or only temperature, with related models, optimization techniques and actuation concepts are also considered in this study. Non-printed structures could be considered to describe new materials for 4D-printed applications,^[11] new actuation measuring techniques^[12] or if they bring potential improvement to the design of 4D-printed equivalent structures.^[13]

Figure 2 presents the evolution of the number of publications including the keyword “4D print*” in the title (from the Web of Science database on the 5th of September 2022^[14]). A total of 593 publications have been found to date, with increasing numbers of papers published every year from 2014.

The graph also presents key publications in the domain. The first two key papers defining the term 4D printing were published in 2014 by Tibbits et al.^[15] and by Ge et al.^[16] Bakarich et al.^[17] measured the mechanical properties and the

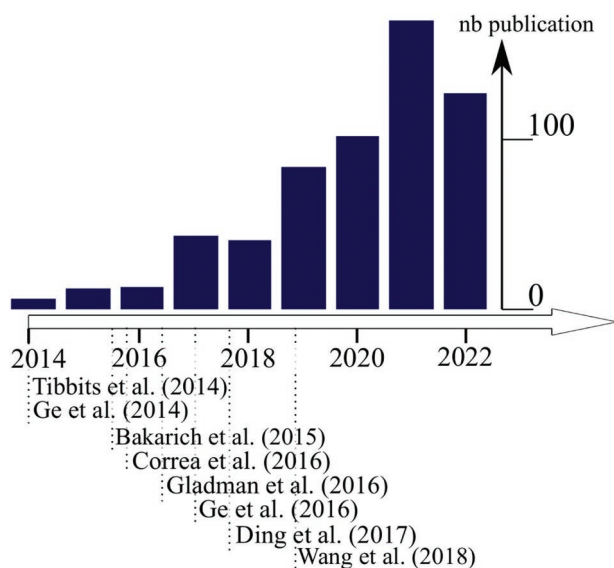


Figure 2. Publication history of 4D printing: Number of publications and key papers. (From Web of science^[14])

deformation properties of hydrogels and proposed them as an efficient material for 4D printing. This paper paved the way for use of hydrogels in 4D-printed actuators. The latter hydrogel route has been taken by Gladman et al.^[18] who published the most cited study of the field by cellulose-reinforced hydrogel-based actuators. Reproducing the actuation generated in this study is still considered as a benchmark for new 4D printing materials.^[18] The same year Correa et al.^[19] produced a study using wood reinforced polymer and mimicking the deformation mechanism of pine cones. Both the material implemented and the bio-mimicking strategy adopted find extensive application in this research area, following Correa et al.’s work. Two of the most important studies for the generation of multi-material actuators have been published by Ge et al.^[20] and Ding et al.^[21] Their use of shape memory polymers broadens the design space of 4D-printed composites. The use of continuous fibers for 3D-printed actuators has started with Wang et al.,^[22] who printed continuous carbon fiber on a flexible and expandable polymer (Polyamide 66 - PA66). From here, many research groups have tried to combine the benefits of using continuous fibers and the flexibility of additive manufacturing.

1.2. Design Process

Design for Additive Manufacturing (DfAM) defines an extensive methodology encompassing all the activities from the concept idea to its prototype.^[23–25] It considers the specificity of 3D printing to make the most of its advantages and drawbacks. According to Rosen,^[23] the general uniqueness of additive manufacturing includes shape, material, hierarchical and functional complexity. For instance, the flexibility of the additive manufacturing technique allows to renew completely the design of mechanically loaded parts.^[26]

The first aim of the present review is to highlight the areas still to explore in the 4D-printed composite hygromorph research field and providing tools to conduct the design, models, and experiments to pursue those explorations. Mapping the knowledge gaps in the area of 4D-printed composite hygromorphs requires taking inspiration from other fields of research (i.e., thermally stimulated 4D-printed research for material distribution, compliance optimization research field for design of fiber-based hygromorphs). Finally, the present literature study aims to compile some design guidelines for humidity-actuated hygromorphs and related adaptive structures. The study is organized around the three main steps presented in **Figure 3**. The three triangles in **Figure 3** present these three steps. Step one relates to the definition of the materials, 3D-printing techniques and objective of the actuation. The second step reviews and discusses the measurement of expansion, stiffness and quality of the materials considered for 4D printing. Finally, the last step presents the modeling, optimization and conditioning techniques implemented to design and build moisture-triggered actuators. In each of these sections, the review aims to critically describe the state-of-the-art knowledge. Following these descriptions, new concepts and generalizations aim to be provided. The guidelines provided to the reader to help the hygromorph design are extracted from the general concepts subsequently defined.

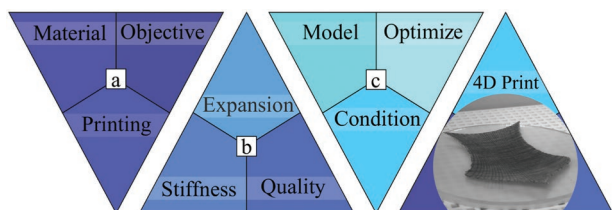


Figure 3. Organization of the present study: a) Define the objective (including at least one actuation function), the material and the printing technique among the options previously described in the open literature, b) Measure the expansion, the stiffness and the quality of the material and propose decision trees based on the type of actuation, material and 3D printing technique selected, c) Implement a model, an optimization technique and a Relative Humidity (RH) conditioning system to improve as much as possible and measure the multi-functionality of the structure. An example of a 4D-printed structure is provided in the last triangle.

Figure 4 presents the design process proposed for the 4D-printed hygromorphs. Here the designer should first define a general conceptual configuration for the actuator, i.e., functionality, range of properties, and dimensions. The designer should then look at the availability of suitable 3D printer(s), material(s) (and related properties measurements), conditioning system for the actuation (immersed or not immersed), and the modeling technique and software. The designer also has to make sure that these elements can be combined: 3D printers can only use specific types of materials, and not every software dedicated to modeling can consider any material constitutive law. The actuation can be controlled by several parameters (i.e., material properties or process parameters). Hence, the designer has to consider the control of the actuation to achieve a desired shape change from an initial design space. Consequently, the following steps consist in adding constraints to restrict this design space. At this point, it is critical to start printing small trial parts to assess the capability of the printing technique. The process parameters (i.e., slicer used, geometry

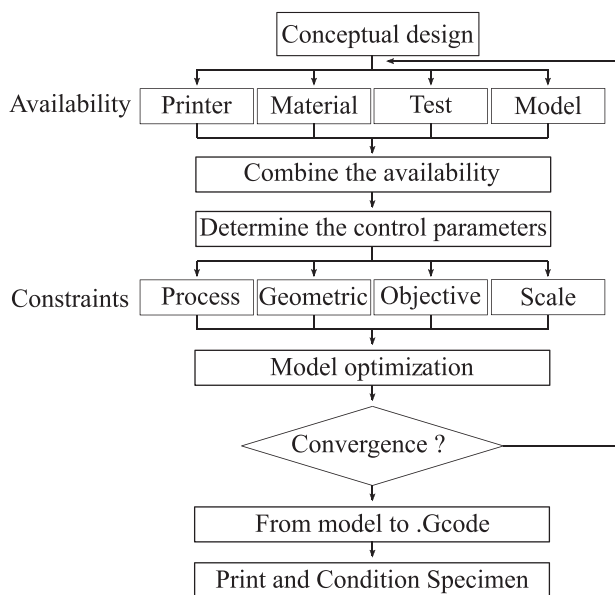


Figure 4. Design process of 4D-printed hygromorph actuators.

achievable) and the functional objective of the 4D-printed structure constrain the design space. The modeling scales for actuators are defined later in the present study as layer scale, phase scale and intra-phase scale. At this stage, the scale of the model has to be selected. In parallel, first simple model techniques (i.e., Timoshenko model, Classical Laminate Theory (CLT)) can be considered to adjust the design space for the optimization run. Genetic algorithms or neural networks are then used to optimize the multi-functionality of the defined structure. In case of a successful convergence of the optimization process, as the last step presented in Figure 4, the configuration can be turned into a printable G-code file.

1.3. Applications

The two main current fields of applications for hygromorphs are biomedical and adaptive structures engineering. In most of the applications presented here as humidity-triggered actuators, temperature has an impact on the actuation. Even though, the present review focuses on the humidity as the main trigger actuation agent (also called stimulus); in most applications, it is impossible to fully de-correlate humidity and temperature, as they influence each other. In most applications highlighted in this section, the humidity triggers the actuation in parallel to the temperature. Outdoor applications undergo stimulus from humidity and temperature at the same time. The idea behind this study is to focus only on the moisture to show the potential to qualify and quantify the impact of these trigger mechanisms on the actuation of different 4D-printed structures. By studying moisture separately, it will be easier to understand its impact on 4D-printed applications when combined with temperature or other sources of actuation.

Wang et al.^[27] used actuators to create a 4D mesh capable of adopting a predefined shape when immersed in water after been printed in a flat shape. Such versatile structure has potentially many applications, from morphing chairs, to body armor and plates. Hygromorphs have also potential as primarily loaded structures. For instance, Jayashankar et al.^[28] created a 3D-printed truss structure actuated with a humidified chitosan layer positioned on top. 3D printing can also help the implementation of non printed hygromorphs by bringing flexibility to the design. For instance, the wooden heat and humidity-triggered actuators proposed by Rüggeberg et al.^[29,30] and actuated by the sun would benefit from a more precise design able to tailor the orientation with accuracy. A solar tracker actuation concept combining shape memory alloy springs and a polymer has also been tested.^[31] Skins for self-regulating buildings have also significant potential for applications as well.^[32,33] However, recent developments of 4D-printed actuators are mostly dominated by heat-stimulated structures. Nonetheless, hygromorph designs can be inspired by those types of actuators. 4D printing facilitates the production of certain parts. For instance, instead of laying up a composite in a complex shape mold, Hoa et al.^[34] have proposed to 3D print asymmetric layouts on the flat surface, with the subsequent actuation placing the structure into the required shape, i.e., corrugated structures placed as core in sandwich panels^[35] or springs.^[36] Momeni et al.^[37] proposed the development of smart flowers-inspired solar concentrators.

Other adaptive structures that could be developed by additive manufacturing are leaves-inspired wind turbine blades.^[38] For these blades, the shape-shifting capability is tailored by the bend-twist stresses coupling generated via the distribution of 3D-printed materials. This coupling is itself controlled by heat. 4D printing also provides designers and engineers with a way of producing ultra-personalized objects, like shoes,^[39] or armor.^[40]

The biomedical and food industry sectors are some of the most important domains of application for hygromorphs.^[41,42] Actuation adds functionality to certain structures. For instance, tissue reconstruction and engineering could benefit from the shape modification induced upon humidity or pH variations in human or animal bodies. The hydrogel-based organs produced by Kang et al.^[43] and Cui et al.^[44] are prime examples of such structures. Zu et al.^[45] have created a hydrogel capsule delivering drugs when reaching specific stimuli. The 4D printing actuation can be used for bone repairing, as shown by You et al.^[46] Adding living cells in the hygromorphs can also help to obtain even greater multi-functionality in the structure.^[47]

Last but not least, as it touches on many aspects of engineering, 3D printing, multi-functionality, material properties and design, 4D printing is considered as a teaching and pedagogical tool.^[48]

1.4. Aim and Objectives

The field of 4D printing started a decade ago and is turning slowly to real technological applications. Although most studies related to 4D printing focus on one source of actuation, a complex network of stimuli needs to be considered for real-life out-of-laboratory applications. The understanding of those synergistic stimuli is essential to qualify and quantify the motion of parts within a 4D-printed component. Among the different stimuli available to actuate 4D-printed structures, humidity is less evaluated than temperature. Among the different types of materials available to provide actuation, composites are capable of specific actuation based on the differences between material properties and on the distribution of the different phases of the materials. One of the critical challenges faced to design parts for 4D-printed applications is the understanding of the impact of the moisture as a trigger to composite actuators.

One objective of the present study is to provide the first overview of the field associated to humidity-actuated, 4D-printed composite materials. The second objective of this work is to provide a practical design process to describe step by step the creation of hygromorphs. Classification and conceptualization of

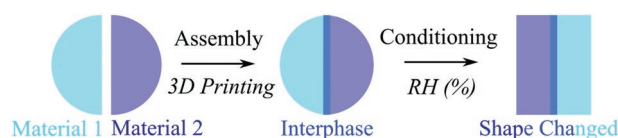


Figure 5. General concept behind 4D-printed composite hygromorph actuator.

the different design steps are also aimed at guiding the reader through the design process. The third objective of this work is to focus on the specificity of the actuation induced by composite materials. The actuation induced by this type of composite adaptive structure requires specific design modeling methods, but also a clear road map of the material selection process. The studies considered to create the holistic overview of the field of composite humidity-triggered macroscopic actuators are critically analyzed. The critical discussions described in this work would potentially lead to ideas about how to improve the design process described, also by observing other types of actuation triggers, or architectures of composite structures. The conclusions of this review also highlight the challenges faced by the research field for most steps of the design process defined along this review.

2. 4D Printing Concept

2.1. 4D-Printed Hygromorphs

Figure 5 presents the concept behind the hygromorph actuators. It includes three main elements: composite materials (i.e., multi-phase non-miscible materials), Relative Humidity (RH) conditioning to actuate the structure and 3D printing to assemble the materials. **Figure 5** shows that the final actuation not only depends on the properties of the original two materials (1 and 2), but also on the properties of the newly created inter-phase. Up to date, the range of studies related to RH-triggered actuators is limited. Hence, other types of actuation (i.e., pH^[6] and temperature^[5]) serve as sources of inspiration for the design of hygromorphs.

Dimassi et al.^[1] have proposed six different actuation functions for 4D-printed structures: bending, folding, twisting, expansion/contraction, and property change (i.e., color or state). In the present review, only bending and twisting are considered as the most common actuation functions found in structural hygromorphs. These types of actuation are presented in **Figure 6**. The actuation displayed is created by a difference between Moisture Content (MC)-triggered expansion between

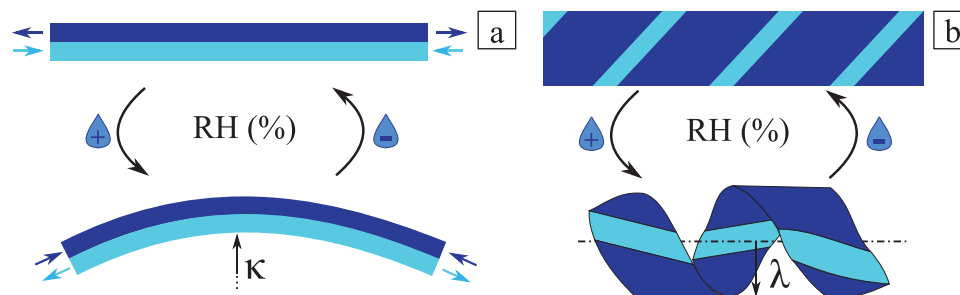


Figure 6. a) Bending actuation. b) Twisting actuation. The types of actuation considered in the present review are a combination of these two actuating mechanisms. κ and λ represent the bending and twisting curvatures, respectively.

Table 1. Synthesis of conclusions drawn by past studies related to 4D printed hygromorph actuation. Conditions to be in the Table: • Continuous fiber composite • 3D-printed • actuator • RH-stimulated. (Followed by Table 2).

Reference	Material	Conclusions
Le Duigou et al. (2019) ^[8]	<ul style="list-style-type: none"> • Continuous Carbon fiber & Polyamide 	<ul style="list-style-type: none"> • Control desorption and responsiveness via electric current heating • Assess the actuation capability of the material system • Show U-shape specimens actuation
Le Duigou et al. (2021) ^[50]	<ul style="list-style-type: none"> • Continuous Flax fiber & PolyLactic Acid (PLA) • Flax fiber & PolyButylene Succinate (PBS) 	<ul style="list-style-type: none"> • Create sequential response • Control actuation with layer height tailoring. • Control actuation and responsiveness with interfilament distance tailoring
de Kergariou et al. (2022) ^[51]	<ul style="list-style-type: none"> • PLA and continuous flax fibers 	<ul style="list-style-type: none"> • Show bio-mimicking actuation (flower).

the materials. Several parameters can be used to quantify this material specific property (i.e., the coefficient of moisture expansion (CME)). The differential between materials expansions triggered by moisture creates stresses perpendicular to the plane of contact between the same materials, hence bending or twisting of the structure.^[49]

Tables 1 (long fiber composite), **2** (short fiber composite), **3** (short fiber composite), **4** (short fiber composite), **5** (multi material) and **6** (multi material) summarize the conclusions of the works carried out by several research groups in terms of RH-actuated structures. All the studies from the literature have in common a search for optimal printing parameters. These tables highlight three main types of general conclusions are drawn in past studies. The first is the presentation of the actuation capability of the material. To achieve this, biomimeticism has been widely addressed. The second conclusion drawn concerns the control the actuation through printing, geometric and material parameters. Most of the time the experimental studies are conducted on simple speci-

mens. Finally, the last type of conclusion concerns applications and the form hygromorphs can take. **Figure 7** provides a synthesis of these conclusion categories, material actuation capability, actuation control with parameters and lastly applications. Each kind of conclusion is described with an example of geometry extensively used to. For material capabilities, flower biomimicking is introduced. For parameters control, usually long slender beam capable of bending or twisting have their actuation measured depending on the variation of a given parameter.

Compared to a humidity stimulation only, greater actuation authority is obtained by combining different expansion triggers. For instance, wetting and heating,^[81] photo actuation and heating^[82] as well as UV light actuation and heating^[83] have all been proposed as combination of actuating triggers. Wang et al.^[10] have also proposed a three-stimuli hydrogel bi-material hygromorph that could be actuated via magnetic fields, solvent composition, and temperature. Even though shape memory actuation is not considered in the present review, it is worth

Table 2. Synthesis of conclusions drawn by past studies related to 4D-printed hygromorph actuation. Conditions to be in the Table: • Short fiber composite • 3D-printed • actuator • RH-stimulated. (Followed by Table 3).

Reference	Material	Conclusions
Gladman et al. (2016) ^[18]	<ul style="list-style-type: none"> • Hydrogel & Short Cellulose Fiber 	<ul style="list-style-type: none"> • Show bio mimicking actuation (Dendrobium helix & calla lily) • Measure filament properties (swelling) • Measure mechanical properties
Correa et al. (2020) ^[52]	<ul style="list-style-type: none"> • Short Cellulose Fibrils & Acrylonitrile Butadiene Styrene (ABS) 	<ul style="list-style-type: none"> • Show bio mimicking actuation (Pinecone) • Control actuation with different printing patterns
Tahouni et al. (2020) ^[53]	<ul style="list-style-type: none"> • Short Wood fiber & ABS 	<ul style="list-style-type: none"> • Demonstrate several complex actuating patterns • Demonstrate the applicability of these design patterns (load carrying, face shield) • Control actuation with hinge crease curvature • Control actuation with interfilament distance
Cheng et al. (2020) ^[54]	<ul style="list-style-type: none"> • Short Wood fiber & ABS 	<ul style="list-style-type: none"> • Show actuation for several complex printing patterns • Demonstrate the applicability of these design patterns (orthotic splint) • Control actuation with mesostructure printing patterns
Tahouni et al. (2021) ^[55]	<ul style="list-style-type: none"> • PLA, PLA & Short wood fiber, ThermoPlastic Copolyester (TPC) 	<ul style="list-style-type: none"> • Create sequential actuation by thickness, filling ratio tailoring • Demonstrate the applicability of these patterns (aperture, cantilever beam)
Zarna et al. (2022) ^[56]	<ul style="list-style-type: none"> • PLA and short wood fibers & PLA 	<ul style="list-style-type: none"> • Demonstrate actuation capability of the material system: cross ply of wood pulp reinforced PLA with a layer of PLA on top. • Show bio-mimicking actuation (flower). • Control the actuation amplitude by adding milled thermomechanical wood pulp in the shape of either fibers or granulate to the PLA.

Table 3. Synthesis of conclusions drawn by past studies related to 4D-printed hygromorph actuation. Conditions to be in the Table: • Short fiber composite • 3D-printed • actuator • RH-stimulated. (Following Table 2, followed by Table 4).

Reference	Material	Conclusions
Cheng et al. (2021) ^[57]	• Short Wood fiber & ABS	<ul style="list-style-type: none"> • Show bio-mimicking actuation (plant: <i>dioscorea bulbifera</i>) • Control actuation with mesostructure printing patterns (interfilament distance, relative orientation of filament layers, thickness) • Demonstrate the applicability of these patterns (orthotic splint)
Le Duigou et al. (2016) ^[58]	• Short Wood fiber & PLA/ PolyHydroxyAlkanoate (PHA)	<ul style="list-style-type: none"> • Assess the actuation capability of the material system • Compare actuation to thermocompressed actuators • Control actuation and responsiveness with printing parameters
Kruger et al. (2021) ^[59]	• PLA & Short wood fibers	<ul style="list-style-type: none"> • Control actuation with mesostructure printing patterns (layer width, layer thickness)
Mulakkal et al. (2018) ^[60]	• Hydrogel & Short cellulose fiber	<ul style="list-style-type: none"> • Show bio-mimicking actuation (flower) • Control deformation with hydrogel composition/cross-linking (citric acid, clay, cellulose fiber)
Lai et al. (2021) ^[61]	• Hydrogel & short cellulose fibers	<ul style="list-style-type: none"> • Show bio mimicking actuation (flower <i>dendrobium helix</i>) • Proof-of-concept for the actuation with densification of the polymer network that depends upon the thickness of material printed • Tailor the composition to achieve printability
Qu et al. (2022) ^[62]	• Hydrogel & Cellulose nanocrystal & Fe ³⁺	<ul style="list-style-type: none"> • Demonstrate actuation capability of the material system: bilayer hydrogel, one layer with cellulose nanocrystal and Fe³⁺. • Control the actuation amplitude and speed with the type of stimuli applied: deionized water or sodium lactate and UltraViolet (UV) light.

highlighting that some research groups have combined bilayer actuation (i.e., silicone/wax and silicone/silica layers) with strain-tailored shape memory materials to explore new deformation possibilities.^[84–86]

2.2. Reversibility

The reversibility is the ability of an actuator to present one and one shape only per actuation stimuli independently of its past transformation, see **Figure 8**. The authors suggest there is no such thing as a reversible or not reversible material, but rather a multi-dimensional spectrum of reversibility for one actuator. This spectrum includes the variables defined in **Figure 8**:

conditioning RH (n_1), the number of repeated cycles (n_2), and the duration of the conditioning (n_3).

The reversibility depends upon the impact of the conditioning on the material properties involved in the actuation. Chabaud et al.^[87] have tested the reversibility of the mechanical properties of carbon fiber reinforced polyamide 66 (PA66) to use this material for hygromorphs.^[8] The interface between the different phases of the composites also affects the reversibility. For instance, Regazzi et al.^[88] show that the leaching, micro fracturing, and decohesion process occurring when natural fiber reinforced composites are immersed in water degrades the reversibility. **Table 7** shows reversibility studies and performed over 4D-printed moisture actuated structures, which have been published in the open literature.

Table 4. Synthesis of conclusions drawn by past studies related to 4D-printed hygromorph actuation. Conditions to be in the Table: • Short fiber composite • 3D-printed • actuator • RH-stimulated. (Following Table 3, followed by Table 5).

Reference	Material	Conclusions
Poppinga et al. (2020) ^[63]	• Short wood and cellulose fibers & ABS	<ul style="list-style-type: none"> • Show bio-mimicking actuation (pine cone scale, lily flower) • Demonstrate actuation of an aperture • Demonstrate actuation of an fly trap via snap through actuation • Proof-of-concept for artificial waterwheel
Langhans et al. (2021) ^[64]	• PLA and Short cellulose or arabocel fillers & ABS	<ul style="list-style-type: none"> • Control actuation with the orientation and amount of fillers
Vazquez et al. (2019) ^[65]	• PLA & Short wood fibers	<ul style="list-style-type: none"> • Control actuation with the relative orientation of printing path between layers, the number of layer and the stacking sequence • Show kirigami structures actuation (i.e., concentric kirigami, multi-material kirigami, extending hinges)
Vazquez et al. (2020) ^[66]	• PLA & Short wood fibers	<ul style="list-style-type: none"> • Control actuation with the interfilament distance, the thickness ration among layers, printing path, and layer height • Show origami modular system actuation
Tomec et al. (2021) ^[67]	• PLA & Short wood fibers and PLA	<ul style="list-style-type: none"> • Control actuation (amplitude and responsiveness) by varying the amount of wood fiber in the PLA and varying the thickness of the layers
Correa et al. (2017) ^[68]	• ABS & Short wood and cellulose fibers	<ul style="list-style-type: none"> • Demonstrate actuation of an opening • Demonstrate double curvature capability

Table 5. Synthesis of conclusions drawn by past studies related to 4D-printed hygromorph actuation. Conditions to be in the Table: • multi material • 3D printed • actuator • RH-stimulated. (Following Table 4, followed by Table 6).

Reference	Material	Conclusions
Baker et al. (2019) ^[69]	• Hydrogel & Elastomer	<ul style="list-style-type: none"> • Show origami actuation (Miura-ori patterns, folding cube, and folding tetrahedra) • Control actuation angle with geometric parameters of hinge-like structure
Liu et al. (2021) ^[70]	• Potato flack/starch gel & plastic	<ul style="list-style-type: none"> • Assess the actuation capability of the material system • Control actuation via drying (by air and/or microwave) • Control actuation via chemical-physical composition of the material (NaCl, fructose syrup, and oil)
Su et al. (2018) ^[71]	• SU-8 (epoxy dissolved in cyclopentanone)	<ul style="list-style-type: none"> • Demonstrate actuation capability of the material: one material with different curing parameters • Show bio mimicking actuation (flower) • Control actuation angle with geometric parameters of hinge-like structure • Show origami actuation (tetrahedron)
Zhang et al. (2019) ^[72]	• In-house resin	<ul style="list-style-type: none"> • Demonstrate actuation capability of the material system: two layers of the same resin with different curing processes
Schwartz et al. (2019) ^[73]	• Acrylate- and epoxide-based monomers	<ul style="list-style-type: none"> • Assess the actuation capability of the material system: two layers of the same resin with different curing processes • Show bio mimicking actuation (flower)
Raviv et al. (2014) ^[74]	• Rigid plastic & photocurable polymer	<ul style="list-style-type: none"> • Demonstrate actuation capability of the material system: one rigid polymer and one UV curable, which turns into hydrogel when immersed in water • Control of the actuation angle, speed and acceleration with geometric parameters of the hinge-like structure • Demonstrate grid-like actuation potential

In Table 7, the results are either presented in qualitative terms (i.e., whether the general shape of the specimen is recovered or not), or in quantitative ones (difference between geometry metrics-like curvature and bending angle). However, the quantitative results are related to a single point of the reversibility spectrum. Only Correa et al.^[19] have tested one structure at two different points of this spectrum by varying the drying process. Another qualitative way of assessing the lack of reversibility of an hygromorph is to look for critical damages in the specimen. For instance, the delamination observed by Correa et al.^[52]

challenges any claim that the structure tested is reversible. To the authors' knowledge, most of the hydrogel-based actuators discussed in the present work and measuring actuating reversibility have been conditioned in water, but the actuation was obtained with a varying temperature.^[18,92–95] Due to the diversity of the tests performed on the different hygromorphs presented in Table 7, it is extremely difficult to provide a precise comparison between the different materials. However, it is apparent that natural materials (such as flax and wood fibers) are not efficient in achieving reversibility, unlike polymeric

Table 6. Synthesis of conclusions drawn by past studies related to 4D-printed hygromorph actuation. Conditions to be in the Table: • multi material • 3D-printed • actuator • RH-stimulated. (Following Table 5).

Reference	Material	Conclusions
Mesa et al. (2020) ^[75]	• Paper and wax	<ul style="list-style-type: none"> • Demonstrate actuation capability of the material system: 3D-printed wax on top of paper. • Show corrugated structure actuation (triangular shape, rectangular shape). • Show self assembling structure actuation (chain formation, pentagonal formation). • Control the actuation amplitude and shape with fiber in paper orientation, wax printed patterns and material distribution.
Zhao et al. (2018) ^[76]	• Elastomer	<ul style="list-style-type: none"> • Assess the actuation capability of the material system: two-photo curable polymers • Show bio mimicking actuation (Flower, leaf) • Show origami folding/deployment actuation (Miura-ori patterns) • Control actuation with mesostructure printing patterns (thickness, material distribution) • Create sequential actuation
Hiendmeier et al. (2022) ^[77]	• in-house resin & luxaprint flex	<ul style="list-style-type: none"> • Demonstrate actuation capability of the material • Show origami actuation (tetrahedron)
Ryu et al. (2020) ^[78]	• Paper & wax	<ul style="list-style-type: none"> • Assess the actuation capability of the material system • Control actuation with the printing pattern • Measure reversibility of the actuator • Show actuation of a grip, a box folding and a self moving robot
Kim et al. (2021) ^[79]	• Liquid Crystal Elastomer (LCE)	<ul style="list-style-type: none"> • Show bio mimicking actuation (flower) • Demonstrate applicability (gripper, self opening vents) • Control actuation with material distribution (twist, grid) and anisotropic stiffness created via extrusion
Bai et al. (2022) ^[80]	• ABS & nylon	<ul style="list-style-type: none"> • Show actuation of a grid-like structure • Control actuation with distribution of printed patterns

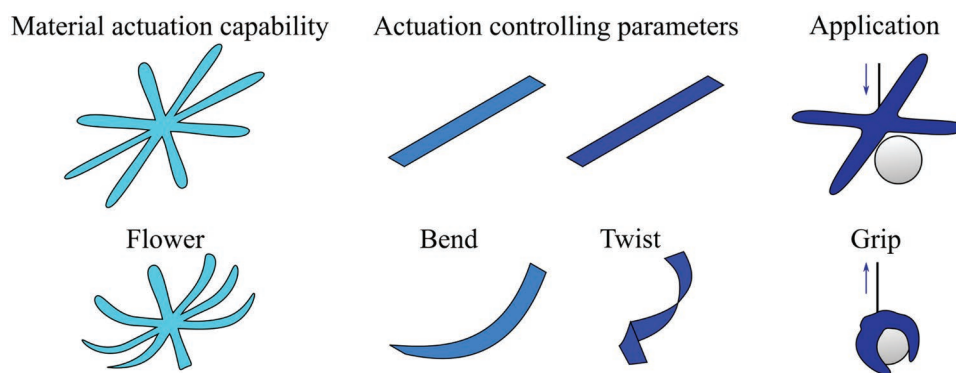


Figure 7. Schematic of the three main types of study conducted on the actuation of 4D-printed hygromorphs (as presented in Tables 1 (long fiber composite), 2 (short fiber composite), 3 (short fiber composite), 4 (short fiber composite), 5 (multi material), and 6 (multi material)). Material actuation capability: Demonstrate the capability of a material system to provide actuation by printing aesthetic hygromorph, i.e., bio mimicking flower, leaf, origami, kirigami. Actuation controlling parameters: Assess the possibility to control actuation by tailoring printing, geometric, dimensional parameters. Application: test the functionality of the hygromorph for potential in-service application, i.e., gripper, aperture, and load lifting device.

ones (polymer, elastomer, and polymeric fibers). **Figure 9** presents a process to follow for measuring the reversibility of the actuation in an hygromorph. Key steps include: definition of a testing point on the reversibility spectrum, including the related set of parameters (n_1 : RH of the conditioning for the reversibility test; n_2 : number of times the specimen is conditioned; n_3 : time of conditioning) defined in Figure 8. This definition includes the setting up of a reversibility criteria to define whether the specimen is considered as reversible for the test conditions or not. Then, the reversibility spectrum is analyzed following the steps presented here.

2.3. Materials and Geometry

This section discusses the way material selections and distributions can be used to control the hygromorph actuation. Priority is given to RH-actuated structures. However, other types of actuation are described, also to propose further explorations of the hygromorph design space.

2.3.1. Actuation Control with Material Distribution

Two main types of composites to produce hygromorphs are described in the open literature: fiber (continuous or short)-reinforced isotropic matrices, and multi-material isotropic matrices (see **Figure 10**). The first type is shown in Figures 10a,b. The architecture of that type of hygromorph involves stacking sequences with different fiber orientations between layers, which induce the actuation. On the other hand, the second type of composite hygromorph makes use of combinations of homogeneous isotropic materials with different properties to obtain similar performances (See Figure 10c). All these actuators are made of materials with different moisture induced deformation capabilities. Materials 1 and 2 are given as example in Figure 10. In the literature the material with the greater moisture induced deformation capability is labelled active, whereas the other one is labelled as passive.^[1,96] The terms “active” and “passive” can also be used to refer to the layer of the hygromorph depending on which layer expand the most.^[55,97] The active and passive behavior of the layers depend on the orientation. In the

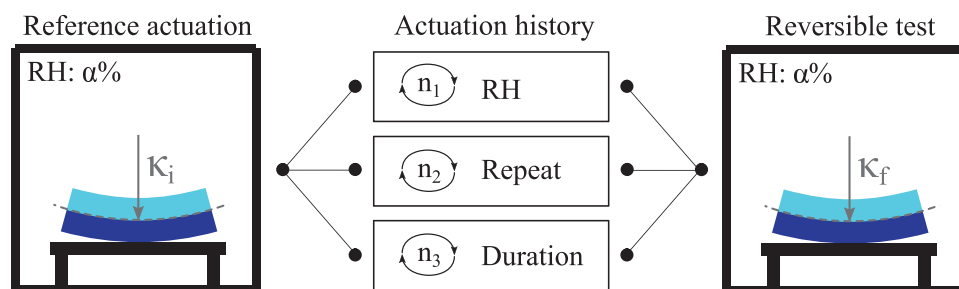


Figure 8. Schematics presenting the reversibility of 4D-printed hygromorph actuation. The measure of the reversibility is to be performed in three steps. First, a reference actuation must be created (specimen placed at a given RH) and the related actuation measured (i.e., initial curvature: κ_i for RH: $\alpha\%$). Then, the hygromorph must be conditioned to the specifications dictated by the designer/experimenter (i.e., at $n_1\%$ RH, for n_2 repeats of n_3 seconds). Finally, the hygromorph must be conditioned in an identical environment to the one of the reference actuation (i.e., final curvature: κ_f for RH: $\alpha\%$). The reversibility can be considered as the difference between the two curvatures measured. In this figure, curvatures are considered as the metrics to quantify the actuation, as it is widely implemented in moisture-actuated 4D-printed structures.^[8,18,52,53,55–57,59] However, many other parameters such as the bending angle, deflection or displacement of the actuation shape can be implemented to account for the deformation. The differences between parameters are discussed later in the review.

Table 7. List of the reversibility studies for 4D-printed composite hygromorphs. The n_1 , n_2 , and n_3 (order of magnitude) correspond to the parameters presented in Figure 8. The last column “Measure” presents the way the reversibility is assessed, either qualitatively or quantitatively with the specified value. Conditions to be in this table: • 3D-printed • actuator • RH-stimulated.

Reference	Material	n_1	n_2	n_3	Measure
Correa et al. (2015) ^[19]	Short natural fiber composite	(oven dried)–100%	4	min	Quantitative: actuation angle loss
Correa et al. (2015) ^[19]	Short natural fiber composite	(air dried)–100%	4	min	Quantitative: actuation angle loss
Li et al. (2019) ^[89]	Polymer & Hydrogel	40%–100%	1	hour	Quantitative: curvature loss
Dingler et al. (2021) ^[90]	Polymer	10%–70%	5	min	Quantitative: curvature loss
Le Duigou et al. (2016) ^[58]	Short natural fiber composite	50%–100%	1	hour	Quantitative: curvature loss
Le Duigou et al. (2021) ^[50]	Continuous natural fiber composite	50%–100%	1	hour	Quantitative: curvature loss
Kim et al. (2021) ^[79]	Elastomer	30%–80%	14	second	Quantitative: curvature loss
Ryu et al. (2020) ^[78]	Paper & Wax	(air dried)–(wet spray)	3	min	Quantitative: folding angle
Tahouni et al. (2020) ^[53]	Short natural fiber composite	(20%:30%)–(90%:100%)	1	hour	Qualitative
Jiang et al. (2021) ^[91]	Polymer & hydrogel	22%–95%	5	min	Qualitative
Le Duigou et al. (2019) ^[8]	Continuous carbon fiber composite	9%–98%	1	hour	Qualitative
Correa et al. (2020) ^[52]	Short natural fiber composite	20%–60%	14	hour	Qualitative

examples provided in Figure 10, the passive layer in the X-direction will be the active layer in the Y-direction.

Table 8 presents 4D-printed composite actuators present in the open literature, classified with the hygromorph categories defined previously. In this table, the ease of implementation (i.e., mainstream slicers and printers) as well as the versatility

and flexibility of the prints increases from left to right (comparison further described in Section 4.3). The number of published results therefore increases as well. On the other hand, the stiffness and bending moment of the structure generally decreases from left to right (comparison further described in Section 3.2). Several studies present combinations of the different material

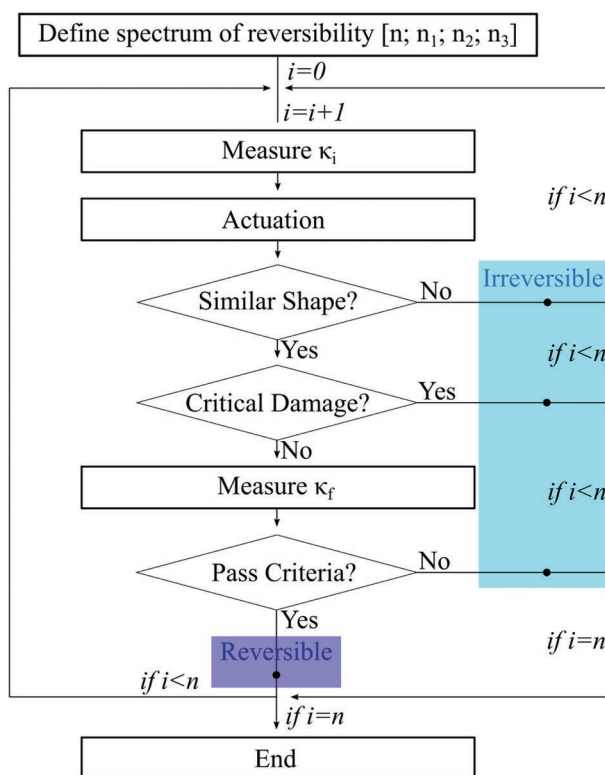


Figure 9. Process to measure the reversibility of hygromorphs (n : number of reversibility tests to perform, i : index for the reversibility tests conducted, $(n_1, n_2, n_3, \kappa_i, \kappa_f)$: reversibility parameters defined in Figure 8). n_1 : Relative humidity value used to actuate an hygromorph. n_2 : Number of repeated actuation cycles. n_3 : Duration of a given stage of actuation. κ_i : Reference curvature to be compared against in order to assess the reversibility. κ_f : Final curvature that has undergone n_1 humidity loading at n_2 % RH during n_3 seconds, to be compared against the reference one to assess repeatability.

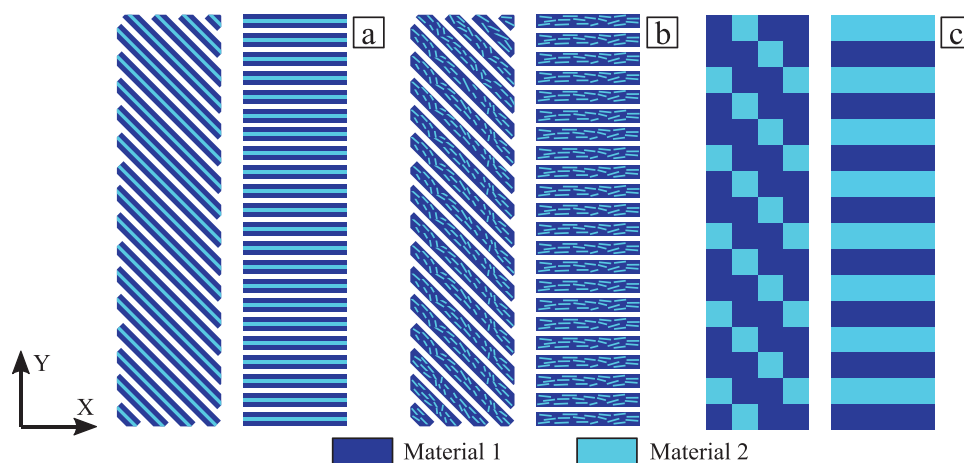


Figure 10. Types of materials distribution used for twisting actuators. For each type of materials, two fiber path layers are presented. When printed on top of each other, twisted actuator is created. a): Continuous fiber filament. b): Discontinuous (short) fiber filament. c): Bi-material (could be generalized in multi-material).

distributions highlighted in Figure 10. Chabaud et al.^[8] as well as Yu et al.^[98] created bilayer hygromorphs with a layer made of continuous fiber composite and the other one made of isotropic material.

The actuation stresses generated within the material distributions presented in Figure 10 are all based on dissimilar materials or printing patterns between layers. However, by changing the post-printing treatment (UV and temperature for instance) between active and the passive layers, Su et al.^[71] have obtained a cross-linking gradient (and therefore of mechanical properties)

through the thickness of a single material in the actuating structure. Sun et al.^[139] have created two materials with distinct properties out of a single resin, depending on the degree of the UV exposure. Schwartz et al.^[73] have proposed similar structures, in which the gradient of the cross-linking is obtained via different photocuring wavelengths (UV and visible lights mainly). Zhao et al.^[145] went a bit further, by proposing a continuously varying cross-linking of the hydrogel implemented, thanks to the variation of photo-cross-linking due to the varying thickness printed. They also created a finite element model

Table 8. Open literature papers divided via the material classification proposed in Figure 10. Conditions to be in this table: • 3D-printed • actuator.

	Continuous fiber	Short fiber	Multi-material
RH	Le Duigou et al. (2021), ^[8] Le Duigou et al. (2021), ^[50] de Kergariou et al. ^[51]	Gladman et al. (2016), ^[18] Correa et al. (2020), ^[52] Le Duigou et al. (2016), ^[58] Tahouni et al. (2020), ^[53] Cheng et al. (2020), ^[54] Tahouni et al. (2021), ^[55] Cheng et al. (2021), ^[57] Kruger et al. (2021), ^[59] Lai et al. (2021), ^[61] Mulakkal et al. (2018), ^[60] Correa et al. (2017), ^[68] Poppinga et al. (2020), ^[63] Langhans et al. (2021), ^[64] Vazquez et al. (2019), ^[65] Vazquez et al. (2020), ^[66] Tomec et al. (2021), ^[67] Zarna et al. ^[56]	Le Duigou et al. (2019), ^[8] Kim et al. (2021), ^[79] Lai et al. (2021), ^[61] Baker et al. (2019), ^[69] Liu et al. (2021), ^[70] Su et al. (2018), ^[71] Zhang et al. (2019), ^[72] Schwartz et al. (2019), ^[73] Raviv et al. (2014), ^[74] Zhao et al. (2018), ^[76] Ryu et al. (2020), ^[78] Hiendleier et al. (2022), ^[77] Qu et al. (2022), ^[62] Zarna et al., ^[56] Mesa ^[75]
RH & Temperature	N.A.	Gladman et al. (2016), ^[18] Boley et al. (2019), ^[99] Stoof et al. (2018), ^[100] Naficy et al. (2017), ^[95] Vazquez et al. (2019), ^[101] Koh et al. (2022), ^[102]	Yu et al. (2020), ^[98] Boley et al. (2019), ^[99] Zeng et al. (2022), ^[103] Naficy et al. (2017), ^[95] Jeong et al. (2019), ^[104] Kacergis et al. (2019), ^[105] Lee et al. (2020), ^[106] Saed et al. (2019), ^[107] Zhou et al. (2020), ^[108] Wang et al. (2021), ^[10] Liu et al. (2019), ^[109] Hua et al. (2021), ^[92] Podstawczyk et al. (2021), ^[93] Zhao et al. (2021), ^[94] Uchida et al. (2019), ^[110] Narupai et al. (2021), ^[111] Hu et al. (2022), ^[112] Shiblee et al. (2019), ^[113] Solis et al. (2022), ^[114] Nishiguchi et al. (2020), ^[115] Li et al. (2022), ^[116] Zou et al. (2022), ^[117] Chen et al. (2019), ^[118]
Other	Wang et al. (2018), ^[22] Hoa et al. (2019), ^[36] Hoa et al. (2020), ^[119] Hoa et al. (2020), ^[120] Hoa et al. (2017), ^[121] Hoa et al. (2022), ^[122] Peng et al. (2021), ^[123] Agkathidis et al. (2022) ^[124]	Bodaghi et al. (2016), ^[125] Piedrahita-Bello et al. (2021), ^[126] et al. (2021), ^[127] Zhang et al. (2019), ^[128] Guo et al. (2018), ^[129] Kokkinis et al. (2015) ^[130]	Zolfagharian et al. (2021), ^[48] Deng et al. (2021), ^[84] Lee et al. (2019), ^[85] Zeng et al. (2019), ^[86] OlgaKuksenok et al. (2016), ^[82] Boley et al. (2019), ^[99] Chen et al. (2021), ^[126] Weng et al. (2021), ^[131] Hamel et al. (2019), ^[132] Yuan et al. (2021), ^[133] Westbrook et al. (2008), ^[134] Mao et al. (2015), ^[135] Liu et al. (2019), ^[136] van Manen et al. (2022), ^[137] Wu et al. (2022), ^[138] Sun et al. (2022), ^[139] Liu et al. (2022), ^[140] Zolfagharian et al. (2018), ^[141] Huang et al. (2017), ^[142] Teoh et al. (2017), ^[143] Benyahia et al. (2022), ^[96] Roach et al. (2022) ^[144]

capable of designing parts actuated with such a strategy.^[146] The photo-polymerization and the consequent through-thickness cross-linking gradient can be tailored with the addition of fillers, such as pollen.^[147] The actuation induced by the gradient-varying properties has not been implemented yet for 4D-printed hygromorph actuation. However, UV-cured hydrogels have been developed for the same application (see Tables 3 and 4). This type of actuation requires the exploration of the design space of its actuation authority for hygromorph applications.

Multi-material actuation does not necessitate of structures made from different classes of materials. For instance, Boley et al.^[99] produced their actuator out of the same material, but with different amount of fillers. Boley et al. also use the orthotropy of the composite material to provide actuation. In that sense, the concept proposed by Boley et al. combines both multi-material and short fiber composite actuation strategies. Ge et al.^[16] use the dimensions of the fibers as design actuation controlling parameters. Consequently, multi-material hygromorphs can be created out of a single material, but with different fiber dimensions. The use of material with orthotropic properties for multi-material structures has been implemented in elastomers^[107] and hydrogels.^[10] Such strategy could increase significantly the design space of the RH-based actuators. However, Tables 1, 2, 3, 4, and 5 show that wood fiber-based polymers currently dominate the field of RH actuators. The use of multi-material approaches would require a more thorough assessment of the moisture-sensitive properties of those new hygromorph materials. Some new promising natural fiber reinforced polymers will be discussed in the section related to the discussion of the mechanical properties of cork,^[148] bamboo,^[148] or hemp^[149] fibers. Again, at this time of writing, their full actuation potential has still to be determined.

2.3.2. Actuation Control with the Geometry

Geometric parameters such as the variation of thickness are also used to control actuation. For instance, Zolfagharian et al.^[150] have implemented a 3D-printed structure stimulated by electrolytic using chitosan hydrogel only. Tahouni et al.^[55] have used geometric parameters such as the variation of the thickness to tailor the speed and the shape of actuation in short fibers actuators. In the latter study, the varying thickness is a controlling parameter, but not the source of the actuation. Other research groups use hinge-like structures to enhance the actuation, by making the use of bi-material 3D printing.^[50,151] Although most of the time the actuators are printed flat, they could also be built out of more complex shapes, such as a cylinder.^[109] Complex shape printing has not been tried for RH actuators. Inter filament distance, layer height, and relative orientation between layers have also been evaluated for the design of 4D-printed hygromorphs (see Tables 1, 2, 3, 4, and 5). These parameters have been mostly tested on wood fiber-based composites. Other types of actuators with complex shape still require to be assessed. Some research groups have gone beyond the conventional bi-layer flat surface to propose more complex architected (or metamaterial) configurations. Lattices structures are one of the most versatile types of architected actuators.^[27,99,152] Assembly of beams made of glass fiber reinforced elastomers

differing by their filler and amount of cross-linking amount were shown to achieve large ranges of actuation authority.^[99] Finally, one of the most flexible shapes to print and deform is a line. Wang et al.^[153] have proposed to print and model a bi-layer PLA line.

2.3.3. Classification of the Materials used in 4D Printing

The selection of material depends significantly on the design objectives assigned to the printed structure. **Table 9** presents the main types of matrix material implemented in past studies, from stiffest to softest polymer/plastic, elastomer and hydrogel. The selection of material type can be made on the potential application fields. The guidelines would be engineering for polymer (high bending moment and stiff), soft robotics for elastomer (large actuation and resilient) and biomedical for hydrogel (biocompatibility and large actuation).

Mixing the different material types increases the size of the actuation design space. High stiffness actuating structures have been produced by Yuan et al.^[133] by printing hydrogel on top of a 3D-printed elastomer layers. In one of the first studies published on 4D printing, Raviv et al.^[74] proposed a bi-material structure printed out of a stiff polymer and a hydro expandable hydrogel to actuate a slender beam. Finally, Lee et al.^[106] proposed the actuation of a bilayer structure made of an elastomer printed on top of a rigid polymer. Such combination has been implemented for temperature actuated hygromorph but not yet for hygromorph. This allows for potential further exploration of hygromorph design space.

Polymer, elastomer, and hydrogel are all implemented as short fiber reinforced and multi-material actuators. For instance, amongst elastomers, the liquid crystal ones are used both as part of short fibers composites (with tailored mesogens orientation) and multi-material actuation. Zhang et al.^[128] propose a liquid-assisted printing technique to orientate crystals in a 4D-printed elastomer. Saed et al.^[107] combined the use of liquid crystal elastomer with multi-material actuation. Elastomers still require their hygromorphic possibility to be assessed to be implemented in 4D-printed actuators.

2.3.4. Actuation Control with Material Selection

For short and continuous fibers hygromorphs, two different types of actuation are implemented. The authors took the initiative of naming these two different sources of actuation presented in **Figure 11**: Fiber Dominated Actuators (FDAs) and Matrix Dominated Actuators (MDAs). The differentiation of the two aforementioned concepts helps looking for new materials serving as actuation sources. For MDAs, the difference of deformation between the different layers generating the actuation is given by restricting the expansion of the fibers in their longitudinal direction. For such deformation to occur, the fibers of the hygromorph must be stiffer in their longitudinal direction than transversely. On the other hand, in the case of FDAs the actuation can be due to either the same difference in stiffness along the different directions of the fibers, or to the orthotropy of the fiber moisture expansion.

Table 9. Type of material implemented in previous studies. Conditions to be in this table: • 3D-printed • actuator.

	Polymer	Elastomer	Hydrogel
RH	Le Duigou et al. (2019), ^[8] Le Duigou et al. (2016), ^[58] Le Duigou et al. (2021), ^[50] Ren et al. (2021), ^[81] Kim et al. (2021), ^[79] Cheng et al. (2020), ^[54] Kruger et al. (2021), ^[59] Zhang et al. (2019), ^[72] Raviv et al. (2014), ^[74] Kokkinis et al. (2015), ^[130] Correa et al. (2020), ^[52] Tahouni et al. (2020), ^[53] Tahouni et al. (2021), ^[55] Cheng et al. (2021), ^[57] Su et al. (2018), ^[71] Schwartz et al. (2019), ^[73] Zhao et al. (2018), ^[76] Correa et al. (2017), ^[68] Poppinga et al. (2020), ^[63] Langhansl et al. (2021), ^[64] Vazquez et al. (2019), ^[65] Vazquez et al. (2020), ^[66] Tomec et al. (2021), ^[67] Hiendlmeier et al. (2022), ^[77] Zarna et al. ^[56] , de Kergariou et al. ^[56]	Kim et al. (2021) ^[79]	Gladman et al. (2016), ^[18] Jiang et al. (2021), ^[91] Mulakkal et al. (2018), ^[60] Lai et al. (2021), ^[61] Raviv et al. (2014), ^[74] Yuan et al. (2021), ^[133] Huang et al. (2017), ^[142] McCracken et al. (2019), ^[154] Baker et al. (2019), ^[69] Liu et al. (2021), ^[70] Schwartz et al. (2019), ^[73] Qu et al. (2022) ^[62]
RH & Temperature	Yu et al. (2020), ^[98] Zeng et al. (2022), ^[103] Jeong et al. (2019), ^[104] Kacergis et al. (2019), ^[105] Lee et al. (2020), ^[106] Stoof et al. (2018), ^[100] Zou et al. (2022), ^[117] Vazquez et al. (2019), ^[101] Koh et al. (2022) ^[102]	Boley et al. (2019), ^[99] Saed et al. (2019), ^[107] Zhou et al. (2020) ^[108]	Gladman et al. (2016), ^[18] Wang et al. (2021), ^[10] Liu et al. (2019), ^[109] Hua et al. (2021), ^[92] Podstawczyk et al. (2021), ^[93] Zhao et al. (2021), ^[94] Naficy et al. (2017), ^[95] Uchida et al. (2019), ^[110] Narupai et al. (2021), ^[111] Hu et al. (2022), ^[112] Shiblee et al. (2019), ^[113] Solis et al. (2022), ^[114] Nishiguchi et al. (2020), ^[115] Li et al. (2022), ^[116] Chen et al. (2019) ^[118]
Other	Wang et al. (2018), ^[22] Hoa et al. (2019), ^[36] Ren et al. (2021), ^[81] Deng et al. (2021), ^[84] Lee et al. (2019), ^[85] Zeng et al. (2019), ^[86] Yu et al. (2022), ^[152] Hoa et al. (2020), ^[120] Hoa et al. (2017), ^[121] Hoa et al. (2022), ^[122] Chen et al. (2021), ^[126] Piedrahita-Bello et al. (2020), ^[127] Weng et al. (2021), ^[131] Goo et al. (2020), ^[155] Liu et al. (2019), ^[136] Benyahia et al. (2022), ^[96] Agkathidis et al. (2022), ^[124] Zolfagharian et al. (2018), ^[141] Feng et al. (2022), ^[156] Roach et al. (2022), ^[144] Wang et al. (2022) ^[157]	Peng et al. (2021), ^[123] Zhang et al. (2019), ^[128] Siddiqui et al. (2022), ^[158] Roach et al. (2022) ^[144]	OlgaKuksenok et al. (2016), ^[82] Lee et al. (2019), ^[85] Guo et al. (2018), ^[129] Benyahia et al. (2022) ^[96]

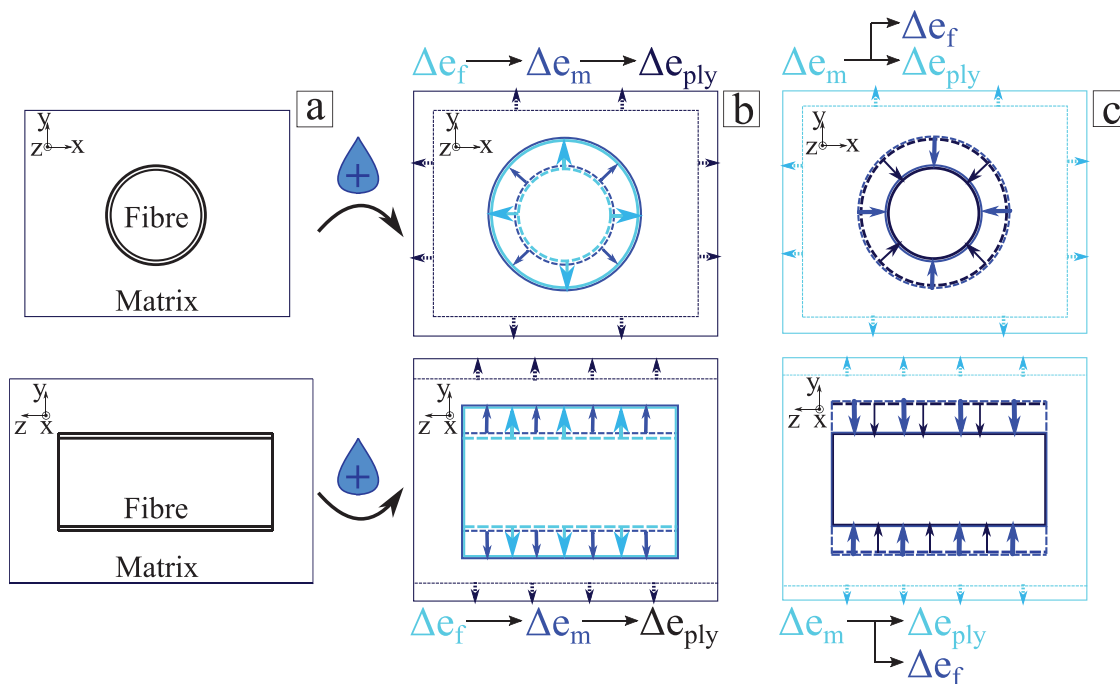


Figure 11. Schematic of the different actuation sources in fibers reinforced actuators. a) Initial distribution of the fiber and the matrix of the composite. The causes of the actuation are highlighted in bright blue, whereas the output of the actuation are in dark blue (Δe : expansion). b) Fiber Dominated Actuation: the actuation is triggered by the expansion of the fibers that apply pressure on the matrix, therefore creating the expected deformation at the scale of the ply. c) Matrix Dominated Actuation: the actuation is triggered directly by the matrix at the ply scale. MDA also exerts pressure on the fiber, but this pressure does not influence the deformation at the ply scale, which is responsible for the actuation.

Table 10. 4D-printed MFA and FDA in the open literature. Conditions to be in this Table: • actuator • 3D printed • fiber reinforced matrix composites.

Type of actuation	References
FDA	Correa et al. (2015), ^[19] Le Duigou et al. (2021), ^[50] Correa et al. (2020), ^[52] Cheng et al. (2020), ^[54] Kruger et al. (2021), ^[59] Correa et al. (2017), ^[68] Poppinga et al. (2020), ^[63] Langhansl et al. (2021), ^[64] Vazquez et al. (2019), ^[65] Vazquez et al. (2020), ^[66] Tomec et al. (2021), ^[67] Stooft et al. (2018), ^[100] Zarna et al., ^[56] de Kergariou et al. ^[51]
MDA	Le Duigou et al. (2019), ^[8] Gladman et al. (2016), ^[18] Wang et al. (2018), ^[22] Mulakkal et al. (2018), ^[60] Kim et al. (2021), ^[79] Lai et al. (2021), ^[61] Boley et al. (2019), ^[99] Saed et al. (2019), ^[107] Guo et al. (2018), ^[129] Kokkinis et al. (2015), ^[130] Weng et al. (2021), ^[131] Van Rees et al. (2018), ^[159] Wang et al. (2015) ^[160]

The **Table 10** presents a classification of the different types of actuation sources found in the open literature.

Table 10 shows that natural fibers and wood extracted fibers (i.e., bamboo) constitute the bulk of reinforcement in FDA structures, and are often associated with non-expandable matrices. Most cellulose and lignin-based materials possess trigger actuation potential due to their hydrophilic and expansion capabilities when placed in a humid environment. The diversity of natural fiber brings a wide range of possibilities for 3D printing applications. Deb and Jafferson^[161] propose a comparison of the different 3D-printed filaments made out of these fibers. Most of these materials have not been yet implemented for 4D printing, and would therefore offer new possibilities to the research field. Muthe et al.^[162] analyzed the use of these fibers combined with PLA in previous studies. They concluded to the great potential of this material association for 4D-printed applications. Greater control and improvement of the actuation are considered as two research opportunities for this field of application. On the other hand, MDA structures are mostly built using gel-type matrices and are associated with any type of fibers. The fillers inside the matrix are used to control the actuation. They are also used to control the hygroscopy of the material.^[163] Mulakkal et al.^[60] added cellulose fibers as well as clay pellets to their 4D-printed flower mimicking hydrogel to tailor the swelling ratio of the material. Another way of tuning the material properties related to actuation is to coat the 3D-printed filament. For instance, Vicente et al.^[164] demonstrated the possibility to modify the water absorption (one of the key actuation parameters) and the strength via the coating of the PLA filament. The use of hygroscopic matrices with polymeric fibers has not been extensively implemented so far, and it opens a great opportunity for designing 4D-printed hygromorphs.^[8] Further development of polymer resin-based hygromorphs can be considered via implementation of superabsorbent resins. An example of such resin is given in the context of 4D printed by Hiendlmeier et al.^[77] It presented a thickness hygroscopic strain of 170% when immersed in water, providing great actuation potential.

2.4. 3D Printing

This section presents the effects of the printing parameters on the actuation of hygromorphs.

2.4.1. 3D Printers

Polymers are mostly printed via Fused Filament Fabrication, whereas hydrogels are largely printed via pneumatic assisted direct ink writing. As de Kergariou et al. discussed^[165] for the case of 3D printing of continuous fiber composites, two solutions are currently available: use of a commercial printer (Markforged), or the modification of an existing printer (such as Prusa or Blade-1) to turn it into a pultrusion machine. In a pultrusion facility, the material is not pushed out of the nozzle; the adhesion to the printing surface during cooling pulls the filament out of the machine itself. Despite the commercial availability of carbon, glass and aramid continuous fiber filaments made by Markforged, to the author's knowledge, there is no such filaments commercially available for natural fibers. To print these materials, two strategies are adopted. The first consists in creating an in-house filament (flax-PLA).^[165] The second strategy is to print with an in-nozzle impregnation (jute-PLA).^[166]

The production of bi-material structures necessitates the use of a machine with two printing heads, or one rig in which the same printing head can switch between different materials.^[167] Printing speed is a key aspect to develop the use of 3D printing. For most bi-material actuators, the two phases are printed one after the other. Ushida et al.^[110] propose, however, to print two hydrogel materials at the same time and in the same filament. This procedure is not applicable to any material system, as it is problematic for printing (i.e., the materials do not feature the same printing parameters). The procedure proposed by Ushida et al. does not also provide the versatility of conventional 3D printing. Another way of accelerating the print of small hydrogel parts is to use digital printing.^[142] In that study, the digitally printed hydrogel-based structure was activated via cross-linking gradient due to variation in light exposure.

2.4.2. Actuation Control with Printing Parameters

The actuation can also be controlled via tailoring the printing parameters. For instance, Alshehly et al.^[168] printed layers at different speeds to induce internal strains in the PLA and, therefore, create the stresses required for the actuation. This study was extended by Rajkumar et al.^[169] to 3D-printed ABS, HIPS and also repeated for PLA. A model was proposed to take into account for the influence of the printing speed on the final properties of the printed structures. The printing speed was also evaluated by Kačergis et al.^[105] for its impact on the actuation within a Thermoplastic PolyUrethane (TPU)/PLA structure. The temperature of the printing plate was also noted as being a parameter of influence. The temperature of the extrusion, the thickness of the PLA layer, the filling density and the printing angle all affected the mechanical properties and, therefore, the performance of the actuation.^[170] Such observations were also made on hydrogels systems: the influence of the printing temperature on the ability of the material to retain water and therefore to actuate has been assessed.^[114] Another research group has used the residual strains generated via the printing path to design a polymer-based actuator,

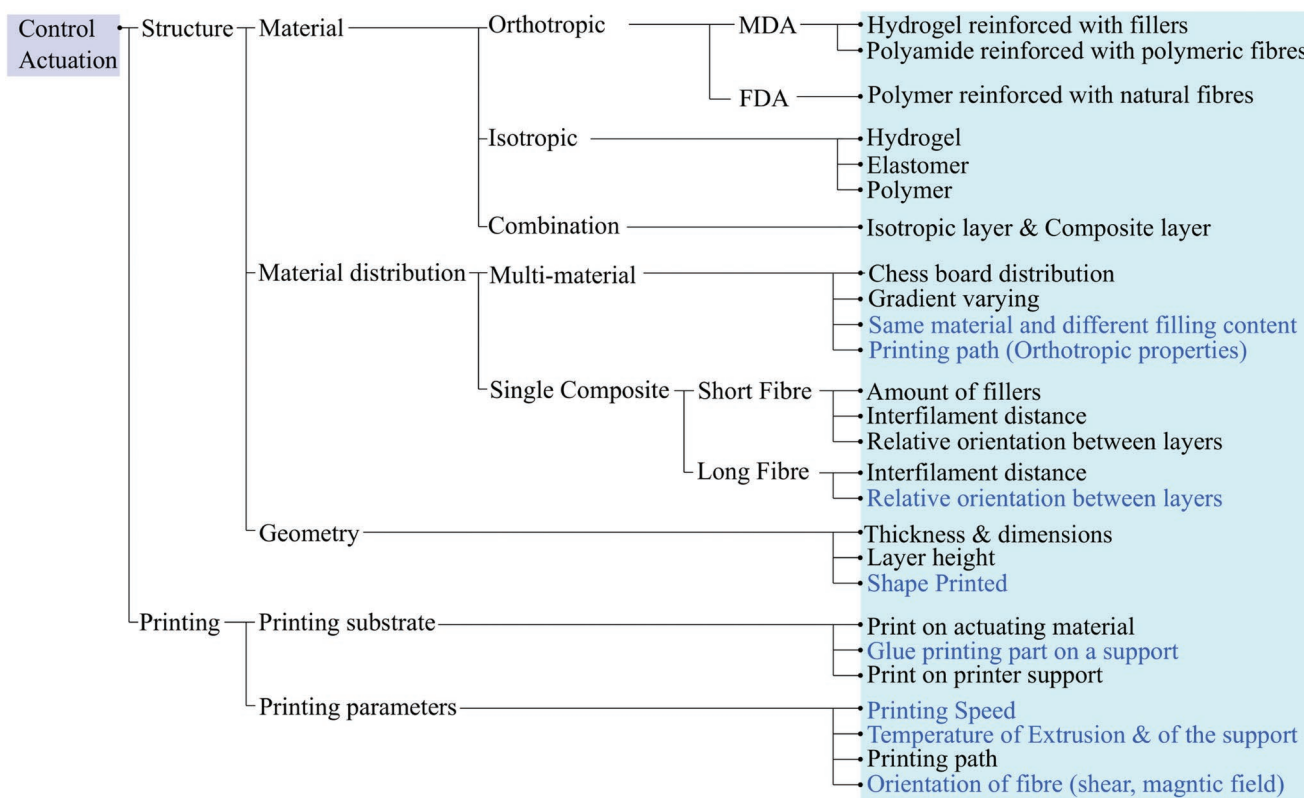


Figure 12. Logic tree presenting parameters studied to control 4D-printed actuation. The parameters on the right side highlighted in turquoise have been considered in previous studies to control actuation. The blue font parameters have not, however, been tested so far on RH-triggered actuators, but offer potential for actuation control.

rather than the printing speed.^[155] Layers of ABS specimens have been printed with different paths to obtain the required deformation. A similar conclusion was drawn by Podstawczyk et al.^[93] for hydrogels with a honeycomb-shaped structure. The relation between the temperature of extrusion and the temperature of the support for printing was considered to orientate along preferential directions the mesogen units inside the elastomeric actuator produced by Zhang et al.^[128] In some other cases the orientation of the filler is provided by applying magnetic fields during printing.^[130] Managing the filament path during printing when filling up the part is also of great interest to control the extent of the deformation. Zeng et al.^[86] compared different infill patterns to create the actuation required. optimization of local properties can be setup before the production of the hygromorph. For instance, Meiabadi et al.^[171] have used an artificial neural network in combination with a genetic algorithm to control the fracture toughness of the PLA with infill percentage, layer thickness and extruder temperature as inputs. The printing parameters presented in this paragraph can be evaluated for their direct impact of actuation. However, similar studies can be conducted for properties influencing actuation, such as stiffness, porosity and hygro expansion. Many of the materials used in 4D-printed hygromorphs presented in this review require to have the influence of their printing parameters thoroughly assessed.

2.4.3. Actuation Control with Printing Substrate

In most studies described in the present review, the actuators are 3D printed in their entirety. However, some research groups are looking to assemble 3D-printed materials with non-3D-printed parts. For instance, Kim et al.^[79] propose to print elastomers on a highly hygro-expansive polyamide 6 to create a 4D-printed hygromorph. Ryu et al.^[78] and Wang et al.^[22] print on paper and PA66 substrate, respectively. In these studies, the substrate is expansible and the printed element serves as a constraining element during the expansion to trigger the actuation. Liu et al.^[136] have showed the possibility to print the polymer layer of an actuator and then glue on top a metal strip after printing, to create the required deformation. Kim et al.^[79] showed these printing techniques to be available for moisture actuated structures. These However, further work is necessary to transfer the design know-how from temperature actuators to hygromorphs.

2.5. Summary of the Actuation Controlling Parameters

Figure 12 presents a summary of the parameters capable of controlling the actuation of 4D-printed hygromorphs. Those parameters have either been implemented in RH-actuated structures, or proposed from other types of actuation.

3. Actuation Control with Material Parameters

When selecting a material to produce an hygromorph, several properties have to be measured and controlled during printing, to ensure that the required actuation is obtained. This section highlights the most important properties to control actuation, i.e., stiffness and hygro-expansion. The quality of the material is also discussed.

It is possible to qualify the dependence of actuation from certain parameters by using the Timoshenko bilayer model presented in Equation (1).^[49] A similar equation is provided by Helfrich et al.^[172] for the twist actuation.

$$\delta\kappa = \frac{6 \times \delta\beta \times \delta MC \times (1+t)^2}{(t_a + t_p) \times (3 \times (1+t)^2 + (1+t) \times ((t)^2 + 1/t \times 1/e))} \quad (1)$$

The deformation ($\delta\kappa$) is influenced by geometrical parameters, such as the thickness ratio of the structure $t = t_p/t_a$. The terms t_p and t_a are the thickness of the passive and active layer, respectively. The passive and active layers correspond to zones that actuate the most and the least, respectively. The material properties also permit to control the actuation, through the stiffness ratio: $e = E_p/E_a$ (E_p and E_a being the Young's modulus for the passive and active layer, respectively) and through the difference of the coefficients of the moisture expansion ($\delta\beta$). This difference then relates the Moisture Content (MC) states reached by the specimens (δMC). This equation is available for a unit width specimen. Kruger et al.^[59] derived however the equation for a non unit width specimen. The calculation of the moisture content is performed via Equation (2), with m_{cond} being the mass of the conditioned specimen and m_{dry} is the mass of the dried specimen.

$$MC = \frac{m_{cond} - m_{dry}}{m_{dry}} \times 100 \quad (2)$$

The influence of the different parameters present in Equation (1) is shown in **Figure 13**. Please note that the absolute values in the figure are not essential. What is significant, on the other hand, is to understand the trends of the parameters influence. For example, the greater is the thickness of the passive layer, the lower is the actuation ($\delta\kappa$). This observation has been experimentally confirmed by Kruger et al.^[59] for wood fibers reinforced PLA. Increasing the active layer stiffness or width leads, on the contrary, to increase the actuation authority. On the other hand, as observable in Equation (1) the increase of such parameters for the design of the passive layer most of the time lowers the actuation curvature achievable.

3.1. Different Scales of Models and Properties

Here are discussed the scales of modeling and the measurement of the properties of both fibers reinforcements and the multi-material composites. **Figure 14** presents these different scales. The "Layer scale" consists in homogenising the properties of the materials that constitute the layers (the actuation requires different expansions between layers).^[19,71,95] The "Phase scale" in **Figure 14** consists of distinguishing the

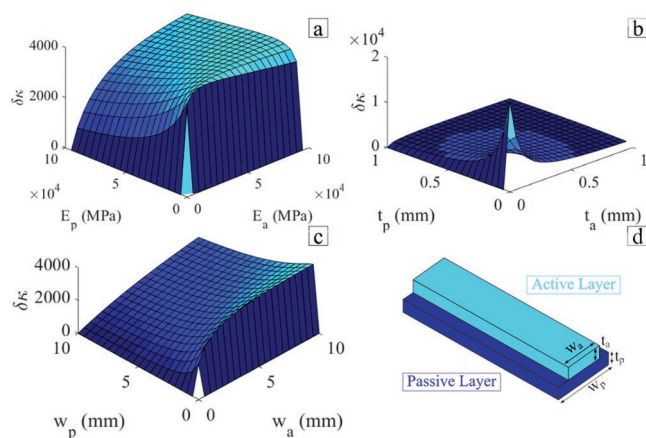


Figure 13. Timoshenko Equation (Equation (1)) adapted from Ref. [59] ($\delta MC = 0.8$; $\beta = 1000$). a) Influence of the passive and active stiffness on the curvature ($t_p = 0.2$ mm, $t_a = 0.1$ mm, $w_p = 1.0$ mm and $w_a = 1.0$). b) Influence of the passive and active thickness on the curvature ($E_p = 30,000$ MPa, $E_a = 5,000$ MPa, $w_p = 1.0$ mm and $w_a = 1.0$). c) Influence of the passive and active width on the curvature ($t_p = 0.2$ mm, $t_a = 0.1$ mm, $E_p = 30,000$ MPa and $E_a = 5,000$ MPa). d) Schematic defining the parameters in the hygromorphs modeled at the layer scale.

different constitutive materials of the composite actuator. For instance, those materials can be separately the fiber and the resin for the fiber composite, or the two materials present at the same time in a bi-material actuator.^[76,89,173,174] In this case, the actuation requires different expansions for the constitutive materials of the composite. In fiber-reinforced composites, the "Intra-phase scale" in **Figure 14** consists in considering the internal architectures of the phases described at the Phase scale, i.e., the yarn of fibers twisted together.^[165] An example of such model for non-actuated structures is provided by Zhang et al.^[175] For multi-material systems, this scale consists in modeling the structure at the filament level and therefore the orthotropic properties of the filament itself (see Refs. [176, 177]).

The layer scale is used for the characterization of the printing patterns influence on the actuation.^[59,95] It can also serve to estimate quickly the potential actuation in complex structures. Often conducted with Timoshenko equation, it will also use Finite Element Analysis (FEA) and CLT when the deformation

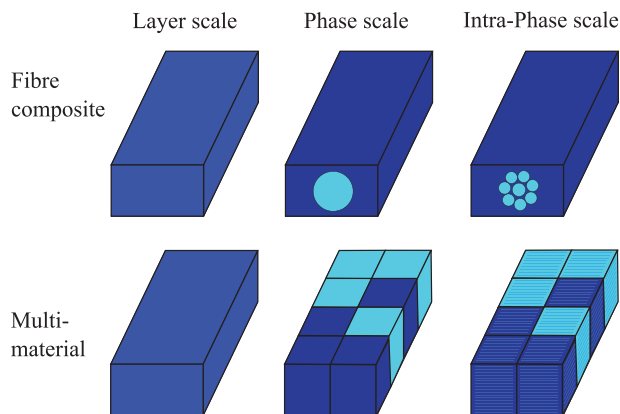


Figure 14. The different scales of modeling for the material distribution described in this study.

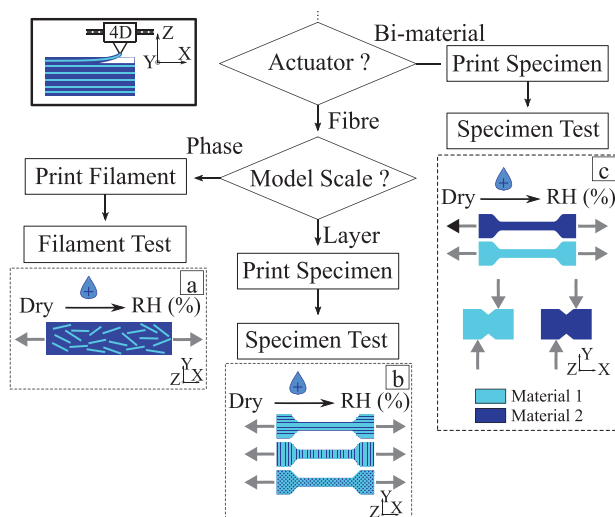


Figure 15. Decision tree to measure the mechanical properties of the material considered for 4D printing. The model scales refer to the terminology presented in Figure 14. Different tests must be performed depending on the scale: a) Filament measurement for composite material. b) Layer scale measurement for composite material. c) layer scale measurement for isotropic material.

required happens to be more complex, for instance, with twisting.^[131] The fiber and filament scale (phase scale) properties are of prime choice to model complex fiber paths, for instance, to model structures like the ones presented by Gladman et al.^[18] This is the preferred scale for the bi-material as it easily adapts to any material distribution.^[76,89,132,178] Finally, the Intra-phase scale brings an additional degree of precision but also of complexity in the creation of the model.^[175,176] To the authors' knowledge, such model has not been used for actuating structure. It would be efficient to describe how the micro-scale influences the macroscale actuation

3.2. Mechanical Properties

3.2.1. Measurement

The rationale for the measurement of the stiffness of 3D-printed materials actuators described in the present review is shown in Figure 15. The stiffness is measured for both dried and conditioned specimens. Figure 15a presents the measurement of the 3D-printed filament properties. The filaments are first printed and then tested when dried, followed by conditioning. The transverse properties of the filament are usually complex to obtain, and an estimation of those properties from transverse test back calculations is presented by Baley et al.^[179] The other option is to perform microscale indentation or compression tests.^[180] Figure 15b presents dog bone or strip-shape specimens printed with filaments orientated at 0° and 90°. If FEA modeling is performed, then the shear stiffness must also be measured, using uniaxial tensile loading on +/-45° specimens. Finally, Figure 15c presents the rationale to test materials for multi-material hygromorph configurations. The material is traditionally considered isotropic, and measuring

only one stiffness independently on the printing path should be sufficient for most modeling purposes. To obtain the shear stiffness, either V-notched test can be performed (Standard example: ASTM D5379^[181]), or the classical isotropic elasticity relation $G = E/(2+2*\nu)$ (G : Shear stiffness, E : Tensile modulus and ν : Poisson's ratio) can be used. In the Material section of this paper was already reported that 3D printing usually creates an orthotropy in the material printed, due to filament shearing in the nozzle. In some cases, it can be therefore recommended to conduct the same test as in Figure 15b. Among all the tensile properties tests described in the open literature, the ASTM D3039, ASTM D638, ISO 527, and GB/T 3354 standards are the most widely used to perform those tests.

For greater details about the measurements of the mechanical properties of materials discussed in this work, the readers are referred to previous specific reviews. Here, such reviews for hydrogels^[182] and polymer/composites are given.^[183–185] The printing parameters can influence the stiffness of the structure. Hence, understanding their influence is the key to make sure the stiffness measured is representative of the one the material provides to the hygromorph. For instance, the interfilament distance and the number of layers printed have been shown to affect the stiffness of continuous flax fiber reinforced PLA.^[186] Part of the gap between the model predictions and the actual actuators performances is due to the evolving properties of the material with the humidity. For instance, the mechanical properties of the material before conditioning are usually considered when using the Timoshenko equation (Equation (1)). Measuring and implementing in models mechanical properties that vary with the humidity is a way to decrease the discrepancy between the predicted and actual deformations of the actuators.^[67,97] For fibers-based hygromorphs, the actuation is often triggered via dissimilar orientations of the fibers between layers. These fibers depositions architectures are a source of delamination between layers due to the presence of peeling stresses.^[187] The strength to delamination of the material and its effect of the stacking sequence can be important for certain hygromorph designs. For instance, Correa et al.^[52] observed their hygromorphs delaminate due to the RH conditioning. Modeling of fiber-reinforced hygromorphs could include the homogenization of the properties at layer scale, and classical laminate theory can be used to this extend. For instance, Malagutti et al.^[188] performed those types of calculations for wood fibers reinforced polymer, a material extensively used for 4D-printed actuators. Zarna et al. implemented this computation method with other similar materials to predict their actuation.^[56] Performance maps of the mechanical properties for different 3D-printed continuous fibers presented in open literature before 2022 have been published by the Authors in a previous study.^[165] This list was updated and is presented in Figure 16 and Table 11. The graphs show that a large proportion of the printed composites described in the open literature are made of polyamide combined with carbon, aramid, or glass fibers. The last two classes of fibers have never been used for 4D-printed hygromorphs. Carbon fibers composites have been used to create MDA hygromorphs.^[8] However, little investigation of their 4D-printed hygromorph design space has been conducted. Aramid and glass fibers have potential for being used in a similar way to create actuation. The data shown in Figure 16

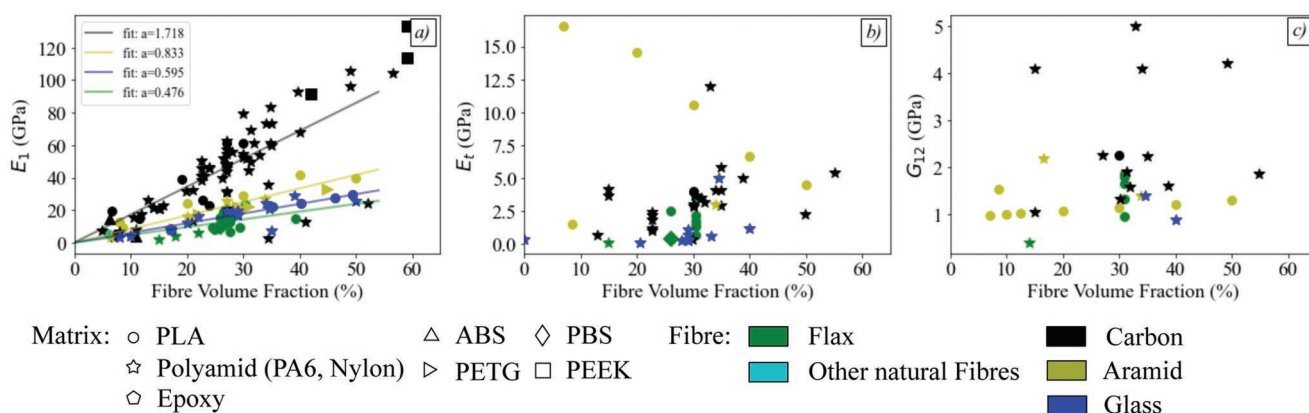


Figure 16. a) Longitudinal. b) Transverse. c) Shear stiffness of 3D-printed continuous fiber reinforced polymers in open literature. For the longitudinal stiffness, the rule of mixture has been adopted to compare different fiber types. (PLA: PolyLactic Acid, PETG: Polyethylene Terephthalate Glycol, ABS: Acrylonitrile Butadiene Styrene, PBS: PolyButylene Succinate, and PEEK: PolyEther Ether Ketone). Plots updated from Ref. [165]. The references are presented in Table 11.)

also highlight the large number of printing parameters available to control the manufacturing and testing of the 3D-printed materials (i.e., printing speed, temperature of extrusion and the temperature of the printing support, amongst others). This reinforces the benefit of testing the material used to model the hygromorph, instead of simply using data available from the literature. The printing parameters influencing the properties of the 3D-printed material can be optimized to obtain properties fitting the application. For instance, Long et al.^[189] optimized the interfilament distance and the printing speed to achieve the best strength for 3D-printed flax continuous fiber composites. Beckman et al.^[190] proposed a review of all the fibers implemented so far in 3D-printed structures. Common resin used in 3D printing are divided based on their hygroscopic ability. PLA, Acrylonitrile Butadiene Styrene (ABS), PolyCarbonates (PC), Polyethylene Terephthalate Glycol (PETG) and PolyEthylene Terephthalate (PET) are considered as hygroscopic, whereas PolyVinyl Chloride (PVC), Polypropylene, Polyethylene, and polystyrene are considered as non hygroscopic. Hygroscopicity is a necessary but not sufficient condition to generate moisture actuation. Hence, even though all these resins have potential to be used as FDA, only PLA, ABS, PC, PETG, and PET have the potential to be used in MDA. Beckman et al.^[190] also ranked fibers in terms of their moisture regain capability. Wool, oak wood, and jute fibers are capable of in-taking more moisture than the flax fiber widely used in hygromorphs. These fibers, as well as hemp (similar moisture regain than flax), show a significant potential to be used in FDA hygromorphs. Additional investigation has to be conducted to confirm the 4D-printed hygromorph potential of these fibers and matrices.

Figure 17 highlights the values of the longitudinal stiffness of short fiber reinforced composites published in the open lit-

Table 11. References for the values presented in Figure 16.

Property	Refs.
Shear modulus	[191–205]
Longitudinal modulus	[50,87,97,166,186,191–230]
Transverse modulus	[50,87,191–195,197,198,200–205,207,217,226,229]

erature. The data do not follow the rule of mixture, due to the variability of the lengths^[231] and orientations^[232] of the fibers. The data presented in Figures 16 and 17 are all based on composites with rigid polymers. Short fiber composites have stiffness about one order of magnitude smaller than their continuous counterparts. Unlike the case of continuous fiber composites, very few studies have been performed on short flax fiber composites. The most widely tested short fibers composite is reinforced by wood. As discussed before, wood fibers have a great potential in terms of actuation potential. Other promising short natural fibers to be used in FDA are hemp,^[149] cork,^[148] harakeke,^[149] and bamboo^[148] if the fiber actuation capability is large enough. Furthermore and similarly to continuous fibers, polyamid-based^[232–235] composites have potential to produce MDA structures, even when reinforced by short fibers. Other types of fillers (not presented in Figure 17) can find application in 4D-printed hygromorphs. For instance, at nano scale, carbon nanotubes,^[236,237] and cellulose-derived fillers^[238,239] have been 3D-printed in polymers and tested for different properties. However, their actuation potential has still to be assessed.

Elastomers and hydrogels are subjected to different classes of mechanical characterizations depending on their properties. Like polymers, tensile tests are sometimes performed.^[18,61,62,73,91,95,118,142] For the hydrogels used in 4D-printed actuators of the present review, the stiffness ranges from 10 kPa to 100 MPa. The elastomers used for 4D-printed actuation have their stiffness varying between 1 kPa and 10 MPa.^[85,158] These stiffness are from two to four orders of magnitude lower than those of composites with rigid polymers presented in Figures 16 and 17. Shear rheometry tests have also been performed to measure the stiffness of those materials.^[60] The testing parameters have also a significant influence on the properties obtained via measurements. Consequently, those parameters must be varied to obtain a set of values representative of the material behavior, i.e., the shear strain,^[10,60,91,93,109] frequency,^[60,61,93] shear stress,^[18] and temperature.^[133] Shear rheometry is extensively performed to compare the mechanical properties of hydrogels or elastomers when fillers are added, or their composition is varied.^[60,61,93] In many cases, the behavior of the material is, however, not elastic, or is elastic within a very

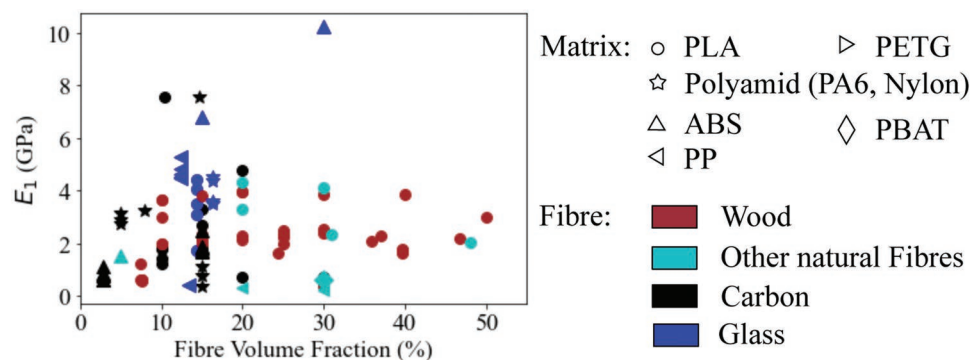


Figure 17. Longitudinal stiffness for 3D-printed short fiber reinforced polymers from the open literature. (PLA: PolyLactic Acid, PETG: Polyethylene Terephthalate Glycol, ABS: Acrylonitrile Butadiene Styrene, PP: PolyPropylene, and PBAT: Polybutylene Adipate terephthalate) Refs: [56, 58, 67, 148, 149, 231–235, 240–257]

small strain range.^[92] The hydrogel could behave elastically when dried, but evolve along a different mechanical behavior when conditioned.^[18] Hence, a single stiffness value becomes a very limited piece of information to represent the overall behavior of the material. Two solutions could be adopted in this case to model this type of material for actuation purposes. The first is to consider the entire mechanical behavior law as input. The second solution consists in considering another equivalent type of constitutive law to represent the hydrogel (for instance, hyperelastic Mooney-Rivlin or Neo Hookean models). The parameters for these models are obtained essentially via compression, shear or biaxial tension tests.^[258,259]

3.2.2. Influence of the Conditioning and Printing on the mechanical properties

The actuation of the hygromorphic structures is triggered by the differential expansion of constituent phases of the composite material. To induce deformation, the moisture has to diffuse within the material, often causing modifications of its properties. Understanding how humidity affects the material properties involved in the actuation is important to improve models. This understanding is also key to evaluate how the relative humidity affects the different types of actuation described in the previous sections. The present study takes into consideration only the permanent state of humidity diffusion within the material. The transient state has been considered in previous studies related to several 3D-printed materials (continuous carbon fiber nylon^[260] and nylon 6^[261]). Lessons from non-3D-printed equivalent materials (i.e., flax fiber reinforced PLA^[262]) can be also applied for printed hygromorphs. As **Figure 18** shows, the influence of the three types of conditioning over the mechanical performance of 3D-printed hygromorphs has been considered in past studies (pre-printing conditioning, as-printing conditioning, and post-conditioning). These three types of conditioning are applied to the filament, the printer and the specimens, respectively. Zaldivar et al. studied the impact of the relative humidity at pre-printing stage on the final properties of ULTEM 9085 resin filaments by measuring the stiffness at the RH level at which the filament was stored.^[263] This thermoplastic filament showed a constant stiffness at low

RH levels. The stiffness then decreased for 0.4% moisture contents and beyond. This reduction in terms of properties is said to be due to the large porosity created during printing by evaporation of the water absorbed by the resin prior to printing.

Greater control of the material properties is obtained when the surrounding environment of the printing is under control (see As-printing in **Figure 18**). For instance, Zeng et al.^[86] tested their TPU Ninjaflex filament-based specimens after printing them at different RH levels in an enclosed box. If the RH value was too low or too high, the print was not feasible. The porosity in the specimens was also significantly affected by the conditions of the printing. To find adequate printing conditions, May et al.^[264] optimized the environment of the printing enclosure by using numerical tools to improve the tensile strength of the printed specimens.

Most of the studies related to the characterization of the effects provided by the relative humidity have been performed during post-printing conditioning. For most materials presented in those studies, this phase of conditioning leads to the modification of the mechanical properties. For instance,

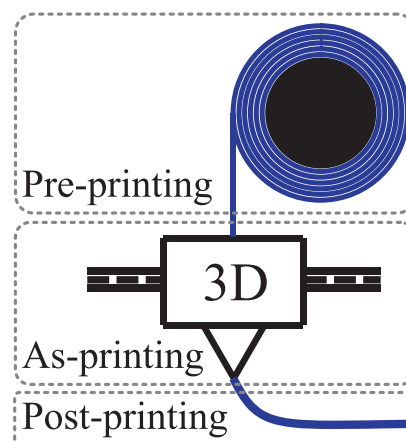


Figure 18. Schematics presenting the different types of conditioning for 3D-printed materials. Pre-printing conditioning: the filament is conditioned ahead of printing. As-printing conditioning: conditioning the entire printer is conditioned during the printing at specific RH and temperature. Post-printing conditioning: any surrounding environmental condition (wanted or not), at which the specimen is subjected to.

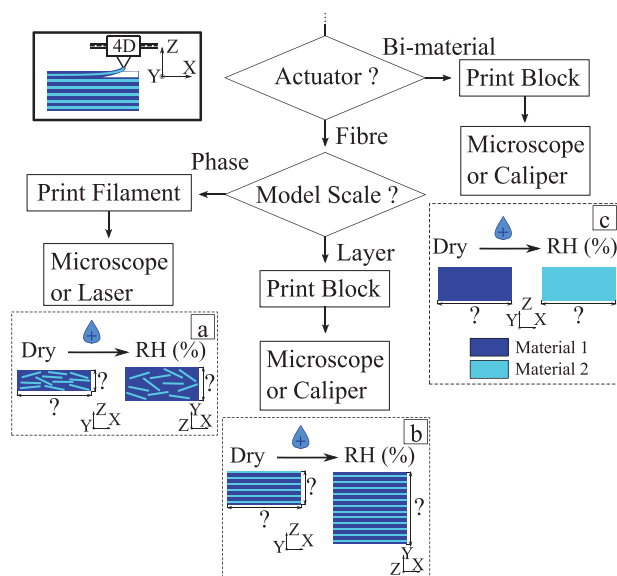


Figure 19. Decision tree presenting the rationale to select the measurement process to detect the hygro-expansion of 4D printing materials. The model scales refer to the terminology presented in Figure 14. The properties are measured depending on the modeling scale of the actuator.

de Kergariou et al.^[165] showed a decrease of shear, longitudinal and transverse stiffness in continuous flax fiber reinforced Poly-Lactic Acid (PLA) composites when the RH ranges from 11% to 98%. That hygromorph material was then used to produce hinge-like structures.^[50] As the material softens at the end of the conditioning, its lower transverse stiffness artificially increases the actuation, compared to what predicted by the Timoshenko model (see Figure 13a). On the other hand, the softening of the active layer tends to decrease the actuation capability of the structure (see Figure 13a). For fiber reinforced filament-based hygromorphs, the amount of reinforcement affects the material properties and hence the actuation. For instance, the more wood fibers in the PLA matrix, the larger the stiffness of the printed composite, up to a certain amount.^[244] Kariz et al.^[265] actually showed a mutual influence existing between the amount of reinforcement and the testing RH conditions on the stiffness of wood reinforced PLA. Below 40% of wood content by weight, the humidity reduces the stiffness; above 40%, the humidity contributes to augment the stiffness. A decrease in stiffness for the same material when the RH increases was described in another paper.^[266] A similar conclusion is drawn for soy bean fibers.^[267] Non-reinforced polymers have been also subjected to the evaluation of their material properties when conditioned in a humid environment. PLA is one of the most widely used matrices for polymer-based hygromorphs, hence the importance of knowing the impact of humidity on its mechanical properties. Chandran et al.^[268] observed the decrease of the stiffness of 3D-printed PLA samples after being immersed in water. Sun et al.^[269] showed an increasing stiffness at low RH values, together with a decrease of stiffness beyond a 40% RH level. Most information needed to understand the influence of water on PLA could be found in the work testing conditioned 3D PLA with specimens printed horizontally and vertically.^[270] Nylon 6, also widely used in 3D printing, was shown to soften

when immersed in water.^[261] The conditioning considerations described in the present paragraph for the most part observed the impact of conditioning on stiffness. These conclusions have to be extended to the production of hygromorphs to add extra control on the production, therefore, on the actuation.

3.3. Hygro-Deformation

This paragraph discusses the measurement of the material expansion when subjected to humidity conditioning. The terms swelling index, swelling ratio or Coefficient of Moisture Expansion (CME) all describe the ability of a material to expand when immersed in varying moisture systems. Figure 19 presents the decision tree for setting up the hygroscopic measurements of the materials to be used as actuators. Measuring the dimensions of the materials sample in dried and humid conditions allows to obtaining parameters that represent the hygro-expansion capability of the materials for modeling purposes (e.i., swelling index and CME). Figure 19a shows the measurement of the hygro-expansion at filament scale. Figure 19b shows the dimension to be measured for a composite actuator modeled at the layer scale. A block of material (usually a cuboid) must be printed along one direction. Then, the dimensions of the cuboid are measured in dried and wet environments. Finally, Figure 19c shows that dimensions to measure, to evaluate the hygro-expansion of the materials used to produce multi-material actuators. The material is usually assumed to be isotropic. However, as described in the material section, 3D printing usually generates an orthotropy in the printed material, due to filament shearing in the nozzle. Hence, for some materials, it is recommended to use the same filling pattern as the one implemented in the final 4D-printed structure, in order to measure the dimensions during dried and wet states. Orthotropic materials also require the measurement of the dimensions in the Z-and Y-directions. Image data processing can be used for the measurement of the dimensions in most materials^[56] systems. Moreover, those image data processing techniques are to be preferred if the material measured is soft, as the contact with the caliper deforms the specimen. Such type of measurements was performed in the case of hydrogels, for instance, by Lv et al.^[271] On the other hand, the caliper could be used for stiffer materials.^[58]

Tables 12 and 13 describe the hygro-expansion measurements performed on materials with the potential to be used as 4D-printed hygromorphs. The moisture expansion of fiber and matrix can be measured separately in the case of fiber reinforced hygromorph composites. Atomic Force Microscopy has been implemented to measure the change of dimensions in cellulose aggregate fibrils with moisture absorption.^[272] A goniometer was used to measure the expansion of technical (bundle of elementary fibers) and elementary (single plant cell) flax fibers.^[273] Models are capable of providing then inverse identification of the hygroscopic properties in composites from the properties of their phases.^[274,275] Another unusual hygroscopic strain measurement technique has been proposed by Hiendlmeier et al.^[77] The technique consists in solving a mechanical equilibrium between the expansion forces during swelling. This methodology however necessitates an “a priori” determination of the mechanical properties of the material.

Table 12. List of hygro-expansion studies performed on materials with 4D-printed hygromorph potential. (Coefficient of Moisture Expansion: (CME); poly(hydroxyalkanoate): (PHA)). Conditions to be in this Table: • 3D printed • material discussed in the present review as having 4D printing potential. Please note that some authors do not provide the RH the specimens are conditioned at. In such cases, a qualitative assessment of the conditioning is provided in the table ("Dry%" and "Ambient RH%" for oven dried and ambient relative humidity, respectively). (Followed by table 13).

Reference	Material	Measurement	Scale	RH range	Properties
Le Duigou et al. (2019) ^[8]	PA6	Caliper	Layer	Dry%-(10, 30, 75, 98)%	CME
Le Duigou et al. (2019) ^[8]	PA6 & continuous carbon fibers	Caliper	Layer	Dry%-(10, 30, 75, 98)%	CME
Zarna et al. (2022) ^[56]	PLA and short wood fibers	Microscope	Layer	Dry%-100%	CME
de Kergariou et al. (2022) ^[51]	PLA and continuous flax fibers	Caliper	Layer	Dry%-(11, 35, 54, 75, 98)%	CME
Tomec et al. (2021) ^[67]	PLA & PLA and wood fibers	N.A.	Layer	20%-80%	CME
Chabaud et al. (2019) ^[87]	Polyamid & continuous glass fiber	Caliper	Layer	Dry%-(10, 30, 75, 98)%	CME
Le Duigou et al. (2016) ^[58]	PLA/PHA & short wood fibers	Caliper	Layer	50%-100%	Hygroscopic strain
Mulakkal et al. (2018) ^[60]	Hydrogel & clay	Caliper	Layer	50%-100%	Hygroscopic strain
Kikuchi et al. (2020) ^[260]	Nylon	Caliper	Layer	Dry%-Ambient RH%-100%	Hygroscopic strain
Kikuchi et al. (2020) ^[260]	PA6 & continuous carbon fibers	Caliper	Layer	Dry%-Ambient RH%-100%	Hygroscopic strain
Kariz et al. (2018) ^[265]	PLA resin & short wood fibers	N.A.	Phase (Filament)	Dry%-(33, 65, 87)%	Hygroscopic strain
Balla et al. (2020) ^[267]	TPC resin & short soy bean fibers	N.A.	Layer	Ambient RH%-100%	Hygroscopic strain

The quantity of reinforcement used in hygromorphs affects the deformation capability of the materials used for 4D-printed hygromorph productions. In wood-reinforced PLA filament, material being used in FDA, the amount of fiber used has a strong influence on the actuation authority.^[265] A similar behavior has also been observed for soy bean fiber reinforced thermoplastic copolyesters.^[267] The larger the amount of reinforcement, the greater the hygroscopic strain. Ayrilmis et al.^[276] investigated the effect of the layer thickness on the thickness swelling in wood reinforced PLA. For those bio-based reinforced thermoplastics, the larger the thickness, the smaller the swelling of the material along the direction of the thickness. Moreover, measurements of the hygro-deformation need to be carried out in an appropriate medium. For instance, Loos et al.^[277] have characterized the absorption using an Archimedes-type of measurement in toluene. In a similar way to the mechanical properties, the assessment of the influence of the humidity on the CME is important to improve the reliability of design models for hygromorphs. The ASTM D1037 standard was adopted to measure the swelling rate of wood fire reinforced PLA filaments.^[278] Those properties are useful to predict the speed of actuation in related hygromorphs. Tables 12 and 13 show the presence of large uncertainties provided by the dif-

ferent measurement techniques associated to the hygro-expansion of the materials considered within the present review. The different results associated to the same parameters also highlights the strong need to define a standardization for those measurements, also to enable a more precise comparison. Such standardization should be performed for measurements at the different scales needed by the design and modeling techniques (layer and phase or filament scales). The shape and dimensions of the specimens also introduce further variability within the measurements. For instance, most studies consider squares specimens of material with parallel printing paths.^[8,58,87,278] Other studies however consider dog bone specimens,^[277,279] or the specific shape of the coupon for which the material is developed for [271]. Finally, a precise evaluation of the range of variation of humidity should be part of a standardization of the measurement techniques. The knowledge of this range of variations would enable a better comparison between datasets present in the open literature. More data are needed to perform the same level of comparison than the one conducted for the stiffness of the materials used in 3D printing. The standardization should be also specific for 3D-printed materials, as the printing path considered affects the expansion obtained along the different directions.^[87,260,280,281]

Table 13. List of hygro-expansion studies performed on materials with 4D-printed hygromorph potential. (Coefficient of Moisture Expansion: (CME)). Conditions to be in this Table: • 3D printed • material discussed in the present review as having 4D printing potential. Please note that some authors do not provide the RH the specimens are conditioned at. In such cases, a qualitative assessment of the conditioning is provided in the table ("Dry%" and "Ambient RH%" for oven dried and ambient relative humidity, respectively). (Following Table 12).

Reference	Material	Measurement	Scale	RH range	Properties
Vonk et al. (2020) ^[280]	Hydrogel filament	Full field topography	Phase (filament)	10%-90%	Hygroscopic strain
Faust et al. (2021) ^[281]	Nylon & short carbon fibers	Laser line probe	Phase (filament)	Dry%-52%	Hygroscopic strain
Hiendlmeier et al. (2022) ^[77]	Superabsorbent in-house resin	Mechanical swelling equilibrium	Layer	Dry%-100%	Hygroscopic Strain
Kreider et al. (2021) ^[279]	Polyamid & short carbon fibers	CT-scanner	Layer	Ambient RH%-100%	Volume change
Loos et al. (2021) ^[277]	Elastomer	Archimedes	Layer	Ambient RH%-100%	Volume change
Lv et al. (2018) ^[271]	Hydrogel	Fluorescent Microscope	Layer	Ambient RH%-100%	Swelling ratio
Yang et al. (2018) ^[278]	PLA resin & short cedar fibers	ASTM D1037	Layer	ASTM D1037	Thickness swelling rate

3.4. Porosity

3.4.1. Impact of Porosity on Actuation

Porosity (sometimes also called void amount^[282]) affects both the stiffness and the moisture absorption of polymers, therefore influencing the actuation of 4D-printed hygromorphs. For thermocompressed flax fiber reinforced polypropylene, Gager et al.^[283] have shown that the increase of the amount of porosity lowers the out-of-plane hygro-expansion. Youssef et al.^[284] looked at the impact of the volumes of the pores on the hygroscopicity of carbon fiber composites. The model created in that study showed that the larger the porosity, the smaller the actuation capability. Mehdikhani et al.^[282] provided an extensive review on the measurement of porosity in polymers and composite materials, as well as on the impact of porosity on the material properties. In addition, 3D printing itself also affects the porosity of the final product. As discussed by Al-Maharma et al.,^[285] additive manufacturing leads to three specific types of porosity: the one between the layers, and those generated by the surface and the sub-surface roughness. Al-Maharma et al. also present the impact of the different types of porosity on the properties of 3D-printed structures, depending on their shape and location. Spherical and irregular pores inside the structure are of interest for the stiffness control purpose. As natural fibers are extensively used as actuation triggers in FDA actuators (see Tables 1, 2, 3, 4, and 5), the specificity of their porosity compared to polymers and polymeric fiber composites must be further understood. The specificity of the natural fiber composite porosity measurement (in this case flax fibers) has been discussed in a past study.^[286] All the aspects highlighted above show the impact of the porosity on the actuation.

3.4.2. Control of Porosity

Porosity can be considered as a defect, but the adaptability of 3D printing also brings the possibility to engineer pores to control actuation. The tailoring of the amount of pores inside 4D-printed hygromorphs is key to obtain the required actuation. As described in the mechanical properties measurement section, pre-printing, as-printing, and post-printing phases of the conditioning are key to achieve a good control of porosity. To this purpose, a list of porosity controlling parameters relevant to the 3D-printed composites is provided in **Table 14**. For sake of repeatability, these parameters have to be specific to each polymeric moisture-actuated actuator proposed. In open literature, porosity sometimes refers to meso structure tailoring via control of the filament path (See Table 14, “Porosity controlling parameters:” • Filament path). This porosity should be distinguished from the micro scale porosity (i.e., fiber matrix interface porosity and resin pores) described, amongst others, by Chabaud et al.^[87] A fully compacted 3D-printed composite does not present voids between the deposited filaments. As the distance increases between parallel printing paths, the size of the inter bead increases. The distinction between inner and inter bead porosity is presented by Keleşet al.^[287] for short carbon fiber reinforced ABS composites. When two neighboring printed filaments are not in contact with each, other meso structure

Table 14. List of parameters used in the past to control the porosity. Conditions to be in this table: • 3D printed • actuators • RH-stimulated.

Reference	Material	Porosity controlling parameters
Le Duigou et al. (2021) ^[50]	PLA & Continuous flax fibers	• Layer thickness
Cheng et al. (2020) ^[54]	PLA & Short wood fibers	• Filament path
Kim et al. (2021) ^[79]	Elastomer	• Filament path
Kruger et al. (2021) ^[59]	PLA & Short wood fibers	• Filament path
Cheng et al. (2021) ^[57]	PLA & Short wood fibers	• Filament path
Kariz et al. (2018) ^[244]	PLA & Short wood fibers	• Amount of wood fibers
Zarna et al. (2022) ^[56]	PLA & Short wood fibers	• Stacking sequence • Shape of reinforcement

porosity, sometimes called infill percentage, is present. Outside the actuators research field, other parameters have been considered to control the amount of porosity in polymer and fiber reinforced polymers. Some of those parameters consist of the speed and acceleration for extrusion,^[256,257,288] the shape of the printing nozzle,^[256,289] the printing temperature,^[256,290] the layer thickness^[257] and the amount of fiber^[289,291].

4. Design

The term “design objective” presented in Figure 3, includes at a minimum, actuation as an objective. However, other objective functions can be added to the actuator (i.e., stiffness, strength, weight). In this section, models capable of accounting for these different objective functions are described. Optimizing strategies enabling precise and detailed design are then analyzed. Finally, obtaining the printing path from the model and the experimental deformation measurement are described in order to test/validate the models and optimization strategies defined. To date, there has been little investigation has been conducted on humidity-triggered actuation models. For most of the modeling strategies, the actuation trigger (i.e., temperature, relative humidity) has no impact on the deformation obtained. Hence, studies conducted with all types of actuation triggers are discussed below. Moreover, there is limited information in the literature on optimization approaches for 4D-printed structures. Consequently, stiffness optimization studies of 3D-printed structures are considered to bring perspective to the design strategies.

4.1. Model

The previous sections of the review have highlighted the need to know—at the minimum—the stiffness and the expansion coefficient of the materials making the hygromorph to model. The knowledge of the geometry and of the material distribution of the actuator are also mandatory to create the virtual structure used in the model. Finally, depending on the precision targeted by the model, additional information may be needed. For instance, the impact of the humidity on the material properties and the diffusivity of the humidity within the material itself are

Table 15. List of References related to models. The "Other analytical" methods include Classical Laminate Theory (CLT) and Energy-based methods. Conditions to be in the Table: • 3D printed • actuator.

	Timoshenko	Other analytical	FEA
Relative Humidity (RH)	Le Duigou et al. (2019), ^[8] Correa et al. (2015), ^[19] Naficy et al. (2017), ^[95] Le Duigou et al. (2021), ^[50] Li et al. (2019), ^[89] Le Duigou et al. (2016), ^[58] Kruger et al. (2021), ^[59] Baker et al. (2019), ^[69] Ryu et al. (2020), ^[78] Erb et al. (2013), ^[292] Langhansl et al. (2021), ^[64] Cheng et al. (2021), ^[293] Verpaalen et al. (2020), ^[294] Ozdemir et al. (2022), ^[295] Tomec et al. (2021), ^[67] Langhansl et al. (2021), ^[64] Bai et al. (2022), ^[80] Zarna et al. (2022) ^[56]	Gladman et al. (2016), ^[18] VanRees et al. (2018), ^[159] Raviv et al. (2014), ^[74] Zarna et al. (2022) ^[56]	Li et al. (2019), ^[89] Su et al. (2018), ^[71] Zhao et al. (2018), ^[76] Ren et al. (2021), ^[296] Ryu et al. (2020), ^[78] Turcaud et al. (2011), ^[173] Wang et al. (2020), ^[174] Bai et al. (2022), ^[80] de Kergariou et al. (2022) ^[51]
Other types of actuation trigger (i.e. Temperature, pH ...)	Zeng et al. (2019), ^[86] Boley et al. (2019), ^[99] Naficy et al. (2017), ^[95] Zeng et al. (2022), ^[103] van Manen et al. (2022), ^[137] Goo et al. (2020), ^[155] Guo et al. (2013) ^[297]	Yang et al. (2017), ^[7] Wang et al. (2018), ^[22] Hoa et al. (2019), ^[36] Boley et al. (2019), ^[99] Hoa et al. (2020), ^[119] Hoa et al. (2017), ^[121] Hoa et al. (2022), ^[122] Liu et al. (2022), ^[140] Zolfagharian et al. (2018), ^[141] Liu et al. (2020), ^[298] Connolly et al. (2017), ^[299] Wei et al. (2021), ^[300] Wang et al. (2021), ^[301] Song et al. (2021), ^[302] Agkathidis et al. (2022), ^[124] van Manen et al. (2022) ^[137]	Wang et al. (2018), ^[22] Zolfagharian et al. (2021), ^[48] Wang et al. (2021), ^[10] Li et al. (2022), ^[116] Liu et al. (2019), ^[109] Hoa et al. (2020), ^[120] Kokkinis et al. (2015), ^[130] Weng et al. (2021), ^[131] Hamel et al. (2019), ^[132] Yuan et al. (2021), ^[133] Westbrook et al. (2008), ^[134] van Manen et al. (2022), ^[137] Lee et al. (2020), ^[106] Yu et al. (2020), ^[98] Sun et al. (2022), ^[139] Jeong et al. (2019), ^[104] Huang et al. (2017), ^[142] Alshebly et al. (2021), ^[168] Goo et al. (2020), ^[155] Zhao et al. (2019), ^[146] Yu et al. (2022), ^[152] Turcaud et al. (2011), ^[173] Guo et al. (2013), ^[297] Wei et al. (2021), ^[300] Wang et al. (2021), ^[301] Jian et al. (2019), ^[303] Su et al. (2020), ^[304] Wu et al. (2020), ^[305] Wang et al. (2021), ^[306] Zou et al. (2022), ^[117] Feng et al. (2022), ^[156] Roach et al. (2022), ^[144] van Manen et al. (2021), ^[307] Safavi et al. (2022), ^[308] Koh et al. (2022), ^[102] Wang et al. (2022) ^[157]

critical to assess the dynamic and several static actuation capabilities. Finally, imaging techniques such as computed tomography imaging can provide a precise account of the geometry for ideal distributions of the materials and the porosity. The modeling techniques used in past studies to design actuators are presented in Table 15.

As described in Table 15, the Timoshenko model has been used extensively to estimate the final shapes of simple materials distributions structures when moisture-actuated. In some works, the format presented in Equation (1) was adapted to investigate the effect of the materials and geometry parameters on the actuation of the hygromorphs. For instance, Dinger et al.^[90] considered adding rheology parameters to Equation (1). Other research groups adapted the bilayer Timoshenko equation to multi-layered structures.^[309,310] Naficy et al.^[95] have adapted the Timoshenko equation to bilayer hydrogels by replacing the stiffness of the material with a power swelling function. Gladman et al.^[18] have discretized the use of the Timoshenko equation for structures composed of layers with varying angle orientations. The Timoshenko model therefore demonstrates a significant versatility to evaluate the influence of the materials or printing parameters on the actuation of the hygromorphs. Other analytical models have been used for 4D-printed actuators. For instance, Classical Laminate Theory (CLT) is considered for actuators made of highly aligned continuous fiber reinforced matrix composites (in the case of 4D printing, see the works of Refs. [36, 119, 122]; for not printed structures, see Refs. [311, 312]). CLT is also sometimes used to model short fiber composites.^[56] A modeling methodology

equivalent to CLT is proposed by van Rees et al.^[159] This technique differs from CLT because of the elastic energy-based actuation calculation. Here, a bilayer structure representing a biomimicking actuator was discretized via triangulations to account for the varying orientations of the angles of the fibers in the structure. The method is efficient in providing qualitative shape predictions, but lacks precision from a quantitative perspective due to the variability in cross-linking and fibril reinforcement orientations. Liu et al.^[298] also proposed an elastic energy-based model (combined with Hooke's law) to study the influence of the thickness ratio on the actuation of bilayer hyper-elastic structures. Based on the classification of the modeling techniques provided in Table 15, Figure 20 presents some general guidelines for the selection of the modeling strategy, depending on the type of material implemented. The Timoshenko model and CLT are limited to simple geometries and layer-scale models, but can also be used for rapid estimations of complex actuation deformations. Elastic energy-based methods can be adapted to more complex hygromorphs, as they also cater for phase models.

The Finite Element Analysis (FEA) is the most widely implemented technique for the modeling of the actuation. FEA consists in dividing a geometry into a mesh to approximate differential equations solutions from element to element. Figure 20 shows how FEA can be used for rapid estimations of the actuation in simple geometries.^[71,76] Finite element techniques constitute a step beyond in terms of fidelity and complexity of the structure to represent, compared to the Timoshenko and the CLT models because FEA can also take into account

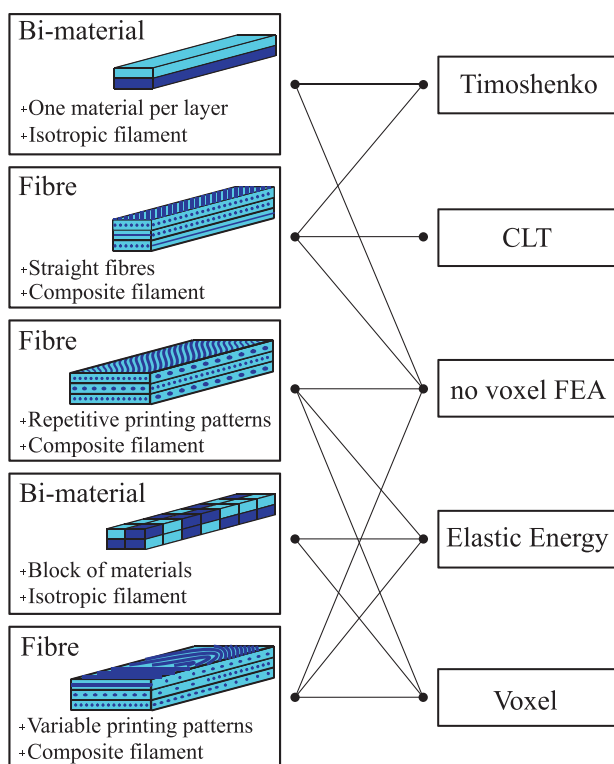


Figure 20. General guidelines for the selection of models related to the different types of 4D-printed hygromorphs. The term “voxel” also includes other modeling techniques, like local homogenized material in which the 2D or 3D structure to design is divided in discrete volume elements.

the presence of complex printed patterns.^[51,313,314] Furthermore, FEA techniques are versatile in terms of handling the materials constitutive laws and their distributions described in the present review. Modeling hyperelastic materials (elastomers, hydrogels, and gels) adds complexity to the design process, due to the large deformations involved. To circumvent this issue, enlarging the number of elements is strongly recommended.^[315] As shown in Figure 20, FEA are usually considered to model complex geometries,^[98] or when the printing path requires to take into account the model at a different scale than the layer one. For instance, studies investigating of the relationship between the material properties at the phase scale and actuation capabilities are lacking for fiber-based morphing structures. These types of studies could be performed using FEA models. Due to their versatility, FEA approaches are also the primary choice for design. A recent example of how FEA can be used to design actuators with accurate and rapid simulations is the isogeometry approach developed by Yu et al.^[152] This technique aims at mixing the benefit of graphical design and FEA tools by fitting the mesh efficiently on complex geometries. Yu et al. have associated this model with a random forest machine learning regressor for each vertex positioned on the grid structure initially designed. These types of neural networks have been used to predict the stresses induced along the beam of the mesh-like structure created to shape the required object (a lamp cover). To model similar mesh-like structures, Raviv et al.^[74] have proposed a spring-mass model particularly suitable to simulate the actuation and the kinematics of the

deformations, in which the shape of the actuation is controlled via stiffness or expansion of the mesh beams. A design strategy suitable to simple geometries is to restrict the number of patterns printable for generating the actuation. Then, the desired actuation is created out of these patterns. For instance, Zolfagharian et al.^[141] have created three different patterns serving as hinge folder. Bai et al.^[80] have measured the hygroscopic deformation of five different meso-scale patterns made of ABS (Acrylonitrile Butadiene Styrene) and nylon bi-layer beams. These patterns were then assembled to provide the required macro-scale deformation. If more printing patterns have to be envisaged, machine learning algorithms should then be considered. Those algorithms are described below in Section 4.2.

Voxel-based models consist in discretizing surfaces or a volume into regular elements, in order to assign discrete properties within the design space. These approaches are often implemented using FEA software. The voxel-based modeling technique is particularly relevant to 3D-printing technologies, as it enables the capturing of the local properties of the structure to measure its global behavior. Sossou et al. have proposed a five steps voxelization strategy, consisting in: the design of the geometry, its discretization, the implementation of the distribution of the material, the computation of the deformation and finally, the computation of the global deformation of the voxelized object.^[316] This open access tool created by Demoly’s research group considers the material distribution skeleton of the part, and then adds the voxel around the skeleton. Several examples of implementation of this tool combined with genetic algorithms have been described.^[96,178] The strategy defined here does not aim at replacing FEA, but rather, at providing a rapid insight into the potential actuation capabilities of multi-material 4D-printed structures. Due to issues still present in the software (i.e. collision, friction, gravity), more in-depth details about the actuation need to be obtained from Finite Elements analysis, if preliminary characterization is made via this technique. According to Momeni et al.,^[317] most actuating structures could be classified into three different categories based on the positioning of the materials patterns: uniform distribution, gradient distributions and distribution with special patterns. These material distributions can be discretized and turned into voxel-based models. Hence, most 4D printing designs can benefit from Sossou et al.’s proposed design strategy. Voxelization has also been implemented by Jian et al.^[303,318] to present self-foldable structures. In such models, different configurations of a given foldable structure are achievable through the use of shape memory polymers and hinges. Finally, de Kergariou et al. have proposed a finite element model in which each pixel of the .png images of the printing gcode was turned into an element with local material properties, orientation and fiber volume fraction.^[151] This technique has been implemented to predict the actuation of a leaf-inspired curling model.

Two other works have described the definition of modeling strategies that could not be classified in the categories presented in Figure 20. Choi et al.^[319] have created a modeling strategy specific to actuators and based on the use of empirical deformations to predict 4D-printed shape morphing. Such kinetic-based software can account for any material, as long as its deformation capability is precisely defined. Simplified models to design 4D printing configurations have also been explored in the past.

Table 16. List of references related to design algorithms implemented in 4D printing and hygromorphs. Conditions to be in this Table: • actuators • 3D printed.

Design algorithm	References
Genetic algorithm	Hamel et al. (2019), ^[132] Sun et al. (), ^[139] Liu et al. (2022), ^[140] Zolfagharian et al. (2020), ^[150] Zolfagharian et al. (2020), ^[167] Sossou et al. (2019), ^[178] Wei et al. (2021), ^[300] Wu et al. (2020), ^[305] Maute et al. (2015), ^[321] de Kergariou (2022) ^[51]
Neural network	Sun et al. (2022), ^[139] Yu et al. (2022), ^[152] Su et al. (2020), ^[304] Zhang et al. (2020), ^[322] Zolfagharian et al. (2021), ^[323] Elgeneidy et al. (2018) ^[324]

These patterns create different actuation amplitudes when printed on a substrate (here pre-strained polystyrene). The analytical and finite element temperature modeling conducted for these different patterns enable the experimenter to control how the part deforms by knowing how the temperature diffuses in the part. Even more simplification is brought by Kwok et al.,^[320] when they proposed a method of fitting a 4D-printed Kirigami structure onto a required shape. The algorithm consists in shaping a flat surface to the geometry required and adding cuts whenever necessary to avoid overlapping the surface and create the folding hinge. To do so, only one pattern of actuation was modeled, all the work needed to go from a local hinge structure to the full deformation is conducted by the optimizer.

4.2. Design Process

Yu et al.^[98] used the previously described models to refine by iteration the design of printed mesh-like structures. Design optimization algorithms are increasingly available and provide efficient tools to automate this process. The optimization strategies currently employed to design actuators are based on genetic algorithms and neural networks. A genetic algorithm is an iterative technique to explore the design space, building up from previous models to finally obtain a series of optimized parameters. A neural network is a classification method that maps complex relationships between inputs and outputs, which allows the user to find ideal inputs for the required out-

puts. **Table 16** shows how these two strategies for the optimization of actuators have been used in the open literature studies. Although optimization algorithms have been extensively implemented in the case of 3D-printed structures, their application to 4D-printed hygromorphs is currently quite limited. Therefore, the majority of the research works literature reviewed in this section is related to 3D-printed, or to not moisture-triggered 4D-printed demonstrators.

4.2.1. Genetic Algorithm

Figure 21 shows the general architecture of a genetic algorithm to design multi-material actuators. This figure also shows the schematics of an optimization of the actuation, based on the tailoring of the distribution of the materials. The first stage consists of creating a population of randomized material distributions. During the same stage, the actuation and all other properties considered in the multi-functional design guidelines (and described by the objective function(s)) are also measured. The following step involves calculating objective function(s) that include at least an actuated shape for every actuator, and then ranking the performance of the different actuators accordingly. Before launching the analysis, a convergence criterion for the objective function is defined. This criterion is checked at every step of the optimization; if it is satisfied, the optimization then ends and the best structural configurations of the print are recorded. Conversely, if the convergence criterion is not satisfied, the last stage then consists in creating a new population. The best actuators from the optimization function are placed in the new population. Actuators whose design parameters are mixed between the higher-end actuators of the previous generation are added to this population. The worst performing actuators are discarded and replaced by new randomly created actuators. This is a non-exhaustive description of the genetic algorithm process by any means; many more options can be added to tailor the convergence (i.e., mutation: random modification of the parameters). Most studies described herein use of material distributions to control the actuation. However, other parameters can also be used. For instance, Zolfagharian et al.^[150] have optimized the deformation of their printed

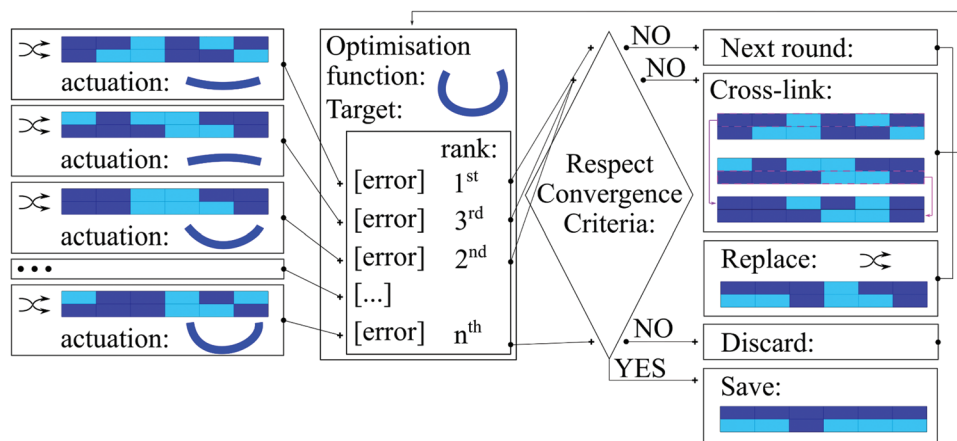


Figure 21. Genetic algorithm structure for bi-material actuators in four stages (from left to right).

Table 17. List of objective functions implemented for the 4D-printed actuation. (“Osmotic pressure” is a particular type of actuation not discussed in the present review based on the gradient evaporation of a solvent inside the printed material.). Conditions to be in this table: • 3D printed • actuator.

Reference	Model	Actuator	Function	Target	Other objective
Hamel et al. (2019) ^[132]	FEA	Multi-material	Displacement	Shape (cosine, sinusoidal)	Minimize active material
Sun et al. (2022) ^[139]	FEA	Multi-material	Position	Shape (periodic, butterfly-like)	No
Liu et al. (2022) ^[140]	Analytical	Multi-material	Folding angle	Scalar	No
Zolfagharian et al. (2020) ^[150]	FEA	Osmotic pressure	Deflection	Maximum	Volume fraction of material
Zolfagharian et al. (2020) ^[167]	FEA	Multi-material	Deflection	Maximum	Volume fraction between materials
Sossou et al. (2019) ^[178]	Voxel	Multi-material	Displacement	Shape (twist)	No
Wei et al. (2021) ^[300]	FEA	Multi-material	Displacement	Shape (parabolic, sinusoidal)	SIMP: density
Wu et al. (2020) ^[305]	FEA	Multi-material	Displacement	Shape (parabolic, cosine, circle)	No
Maute et al. (2015) ^[321]	FEA	Multi-material	Displacement	Shape (parabolic, cosine, twist)	Smooth of the surface
de Kergariou et al. (2022) ^[51]	FEA	Continuous fibers	Curvature	Shape (discontinuous target curvatures)	No

structures by varying the thickness along the actuator. Looking at Figure 4, before “Model optimization”, it is advised to “Determine the control parameters.” Each of these parameters is a dimension in the design space of the actuator. The use of genetic algorithms includes tweaking these parameters to guide the optimization towards the design optimum (local or global). The authors describe here two ways of obtaining restrictions of the design space to guide the optimization. The first one, called pre-optimizing restriction, consists in banning values of the control parameters before the optimization run. For instance, Wu et al.^[305] have calibrated the size of the voxel in the chess-board used for the optimization by looking at the influence of the parameters on the ease of print. Zhang et al.^[322] have forced the optimized actuator to be designed as symmetric. Zolfagharian et al.^[150] proposed a volume constraint approach to monitor the stiffness of the actuator. Another example is provided by Maute et al.,^[321] who have implemented a Level-set optimization to control the phase boundaries inside the geometry. This type of restriction of the design space should be as limited as possible, as the interaction between parameters is in general complex to understand ahead of the optimization run. Hence, over-limiting the design space has the potential to eliminate local optima, or even a global optimum. The second strategy, called optimizing restriction, consists of assigning penalties to actuators if they do not respect the design guidelines set before the optimization. An example of this strategy is the Solid Isotropic Material with Penalisation (SIMP) model^[325] that has been extensively applied within the few genetic algorithms used in 4D printing.^[150,167,300] It is critical to keep penalties and rewards relatively small in magnitude, to prevent an over con-

straint of the exploration of the design space.^[326] Even though penalties and rewards are simple ways of adding additional constraints to the model, they are known as being computationally fairly costly, and their use should be limited.^[327] Penalties are of prime interest when multiple objective functions are assigned to hygromorphs. In that context, a penalty is assigned for each function not satisfied by the actuator. A modified version of the genetic algorithm presented in Figure 21 is described by Zolfagharian et al.,^[167] as well as by Wei et al.^[300] In their studies, the authors have been looking at generating the largest possible deflection for the actuator. At each iteration of the optimization process, the sensitivity of the strain to the variation of the materials distribution was calculated. After filtering, those sensitivities triggered new material distributions evaluated for the next generation. Liu et al.^[140] have proposed a similar optimization process by using an analytical model, considered as more efficient than the FEA-based optimization.

The second parameter of importance for genetic algorithms is the objective function. Different types of function can be assigned for the optimization process of an actuator. For an actuator, the shape objective function aims at describing the physical state of actuation. Table 17 presents all the shape objective functions for the different genetic algorithms used in past studies for the design of 4D-printed actuators.

Table 17 shows that design optimization of actuators has been mainly conducted on multi-material structures with FEA or FEA-like models (i.e., voxel-based models). The different parameters used to define the shape objective functions are presented in Figure 22. They are classified into two categories, the global and the local shape objective function. In the former,

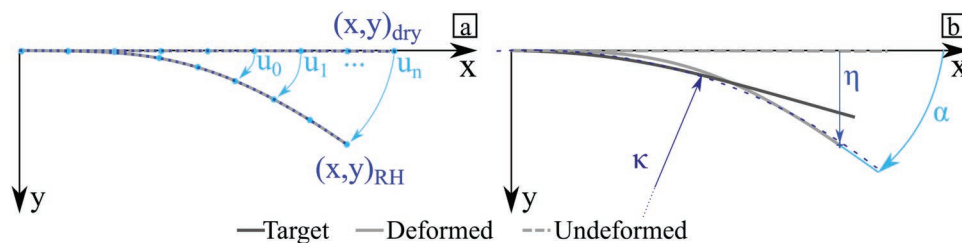


Figure 22. Shape objective function parameters: a) Local objective function with u_i : Displacement or (x,y) : Position. b) Global objective function with α : Bending angle or η : Deflection or κ : Curvature.

the local aspect of the actuator is compared to the target shape. In the latter, a global parameter is used to encompass the global shape of the structure and this unique scalar is compared to the target shape. For the local parameters, the difference between position and displacement is that displacement considers the history of the motion of the points considered for the objective function whereas the position, only accounts for the final state of the deformed structure. For the global parameters, the curvature and bending angle are equivalent and provide additional information when compared to the deflection. They account for the entire shape of the actuator, whereas the deflection only accounts for the position of the tip of the actuator and is independent of the shape of the structure. As presented in Table 17, local objective functions require a shape to be considered as output whereas the global ones require either a scalar (e.g., curvature, bending angle, and twisting angle) or a direction (maximum, minimum) to be assigned. For instance, Sun et al. used a cosine ratio of position to create a fitness function capable of converging towards the sinusoidal profile required.^[139] When choosing the objective function for the deformation of the actuator the experimental test must be considered. Liu et al.,^[140] Zolfagharian et al.^[150,167] and Sun et al.^[139] considered the comparison between the optimized geometry and the experimental work with the same parameters as those used in the objective function, respectively, folding angle, deflection and position. From the easiest to the most complex to measure experimentally the parameters are: deflection (one geometrically unique point to position at the final stage of deformation), folding angle and curvature (obtained with geometric construction on the actuator final deformation stage), position (easy to track point position on a model but on an experimental structure extra equipment is required, video gauge or digital image correlation to track the points during deformation) and displacement (compared to the position extra calculation is needed to determine the path taken by points when they move.). Greater discussion about the selection of the deformation measuring technique is proposed in Section 5. To the authors' knowledge, only 2D deformations have up-to-date assessment. However, the conclusions drawn from the 2D systems could be extended to 3D problems.

Finally, additional objectives can be added to the convergence function. An example of a multi-parameter convergence function to design a structure was demonstrated by Hamel et al.^[132] Here, they attempted to minimize the amount of active material in the thermo-sensitive actuator, while limiting the gap between the displacement of points along the structure for the target and the population deformed geometry. Adding targets in the objective function tends to lower the speed of convergence of the function, but can allow the development of multi-functional composite actuators.

Multi-material optimization has been extensively discussed above. However, to observe optimization for fiber reinforced composites, it is necessary to consider 3D-printed compliance and geometric optimization (Table 17 shows that no fiber reinforced actuators had their design optimized in past studies). In addition to material distribution, fiber composites require fiber orientation to be defined. The geometry to be optimized is divided into squares (2D) or cubes (3D) and the orientation of the fiber can be defined via analytical calculation, for instance,

principal stresses.^[328] Then a genetic algorithm can be conducted to position the fiber along the streamlines (representing the local fiber orientation) previously defined.^[329,330] Otherwise, a fiber path can be proposed, for example, inspired by actuation observable in nature,^[63] and then through sensitivity calculation this path could be improved via several iterations to achieve the required deformation. For the most common type of optimization model, voxel-based FEA, the number of values of the optimized parameter is increased compared to multi-material structure. Each voxel or element must have material properties and a material orientation, both chosen in continuous intervals, assigned to it. Several research groups created optimization process for short fiber composites.^[331–334] Chandraskhar et al.^[332] used the widely implemented SIMP to adjust the local infill of the part designed. The thermal compliance optimization is conducted on the same geometry to define the local short fiber orientation. To avoid extremely erratic printing paths, local filters can be applied to average the orientation of the fiber.^[334] 3D optimization was conducted by Kubalak et al.^[331] using a quaternion-based continuous fiber angle optimization. Among continuous fiber hygromorphs two categories can be distinguished. On the one hand, a continuous filament could be cut using a Markforged Mark 2 printer.^[329,335] On the other hand, such filament cannot be cut when used for pultrusion in a modified Prusa or Tevo for example.^[165,203] Either way, the optimization of continuous filament structure is more complex. Blom et al.^[336] conducted a maximum thickness and smoothness optimization for overlapping tow placement. The difficulty in continuous fiber optimization is obtaining continuity in the filament, hence, little variation between neighbouring streamlines. To achieve this, Blom et al. provided the general shape of the tow placement via orientation functions. These functions have their variable optimized for maximum thickness and smoothness, leading to new streamlines, therefore, new orientation for the tow placement. A similar optimization method was considered by Brampton et al.^[337] to optimize compliance of an automated fiber placement fabricated structure. To achieve this, the researchers defined an initial fiber path to be discretized so as to measure the element fiber orientation in the structure. In this way, the sensitivity of the compliance matrix to modification of the local fiber orientation is measured. The fiber path is updated thanks to a Hamilton Jacobi formulation, which takes into account the sensitivity previously measured and the calculation of a continuity score. Several runs of this process are then conducted until the compliance required is achieved. Boddeti et al.^[314] built up on this optimization technique by adding density requirements for the structure and allowing the optimizing method to remove parts of the initial block of the design material. The optimization they proposed is conducted at different scales via the Mori-Tanaka homogenization method to obtain the properties of the element position in the optimization from the material properties set up as inputs (the fiber orientation and the fiber volume fraction depending on the position over the optimized geometry). Papapetrou et al.^[338] added strategies to the model proposed by Brampton et al. to automatically define the fiber path proposed for optimization by imposing an offset from the boundaries of the solid domain. A set of parallel and distanced lines with an offset is then created until two lines intersect or

one line reaches an opposite boundary. These lines could potentially be divided manually to fit geometries more efficiently. The Equally-Space method proposed in this same study goes a step further by setting up the filament path on the most constrained part of the geometry to obtain smooth fiber paths. Li et al.^[339] present a design strategy closer to the one used for multi-material optimization. In this approach the optimization is obtained via filling of a chessboard pattern with a distribution of two isotropic materials, one for the fiber and one for the matrix. The continuity of the fiber is achieved by forcing the local proportion of fibers. Instead of considering two isotropic materials, a similar optimization method can be conducted with homogenized composite blocks distribution.^[340] For instance, Kim et al.^[340] obtained the homogenized properties for three different fiber lay-outs and used these properties to distribute the fiber across their compliance optimized structure. Yang et al.^[341] begin the compliance optimization of their printing path with a definition of density and orientation for each element based on the directions of the principal stresses. The optimization then implies the use of monoblocks, as blocks of elements whose orientation is within a range of 45° compared to the neighbouring blocks. This necessarily leads to overlaps in the monoblocks defined. The different layers in the structure would serve to prioritize one or others blocks at the location of the overlap. The monoblocks are then mostly printed one by one. Similarly to Wang et al.,^[342] to the authors, knowledge, the way the printing monoblocks are connected is not specified. Works have been also published about techniques to join continuous fiber 3D-printed parts by avoiding any cut in the filament. For instance, Huang et al.^[343] propose a discrete finite element compliance optimization technique, in which each element is assigned a set of density and orientation values. The geometry obtained is then divided into monoblocks according to macro-scale features of the part. Inside these blocks, continuity of the orientation is ensured by setting the orientation of the elements as equal or close to the surrounding elements. The monoblocks are modeled as nodes to solve the printing path definition problem as a NP-complete problem. A Hamilton path is then used to find a solution to this problem by avoiding overlaps and voids. Finally, the frame of the printing path defined is then adjusted to make the structure printable. Therefore, adjustments are provided to the distance between printed filaments and to the angle definition. de Kergariou et al.^[51] propose a design optimization technique providing less freedom in terms of definition of the printing path compared to the strategies previously commented. In their model, de Kergariou et al. define a printing path before running the optimization. The printing path is then parameterized to define the boundaries of the design space for the optimization. A .png image of the gcode is then turned into a FE model, with each pixel of the model becoming an element. Each element is given a set of density and fiber volume fraction depending on the grayscale of the corresponding pixel in the .png image. Each element also receives an orientation via the calculation of an Hessian matrix. In [51], two examples of models were run, one related to a leaf-inspired hygromorph, and another linked to a cross-ply hygromorph with varying distances between fibers. A fiber path optimization is then performed via evolutionary algorithm on the parameters defining the gcode. There are few lessons learnt for

fiber composite actuator optimization from the discussion about mostly mechanical optimization discussed here. Accordingly, adapting these optimization methods to actuation could be conducted in different ways. The first one is to determine a set of analytical equations capable of linking the local orientation of fiber to the final actuation. This would help define the streamlines that could serve as a basis to position either short or continuous fibers. The second strategy consists of implementing an evolutionary algorithm, in which the main difference will be the actuation function. Here, the actuation functions defined for multi-material optimization presented in Table 17 could have their use extended to both continuous and discontinuous fiber composites.

Although conducted on shape memory 4D-printed actuator, the design strategy proposed by Paz et al.^[344] is of great interest, as it employs a genetic algorithm to optimize two different geometries at the same time. These geometries corresponding to the two deformed configurations of the actuator. Using this approach, Paz et al.^[345] combined a neural network and a genetic algorithm to converge toward the desired deflection solutions. The optimization, in this case, is not conducted on the actuation itself but on the characteristics of the two deformed shapes: weight and manufacturing cost. The actuation is implemented in the code as a constraint penalising the solution which do not present the required shape. A preliminary step of selection of design called “Design of Experiments” is conducted to gather information about the model. Similar to what the same research group conducted in the past for stiffness optimization, extreme values of variables and Latin Hypercube selected variables are tested through the genetic algorithm. This algorithm drives the Kriging prediction methods to approximate the optimal answer. In the optimization stage a group of designs is selected with a fairly lenient convergence criterion. Finally, the last stage consists in running the same genetic algorithm combined with Kriging method on the population defined in the previous step but without penalty and only selecting one optimized design. Sun et al.^[139] combined an evolutionary algorithm and a Voxel FEA to create bi-material high aspect ratio structures. They compared the computational cost between the same optimization conducted from the Recurrent Neural Network (RNN) and from an evolutionary algorithm. The recurrent neural network is several orders of magnitude quicker, when not considering the time needed to create and train the models.

4.2.2. Neural Networks

The neural network modeling technique is a data-driven optimization techniques (with among others, Regression Analysis^[346]), which could be used to classify hygromorphs or predict actuation depending on printing parameters.^[324] Among the not neural network data driven techniques available, k-nearest neighbour (principle explained in **Figure 23**) was described as inefficient with little training data to account for material distribution in multiple material actuators.^[322]

Linear regression algorithms have also been implemented by Zhang et al.^[322] They were shown to reduce average validation loss compared to the k-nearest neighbor algorithm. However,

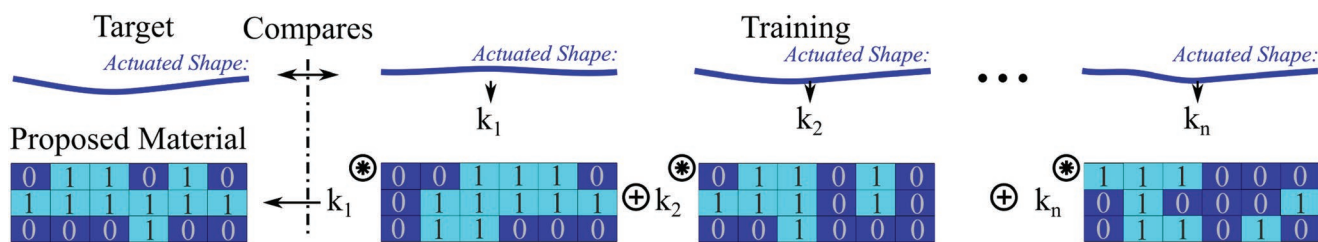


Figure 23. Structure of k -nearest neighbor algorithm applied to a bi-material example. The target shape is compared to every training shape. This allows obtaining a coefficient (k_i) as high as the difference between the two actuated shapes is high. Then the coefficients are used as a multiplier to the actuators parameters (distribution of material) to “rank” the importance of the training data.

they were described as far worst predictors than the neural network algorithm (Convolutional Neural Network (CNN) in this study).^[322] Artificial neural networks are also described by Zolfagharian et al.^[323] as more suited to solve a non-linear problem than regression and analytical models. Consequently, from here, only neural networks are discussed in this review. For 4D-printed structures, neural network algorithms map the influence between the input parameters highlighted in the previous sections (i.e., material distribution, geometry, and fiber orientation) and the actuation of the structure (bend angle, curvature, position, and displacement). The neural network algorithm could be applied to experimental data^[304,346] or to numerical models.^[139,322,323] However, if model-based optimization is to be implemented, the model efficiency must be pre-emptively assessed. For instance, the optimization of a 4D-printed pneumatic actuator has been realized by Zolfagharian et al.^[323] via an artificial neural network trained with FEA models.^[347] Before launching the analysis, this research group tested several FEA

configurations and compared them to the specimens printed. Different types of neural networks have been used in past studies to optimize hygromorph actuation. The two primary examples, RNN and CNN, are presented in **Figure 24**. CNN learns the link between patterns of material distribution and the obtained deformation in all the members of the training population by applying different filters. Each filter is associated with a weight (a number, presented in the grids at the bottom of the figure) representing what the algorithm has learnt. These weights are then called when the validation population asks for a deformation similar to one obtained with a pattern observed in the training. RNNs set up a random box of coefficients that links the material used to the deformation obtained. The box of coefficients is adjusted with the error between the deformation of the training material and the deformation obtained with the box of coefficients. On the one hand, RNNs are efficient in considering past trials to converge to the required solution. On the other hand, CNN is capable of detecting patterns and their

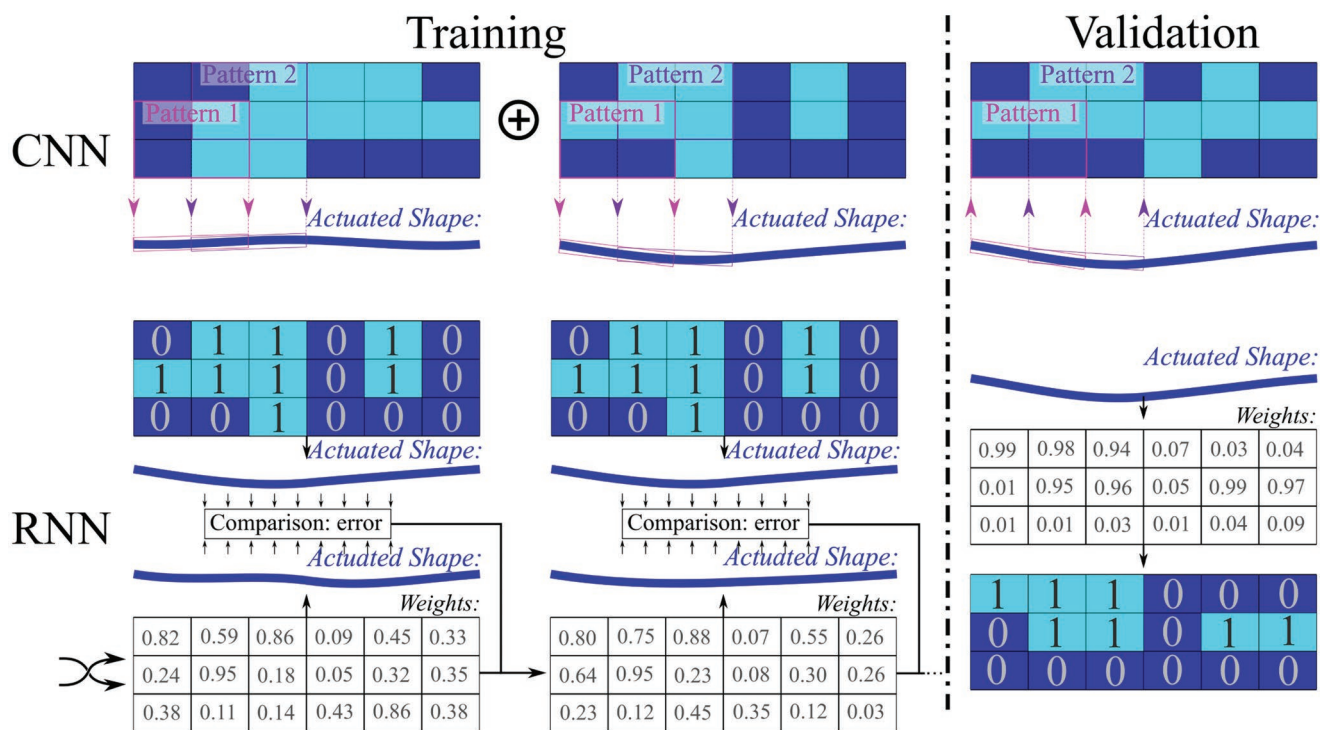


Figure 24. The structures of CNN and RNN applied to a bi-material shape changing actuator.

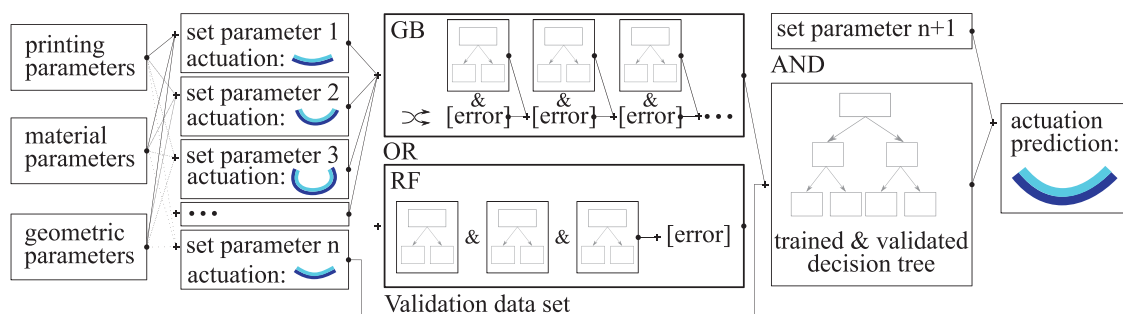


Figure 25. Structure of random forest and gradient boosting algorithms.

influence on the resulting deformations. Such an algorithm uses the different patterns analysed to propose a general distribution of materials in the structure. The comparison of these two neural networks conducted by Sun et al.^[139] showed that the even though CNN showed accurate prediction (coefficient of determination: $R^2 \approx 0.9$), RNN performed better (coefficient of determination: $R^2 > 0.999$). Zhang et al.^[322] found CNN as the best for the accuracy. In the context of humidity-stimulated structures, neural networks can be implemented in the same way described for empirical training and validation data of temperature actuated structures presented here. However, for materials with low coefficients of moisture diffusivity, the deformation of the hygromorph has to be recorded along with the Moisture Content (MC) inside the specimen. The relative humidity record is not sufficient as the diffusion of humidity from the air to the material tested can be slow. Data augmentation algorithms can be implemented to have more training and validation data.

By mapping the influence of inputs on outputs, neural networks are capable of ranking the influence of each parameter on the actuation. Random forest and gradient boosting algorithms were implemented by Su et al.^[304] to work out such influence, (the principle behind these two algorithms is presented in **Figure 25**). Both algorithms start the same way in that they need numerous sets of parameters and the corresponding actuation value as input. This list of parameter sets and the corresponding actuation is divided into training and validation data sets. The training data set is then used in different manners depending on the machine learning algorithm implemented. On the one hand, Gradient Boosting consists in creating a random list of errors. Comparing these errors and a decision tree fitted to the training data set leads to an updated error. This is repeated as many times as set up by the experimenter. On the other hand, if the training data is used in a random forest algorithm, then a large number of decision trees are fitted to the training data in parallel. The results of these trees are then averaged out to obtain a fitting decision tree and the error resulting from it. The trees created must then be validated with the validation data set saved for this occasion. If the validation is satisfying, then it could be used to make predictions. Processing, structural and conditioning parameters were ranked in this study in terms of relative importance. From a design perspective, it is needed in order to select the most appropriate parameters of control and the quickest way to define printing parameters. The gradient boosting algorithm was highlighted as the most accu-

rate way to predict the actuation. When basing the machine learning algorithm on experimental data, obtaining experimental data is in some complex cases. Su et al.^[304] have proposed a Gaussian-based data augmentation technique to create additional training sets of data. Finally, this research group also proposed a deformation forecasting technique based on three different algorithms: exponential smoothing, long short term memory and echo state network. Depending on the material, the geometry involved and the conditioning environment, the experiment conducted to observe deformation can run over several weeks or months (i.e., thick actuator, certain polymers, out of water conditioning). In that case, using an algorithm to predict its final deformation could be of great use in design.

Neural network and topological optimization were combined to optimize the bulk and shear modulus as well as the Poisson's ratio of metamaterials.^[348] The design space was made as large as possible initially by randomly selecting parameters describing the representative unit cell serving as input in the topological optimization. The optimization run gave a set of input properties leading to a maximized modulus and a minimized Poisson's ratio. Then these data were restructured to obtain an image for a set of input parameters for the training of the CNN. The model was described as robust with respect to accuracy and time even when the CNN was run on low-performance computers. A similar conclusion was drawn by Sosnovik et al.,^[349] who prematurely ended a topological optimization to let a CNN finalize the optimization job in order to accelerate the convergence. This technique has to the authors' knowledge not been adapted for actuators as yet. Other optimization techniques, like ant colony optimizer,^[350] are also available to researchers, but have not been implemented yet for 4D printing applications. The authors prefer not to give any guidelines for the selection of the optimization techniques as the techniques presented here are quite general and could be adapted to most structures. Finally, recently Akbar et al.^[13] implemented gradient boosting and random forest regression algorithm to predict the deformation of glued (not 3D-printed) bilayer wood (not composite) hygromorphs. In this study, the surface of the wood pieces assembled to form the hygromorph are scanned. From these scans, the wood grain orientations are obtained. In parallel the curvature deformation of the hygromorph is measured while the specimen deforms from 26% to 95% RH. The grain orientation and the curvature values are used as training data for the model. For the structures considered in the present review, a similar methodology could be applied by replacing the

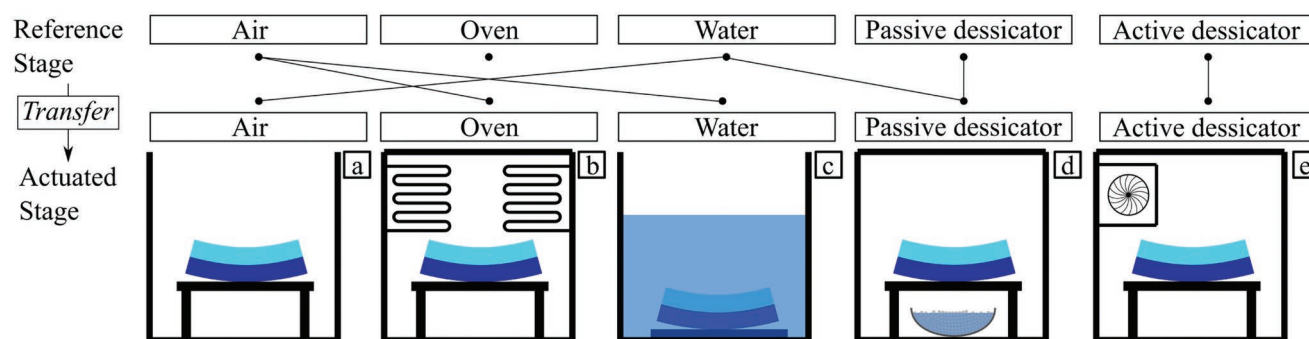


Figure 26. Different conditioning systems described in past published studies: a) Air Conditioning with a Relative Humidity (RH) \approx 50%. b) Oven drying with RH \approx 0% (vacuum drying can be used in the oven). c) Water immersed with Relative Humidity 100%. d) Passive desiccator with RH created by water saturated with salts or driers. RH available: RH corresponding to the salts available (i.e., 11% RH with Potassium Hydroxide). e) Active desiccator. Continuous range of humidity depending on the specification of the part.

grain orientation by the fiber orientations of each 3D-printed layer. One potential axis of development for the use of neural networks in the field of 4D printing consists in using them for more complex actuation types such as twisting or combination of twisting and bending deformations. They also present the potential to be used to program the deformed shape of more complex structures, such as mesh structure.^[27,74]

4.3. Optimized Geometry to Printing Parameters

The derivation of the printing parameters from optimized geometry of bi-material structures is mostly a straightforward process, because one can use conventional slicers and CAD models (i.e., Ultimaker Cura, Slic3r, PrusaSlicer). For instance, the g-code of voxel-based models obtained with Rhinoceros3D^[54,96,124,316] can be obtained from the “voxel2G-code” github library.^[54] Fernandez et al.^[351] proposed an optimization technique to minimize the printing costs. The resin sometimes used to develop multi-materials configurations can lead to the presence of anisotropic properties within the printed filaments (e.i., PLA or ABS based-filament^[352]). The filling patterns of the printed block of materials printed must be therefore carefully chosen. Multi-materials structures can be obtained by stacking different materials with the same printer on top of each other.^[167] The multi-materials configurations can be also printed with one ink, and then by varying the post-processing of the single material phase.^[139] Finally, the different materials can be printed separately and assembled after printing.^[96] The latter study describes an initial distribution of materials, then an iterative procedure is put in place to modify the distribution until the structure could be assembled. The difference in actuation (i.e., displacement) obtained before and after the modification is calculated, to make sure a target range of actuation is achieved. This fabrication technique is useful when the materials used cannot be printed from the same machine.

Conventional slicers can also serve to print the short fiber-based composite actuators presented in Figure 20. Specific slicers have to be used for slightly more complex material to print, for instance, continuous fiber composites. For instance, Chabaud et al.^[8] printed U-shape actuators made of contin-

uous carbon fiber reinforced polyamide 6 composites with the Markforged slicer Eiger.io, specific to the printer. Complex filament paths (i.e., the repetitive and variable printing patterns shown in Figure 20) require extra steps and processing from the model to the additive manufacturing phase, as the conventional slicers cannot achieve the desired path. A user defined algorithm can be created to link the streamlines of the materials orientations in the model to the gcode. For short fibers, the problem was partially solved by van Rees et al.^[159]. This research group discretized the model to anticipate the actuation of the hygromorph. From this discretization via triangulation, the density of the required material was obtained by looking at the distances between the neighboring orientation vectors. The orientation of the printing path was then obtained via smoothing of the same orientation vectors. In stiffness optimization applications, Kubalak et al.^[353] developed a methodology to turn the streamlines into a printable path for multi-axis printing. Several research groups have created algorithms capable of turning continuous fibers orientation streamlines into cut continuous fiber printing paths.^[314,336–339] Such a technique has been adapted for continuous fiber composites with uncut filament by Wang et al.^[342] The authors partitioned the geometry with Voronoi diagrams to obtain at the interface of the Voronoi region a “medial axis” serving as a basis for the fiber path. Each point of the fiber path was then updated, so that its orientation was as close as possible to the nearest orientation of the stress streamlines. Each section of the geometry ended up being filled with almost parallel continuous fibers. These segments of the fibers were finally joined together to avoid any cuts during the additive fabrication. Wang et al.^[342] did not specify however how these segments were joined.

5. Measurement of the Deformation

To validate the models considered for the design of hygromorphs, the deformation of the 3D-printed specimens must be measured. Fives main techniques of conditioning are presented in Figure 26. Their implementation in past published studies is presented in Table 18. Here are the main criteria considered to select the conditioning technique, depending on the final application for the structure:

Table 18. Distribution of the different systems of conditioning used in the open literature. The column represents the actuated stage and the row represents the reference stage. Conditions to be in this table: • 3D printed • actuator • RH-stimulated. (⊗: Impossible).

	Air	Oven	Water	Passive desiccator	Active desiccator
Air	⊗	[70]	[18,54,56,60–63,69,72–76,79]	[64–67,80]	N.A.
Oven	N.A.	⊗	[77]	N.A.	N.A.
Water	[50,53,55,58]	N.A.	⊗	[52]	N.A.
Passive desiccator	N.A.	N.A.	N.A.	[8,51]	N.A.
Active desiccator	N.A.	N.A.	N.A.	N.A.	[53,54,57,59]

- Range of humidity.
- History of humidity.
- Access to the specimen for the measurement of the deformation.

Figure 26 shows the presence of two stages during the conditioning for measuring the actuation (reference and actuated stages). The change of humidity between these two stages gives the RH range used to measure the actuation. The change could be an increase (i.e., Oven⇒Water) or a decrease (i.e., Water⇒Passive desiccator). The reference stage consists in stabilizing the humidity content of the actuator at a specific RH value at which the measure of the actuation will start. The actuated stage is related to the conditioning at which the actuation will end. The reference stage can be obtained by drying the specimen in the oven, immersing it in water, or placing it in a desiccator at a given RH. Then the specimen is transferred to one of the conditioning environments presented in the actuated stage. The authors also emphasize the importance of carefully conducting the transfer from the reference to the actuated stages, as that could lead to detrimental effects on the actuation measured. The figure shows the transfers from reference to actuated stage implemented in past studies, but any other combination is possible as long as the relative humidity changes. Table 18 shows that the most widely used actuation with RH variation is the air, as reference stage, to water immersion, as actuated stage. It is implemented to qualitatively assess actuation capabilities of a material as it induces a large and quick actuation. On the other hand, water to air desorption is used for a quantitative evaluation of the actuation, because it enables a precise tracking of the deformation. Active desiccators have been used for cyclic conditioning of the specimens (e.g., for testing the actuation reversibility). The reference stage of the actuation considered in this section is a permanent stage of deformation. Reaching this permanent stage must be performed with as little as possible impact on the structural integrity of the actuator. For this reason, gentle conditioning techniques must be implemented. For instance, de Kergariou et al.^[165] conditioned continuous flax fiber reinforced PLA composites at a lower temperature than suggested by the standard, to avoid post-printing re-crystallization of the resin. Another example of gentle conditioning is the one proposed by Hiendlmeier et al.^[77], who dried their super absorbent resin in vacuum.

After or while being conditioned, the actuation must be measured. As described in Section 4.2, five different parameters can be tracked to assess the deformation of the structure: the deflection, the curvature, the bending angle, the position and the displacement. The applications of hygromorphs require

the monitoring of the evolution of at least one of these parameters. The techniques described in the open literature to conduct the measurements are partitioned into three groups presented in Table 19. Each group is referred to the parameters it can measure. The simplest, yet rarely used one consists of taking the specimens out of their conditioning medium and measuring manually their curvatures by plotting their imprint shape on a piece of paper. For instance, this technique was employed by Popineau et al.^[12] A slightly different measuring technique consists in printing a curvature jig (scale) consisting in a long bar with known varying curvature.^[66] The curvature of the specimens is then compared against the reference curvature on the jig. These techniques are well suited for stiff hygromorphs because any soft specimen would be permanently deformed during the operation. These techniques are also adequate for immersed actuators, as the optical methodologies proposed later on tend to feature images diffracted by the water. Another technique, named measure on photos, consists in taking images of the specimens while deforming and measuring the curvature,^[8,18,56,58,59,79,81,108,119,130,133] the twisting angle,^[81,119,354] the bending angle,^[48,62,74] the deflection^[64,67,150,167,323] and the position^[139] representative of the deformation. The post-processing of these images is usually conducted by using commercial codes, such as Fiji. These techniques are easy to implement, if only the permanent state of deformation is of

Table 19. Advantages, issues and list of parameters measurable by using the different actuation measurement techniques.

	Advantages	Issues	Parameters (Figure 22)
Physical	No image bias	Not automatic	Curvature (2D)
	Cheap	Open the chamber	Bend angle (2D)
	Quick to set up	Can deform specimens	Twist angle (2D)
	Adaptable	Very limited geometries	Deflection (2D)
	Run tests in parallel		Displacement (2D)
Measure on photo	Use any chamber		
	Not opening chamber	Image bias	Curvature (2D)
	Cheap	Lot of equipment needed	Bend angle (2D)
	Can be automatic	Constraining chamber choice	Twist angle (2D)
Pol tracking		Limited geometries	Deflection (2D)
	All geometries	Image bias	Position (2D)
	Not opening chamber	Lot of equipment needed	Displacement (2D)
	Automatic	Expensive	Curvature (2D & 3D)
	Full field of deformation (DIC not VG)	Constraining chamber choice	Bend angle (2D & 3D)
			Twist angle (2D & 3D)
			Deflection (2D & 3D)
			Position (2D & 3D)
			Displacement (2D & 3D)

interest to the researcher. Parlevliet et al. simplified the determination of the curvature from side images of the specimen by implementing Equation 3.^[355] In (3), L is the chord length of the specimen and h is the deflection at the centre of the specimen itself. The equation has also been implemented by Zarna et al. for 4D-printed wood reinforced PLA hygromorphs.^[56]

$$\kappa = \frac{8h}{L^2 + 4h^2} \quad (3)$$

The final set of techniques, called by the authors PoI (Point Of Interest) tracking, only differ from the previous ones by the type of post-processing. Video Gage (VG) and Digital Image Correlation (DIC) can track the position of PoIs on 2D or 3D images. These techniques record images at regular intervals, with the tracker points positioned on the specimens are automatically detected by the post-processing software. This enables to position as many points in space as desired and to obtain the displacement or curvature needed for the comparison with the models. VG consists in a discontinuous measurement. Specific patterns are positioned locally over the structure and the positions of these patterns are obtained independently from each other. On the other hand, DIC tracks the deformation continuously over a surface that has been painted with speckled black on white background. Bai et al.^[80] use DIC to track deformation of a grid-like structure and calculate the global deformation (curvature, gradient angle, shear angle). An example of VG measurement for immersed hydrogel silicone actuating structures is given by Pfeil et al.^[356] In this study, the pattern used for discontinuous position tracking is a square of a speckled black paint on white background, which is characteristic of DIC measurements. A summary of the pros and cons associated to each technique is presented in Table 19. Image biases include perspective and light issues. The price of the experiment is of prime interest, as the deformation can take up to several weeks to deform, depending on the material, geometry and the conditions. For long experiments, making the recording of deformation is a significant advantage. “Not opening the test chamber” is a key aspect, as any opening of the chamber modifies the RH inside the test room. PoI tracking is extremely adaptable and can be used for “every geometry” and parameters to measure. Finally, optical measurements (Photo or PoI) include a “closed controlled chamber”, as it needs to be transparent to record from the outside.

Other methods can also be adapted to humidity-immersed actuating structures. Laser measurement was implemented by Hoa et al.^[120,122] However, to the authors’ knowledge, this technique has only been considered for actuation occurring at room temperature and humidity. 3D scanning techniques have also been used for 3D-printed structures, but have not been developed for 4D printing yet. For instance, design^[39] and biomedical^[357,358] based applications use scanners to obtain an image of one’s body part and consequently 3D print a highly personalized component. Some of the actuation tests conducted would benefit from having regular 3D scans of the actuated part, to obtain the full field of deformation of the part itself. 3D scanning techniques have been used for instance by Blonder et al.^[359] to measure the curvature on not-3D-printed actuators similar to the ones described in the present review. Only Vazquez et al.^[65]

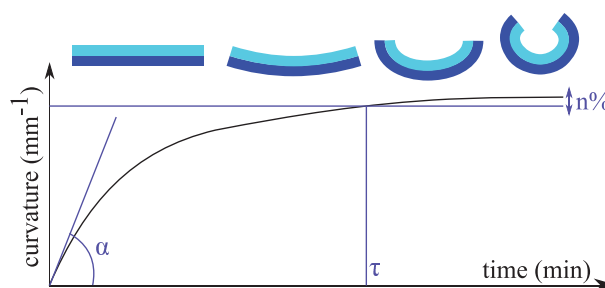


Figure 27. Definition of the actuation speed. α : derivative of the curvature, which can be calculated at any stage of the actuation, but usually considered at the beginning. τ : Actuating time: time to reach the final stage of the actuation. A percentage of the interval of curvature is usually defined as the criteria to identify the actuating time.

used 3D scanner for 4D printing actuation measurements. Unfortunately, only qualitative assessment of the deformation of the related Kirigami structure was performed.

All these techniques can be used to measure the speed of the deformation by deriving the actuation versus time.^[8,50,58,67] The speed is called responsiveness and can correspond to different either qualitative or quantitative parameters. The quantitative parameters are described in Figure 27.

Tables 20 and 21 present the conclusion drawn about the actuation speed of the 4D-printed composite hygromorphs. On the one hand, the derivative of the curvature has been used to observe the influence of the different parameters on the actuation speed.^[50,58] However, the initial derivative of the curvature cannot be used to control the sequential actuation as a varying α does not necessarily means the permanent stage of actuation will be reached at different stage. Consequently, Zhao et al.^[76] and Tahouni et al.^[55] show that designing sequential actuation require the speed of actuation to be tested with actuation time. In these studies the impact of parameters on the actuation speed via measurement of the actuation time is assessed. As can be observed in Tables 20 and 21, a limited number of parameters have been tested for their influence on the actuation speed of a limited number of materials.

6. Concluding Remarks and Outlook

This opinion paper aims to provide review and design guidelines for 4D-printed composite materials stimulated by moisture. In this comprehensive analysis of the specific research domain, the following observations and conclusions can be drawn:

- A full design process has been generalized, from design concepts to the additive manufacturing and measure of the actuation. Other phases of the design process include the selection of materials and parameters to control, modeling and optimization.
- Actuation reversibility tests conducted in past studies have been analysed and discussed in a critical manner to further the understanding of the potential for reversibility shown by the test cases considered. Up to now, 4D-printed hygromorphs are mostly produced by using natural fiber-based

Table 20. Conclusions about actuation speed for humidity triggered actuators. Conditions to be in the table: • 3D printed • actuator • RH-stimulated. (Followed by Table 21).

Reference	Type speed	Material	Conclusions
Le Duigou et al. (2019) ^[8]	Qualitative	Continuous carbon fiber and PA6	<ul style="list-style-type: none"> The higher the conditioning RH the higher the initial curvature derivative The conditioning RH has no influence on the actuating time.
Le Duigou et al. (2021) ^[50]	Initial curvature derivative	Continuous flax fiber and PLA	<ul style="list-style-type: none"> The higher the interfilament distance the higher the initial curvature derivative The bigger the hinge gap the greater the initial curvature derivative.
Le Duigou et al. (2016) ^[58]	Initial curvature derivative	Short wood fiber and PLA/PHA	<ul style="list-style-type: none"> 3D printed hygromorphs present greater initial curvature derivative than thermocompressed actuators. The larger the printing width the greater the initial curvature derivative.
Tahouni et al. (2021) ^[55]	Actuation time at 95%	Short wood reinforced polymer	<ul style="list-style-type: none"> The bigger the filling ratio of active restrictive or blocking layer, the higher the actuating time. The larger the number of active layer the higher the actuating time. Proves of concept for sequentially actuated aperture prototypes and cantilever beam lock.
Baker et al. (2019) ^[69]	Qualitative	Elastomer and hydrogel	<ul style="list-style-type: none"> The bigger the hinge gap, the higher the initial curvature derivative The hinge gap has no influence on the time to reach permanent state of actuation.
Su et al. (2018) ^[71]	Actuation time	SU-8	<ul style="list-style-type: none"> The larger the thickness of the actuator the larger the time needed to reach actuation.
Zhao et al. (2018) ^[76]	Actuation time at 85%	Poly(Ethylene Glycol) DiAcrylate (PEGDA) and Poly(ProPylene Glycol) DiMethAcrylate (PPGDMA)	<ul style="list-style-type: none"> The larger the thickness of the PPGDMA (passive material) layer the larger the actuation time. Proofs of concept for sequentially actuated flower and worm.
Tomec et al. (2021) ^[67]	Actuation time at 63.4%	Wood & PLA and PLA	<ul style="list-style-type: none"> The larger the thickness of the PLA (passive material) layer compared to the thickness of the wood & PLA layer the smaller the actuation time. The amount of fillers inside the PLA has little impact on the actuation time.

composites. However, polymeric fiber and polymeric multi-material composites have also recently displayed interesting actuation capabilities. Multi-materials composites also show better actuation reversibility than the natural fiber-based ones. One of the main challenges for the implementation of moisture-triggered 4D-printed structures is to account for all the reversibility tests required for understanding the evolution of the actuation capability of the structure. Modeling such evolution is necessary to achieve long-term control of the actuation. A potential solution to this issue is to perform automatic recordings of the deformation and the moisture variation within the actuators, to then simulate efficiently the long-term actuation.

- This paper proposed a classification of the different material distributions (short fiber composites, long fiber composites, multi-material), as well as the materials compatible with them. This classification is aimed to guide the reader to the development of targeted actuated hygromorph structures. Continuous fiber composites currently provide significant mechanical performance, but they are more difficult to print compared to short fibers and multi-materials structures.

Table 21. Conclusions about actuation speed for humidity triggered actuators. Conditions to be in the table: • 3D printed • actuator • RH-stimulated. (Following Table 20).

Reference	Type speed	Material	Conclusions
Qu et al. (2022) ^[62]	Time of actuation	Hydrogel	<ul style="list-style-type: none"> Water triggered actuation slower than sodium lactate and UV stimulated actuation.

Combining actuation triggers and architecture of the actuators are key to tailoring the overall actuation. Multifunctional structures provide big challenges (but also opportunities) for the materials selection in 4D printing technologies. For instance, continuous fiber 4D-printed materials have an intrinsic actuation function, together with the load-carrying one. New potential applications can emerge from adding functions to the actuating structures (i.e., mechanical, optical, and acoustic).

- The understanding of the actuation trigger mechanisms for hygromorphs (matrix-dominated and fiber-dominated actuation) is key to propose new materials allowing for a greater exploration of the 4D printing hygromorphs design space. Examples of these materials are natural fibers and polyamide-based filaments.
- The scales of modeling of the actuators (layer, phase, and intra-phase) have been classified to understand how to measure the relevant mechanical and physical properties responsible for the actuation. Fiber-based actuators require more investigations to be performed, to better understand the influence of the phase scale material properties on the 4D printed actuation. Developing robust modeling approaches to describe what occurs at intra-phase scale for both multi-materials and fiber-based actuators constitutes a central tenet to understand and predict the influence of the printing parameters on the hygromorphs actuation.
- Printing parameters such as the printing temperature, speed, and path have been described as key to control the actuation of the structure. Several other parameters controlling actuation in other fields of 4D printing have also been discussed.

A key challenge for the development of 4D printing hygromorphs will be to test all those parameters for humidity-triggered actuators. Another challenge for researchers working in the field of moisture actuation 4D-printed structures is to generate a standard capable of defining a clear process to measure the actuation amplitude and the control capability of a given structure. Such a standard would help to eliminate part of the confusion created by the diversity of actuation measuring parameters (i.e., position, curvature), as well as the conditioning processes adopted, which currently differ between research groups. This makes difficult to compare between materials and actuated structures described in open literature.

- The material properties responsible for the actuation control and the techniques to quantify those have been here discussed to allow for a better understanding of the design space of the 4D-printed hygromorphs actuators. Guidelines to measure the mechanical hygro-expansion and the porosity of the materials have also been given.
- Three types of conditioning phases have been here defined: pre-printing, as-printing, and post-printing conditioning. Each of them had its influence on the material properties responsible for the actuation. The first two conditioning phases tend to impact the quality of the hygromorph printed, whereas the post-printing conditioning can accelerate the deterioration of the material properties of the actuator over time.
- Strategies available to model the actuation of 4D-printed hygromorphs have been presented. Those strategies involve the use of Timoshenko bi-layer beam-inspired models, classical laminate theory, finite element analysis, elastic energy, and voxel-based models, and others other mathematical frameworks less extensively used. Each modeling technique was critically discussed and associated to specific configurations of actuators. One challenge for modeling techniques applied to moisture-triggered actuators is to account for the water diffusion through the material. The gradient of water inside the material generated by the diffusion of the humidity affects the temporary deformation state of the structure. All the modeling methods presented here would benefit from accounting for this water gradient evolution through the material itself.
- In past studies, the optimization of the structure of the 4D-printed hygromorph actuator has been mostly performed via either genetic algorithms, or neural networks. In this paper, genetic algorithms are mainly discussed for multi-materials structures. However, the present paper also suggests few directions to follow in order to apply these predictive methods to fiber-reinforced actuators. The paper has presented genetic algorithms used in past studies, with their objective functions and deformation measuring parameters. To the Authors' knowledge, no genetic algorithm based-optimization has been performed so far to design 4D-printed short fibers or continuous fiber hygromorph actuators. The paper therefore discusses potential developments about the use of models inspired by stiffness optimization, to further the design space and production of future 4D-printed hygromorphs. The different design trials performed using data-driven algorithms have been also discussed (i.e., k-nearest neighbor and linear regression). Only convolutional and recurrent

neural networks have been here discussed at length, as they are considered the most promising optimization techniques available in the field of 4D-printed hygromorphs.

- The different ways of conditioning the hygromorph actuators have been here presented and classified. Conditioning techniques discussed involve the use of air conditioning, oven/vacuum drying, water immersion, salt-saturated water (passive desiccation) and active desiccation. The criteria used to select the proper methods for conditioning are also introduced in this paper as guidelines.
- The different techniques to measure the deformations have been here classified into three groups: physical, photo or point of interest tracking. These measurement techniques (with their pros and cons) have been associated with the parameters responsible of the actuation of the hygromorphs. Techniques to measure the speed of actuation are also discussed. Limited work has been performed so far on improving the actuation speed of the materials considered. The creation and use of dynamic actuation will require tests and custom modeling to analyse the influence of the printing parameters and material properties for this specific application. Ideally, a standardization of the tests should be created for comparing the dynamic behavior of materials and structures actuated within the different research groups invested in 4D printing worldwide. To conduct such tests, the water conductivity of the printed materials would be an additional material property to be measured for generating ad-hoc models.

The 4D printing paradigm introduced in 2013 by Tibbitts et al. has also found applications highlighted in humidity-triggered test cases. Engineering applications such as smart solar concentrators and trackers, humidity self-regulating buildings and highly personalized clothing are among those in which hygromorph materials could find an avenue. Biomedical is the second predominant field of application, as it makes use of hygromorph principles for drug delivery and tissue engineering. The paper demonstrated that 4D printed hygromorphs are at an early stage of development, and part of the research studies discussed here have been also performed for temperature-stimulated structures. In the case of design optimization of hygromorphs, also compliance-based methodologies have been used to highlight new potential avenues to design hygromorphic materials and structures. For all the aspects touched on in this study, the authors have also tried to present potential directions of research and development for 4D-printed hygromorph materials.

Acknowledgements

The author would like to thank the UK Defence Science and Technology Laboratory for the funding received for this project through the UK-France Ph.D. Scheme. Fabrizio Scarpa also acknowledges the support from ERC-2020-AdG-NEUROMETA (No. 101020715).

Conflict of Interest

The authors declare no conflict of interest.

Keywords

4D printing, composites, designs, hygromorph actuators, optimization

Received: September 5, 2022

Revised: November 6, 2022

Published online:

- [1] S. Dimassi, F. Demoly, C. Cruz, H. J. Qi, K. Y. Kim, J. C. André, S. Gomes, *Computers Industry* **2021**, 126, 1.
- [2] Y. Zhou, C. B. Parker, P. Joshi, A. K. Naskar, J. T. Glass, C. Cao, *Adv. Mater. Technol.* **2021**, 6, 1.
- [3] A. F. Ghazal, M. Zhang, Z. Liu, *Food Bioprocess Technol.* **2019**, 12, 1627.
- [4] Q. Ji, X. V. Wang, L. Wang, L. Feng, *Sci. Rep.* **2022**, 12, 1.
- [5] Z. Hu, X. Zhang, Y. Li, Z. Hu, X. Zhang, Y. Li, *Science* **1995**, 269, 525.
- [6] H. Nakagawa, Y. Hara, S. Maeda, S. Hasimoto, *Polymers* **2011**, 3, 405.
- [7] C. Yang, B. Wang, D. Li, X. Tian, X. Tian, *Virtual Phys. Prototyping* **2017**, 12, 69.
- [8] A. Le Duigou, G. Chabaud, F. Scarpa, M. Castro, *Adv. Funct. Mater.* **2019**, 29, 1.
- [9] D. J. Roach, X. Kuang, C. Yuan, K. Chen, J. Qi, *Smart Mater. Struct.* **2018**, 27, 1.
- [10] L. Wang, F. Liu, J. Qian, Z. Wu, R. Xiao, *Soft Matter* **2021**, 17, 10397.
- [11] S. Réquillé, A. Le Duigou, A. Bourmaud, C. Baley, *Composites, Part A* **2019**, 123, 278.
- [12] V. Popineau, A. Celino, M. Peron, C. Baley, A. Le Duigou, *Composite Part A: Appl. Sci. Manufac.* **2022**, 158.
- [13] Z. Akbar, D. Wood, L. Kiesewetter, A. Menges, in *27th Int. Conf. Assoc. Computer-Aided Architectural Design Res. Asia*, **2022**, pp. 393–403.
- [14] 4d print* (Title) – 565 – Web of Science Core Collection.
- [15] S. Tibbits, *Archit. Des.* **2014**, 84, 116.
- [16] Q. Ge, C. K. Dunn, H. J. Qi, M. L. Dunn, *Smart Mater. Struct.* **2014**, 23, 1.
- [17] S. E. Bakarich, R. Gorkin, M. I. H. Panhuis, G. M. Spinks, *Macromol. Rapid Commun.* **2015**, 36, 1211.
- [18] A. Sydney Gladman, E. A. Matsumoto, R. G. Nuzzo, L. Mahadevan, J. A. Lewis, *Nat. Mater.* **2016**, 15, 413.
- [19] D. Correa, A. Papadopoulou, C. Guberan, N. Jhaveri, S. Reichert, A. Menges, S. Tibbits, *3D Print. Addit. Manuf.* **2015**, 2, 106.
- [20] Q. Ge, A. H. Sakhaei, H. Lee, C. K. Dunn, N. X. Fang, M. L. Dunn, *Sci. Rep.* **2016**, 6, 1.
- [21] Z. Ding, C. Yuan, X. Peng, T. Wang, H. J. Qi, M. L. Dunn, *Sci. Adv.* **2017**, 3, 1.
- [22] Q. Wang, X. Tian, L. Huang, D. Li, A. V. Malakhov, A. N. Polilov, *Mater. Des.* **2018**, 155, 404.
- [23] D. W. Rosen, *Virtual Phys. Prototyping* **2014**, 9, 225.
- [24] M. Kumke, H. Watschke, T. Vietor, *Virtual Phys. Prototyping* **2016**, 11, 3.
- [25] S. Yang, Y. F. Zhao, *Int. J. Adv. Manuf. Technol.* **2015**, 80, 327.
- [26] J. Plocher, A. Panesar, *Mater. Des.* **2019**, 183, 108164.
- [27] G. Wang, H. Yang, Z. Yan, N. G. Ulu, Y. Tao, J. Gu, L. B. Kara, L. Yao, in *UIST '18: Proc. 31st Annu. ACM Symp. User Interface Software and Technology*, ACM, New York **2018**, 623–635.
- [28] D. Kumar Jayashankar, Sachin, S. Gupta, N. D. Sanandiya, J. D. Fernandez, K. Tracy, *Int. J. Adv. Manuf. Technol.* **2020**, 109, 1493.
- [29] M. Rüggeberg, I. Burgert, *PLoS One* **2015**, 10, 1.
- [30] P. Grönquist, D. Wood, M. M. Hassani, F. K. Wittel, A. Menges, M. Rüggeberg, *Sci. Adv.* **2019**, 5, 1.
- [31] O. Testoni, T. Lumpe, J.-L. Huang, M. Wagner, S. Bodkhe, Z. Zhakypov, R. Spolenak, J. Paik, P. Ermanni, L. Muñoz, K. Shea, *Smart Mater. Struct.* **2021**, 30, 1.
- [32] H. Yi, Y. Kim, *J. Build. Eng.* **2021**, 43, 1.
- [33] E. Vazquez, C. Randall, J. P. Duarte, *J. Facade Des. Eng.* **2019**, 7, 93.
- [34] S. Hoa, B. Reddy, D. Rosca, *Compos. Struct.* **2021**, 272, 1.
- [35] S. Hoa, M. Abdali, A. Jasmin, D. Radeschi, V. Prats, H. Faour, B. Kobaissi, *Compos. Struct.* **2022**, 290, 1.
- [36] S. V. Hoa, *Compos. Struct.* **2019**, 210, 869.
- [37] F. Momeni, J. Ni, *Renew. Energy* **2018**, 122, 35.
- [38] F. Momeni, S. Sabzpoushan, R. Valizadeh, M. R. Morad, X. Liu, J. Ni, *Renew. Energy* **2019**, 130, 329.
- [39] T. R. Nachtigall, O. Tomico, R. Wakkary, S. Wensveen, P. Van Dongen, L. Tenthof Van Noorden, L. Suzanne, in *CHI EA, 18: Extended Abstracts of the 2018 CHI Conference on Human Factors in Computing Systems* **2018**, 1–9.
- [40] Y. Tao, J. Gu, B. An, T. Cheng, X. A. Chen, X. Zhang, W. Zhao, Y. Do, T. Zhang, L. Yao, in *CHI EA, 18: Extended Abstracts of the 2018 CHI Conf. on Human Factors in Computing Systems*, ACM, New York **2018**, 1–4.
- [41] X. Kuang, D. J. Roach, J. Wu, C. M. Hamel, Z. Ding, T. Wang, M. L. Dunn, H. J. Qi, *Adv. Funct. Mater.* **2019**, 29, 1.
- [42] A. Fathy Ghazal, M. Zhang, A. S. Mujumdar, M. Ghamry, *Crit. Rev. Food Sci. Nutr.* **2022**, 0, 1.
- [43] H.-W. Kang, S. Jin Lee, I. Kap Ko, C. Kengla, J. J. Yoo, A. Atala, *Nat. Biotechnol.* **2016**, 34, 1.
- [44] C. Cui, D.-O. Kim, M. Y. Pack, B. Han, L. Han, Y. Sun, L.-H. Han, *Biofabrication* **2020**, 12, 45018.
- [45] S. Zu, Z. Wang, S. Zhang, Y. Guo, C. Chen, Q. Zhang, T. Liu, Q. Liu, Z. Zhang, *Mater. Today Chem.* **2022**, 24, 1.
- [46] D. You, G. Chen, C. Liu, X. Ye, S. Wang, M. Dong, M. Sun, J. He, X. Yu, G. Ye, Q. Li, J. Wu, J. Wu, Q. Zhao, T. Xie, M. Yu, H. Wang, *Adv. Funct. Mater.* **2021**, 31, 1.
- [47] L. K. Rivera-Tarazona, T. Shukla, K. Abhay Singh, A. K. Gaharwar, Z. T. Campbell, T. H. Ware, L. K. Rivera-Tarazona, K. A. Singh, A. K. Gaharwar, T. H. Ware, T. Shukla, Z. T. Campbell, *Adv. Funct. Mater.* **2022**, 32, 2106843.
- [48] A. Zolfagharian, H. R. Jarrar, M. Bodaghi, *Bioprinting* **2021**, 24, 1.
- [49] B. Y. S. Timoshenko, *J. Opt. Soc. Am.* **1925**, 11, 233.
- [50] A. Le Duigou, T. Fruleux, R. Matsuzaki, G. Chabaud, M. Ueda, M. Castro, *Mate. Des.* **2021**, 211, 110158.
- [51] C. de Kergariou, B. C. Kim, A. Perriman, A. Le Duigou, S. Gueasmas, F. Scarpa, *Addit. Manuf.* **2022**, 59, 103144.
- [52] D. Correa, S. Poppinga, M. D. Mylo, A. S. Westermeier, B. Bruchmann, A. Menges, T. Speck, *Philos. Trans. R. Soc. A* **2020**, 378, 1.
- [53] Y. Tahouni, T. Cheng, R. Sachse, R. Thierer, M. Bischoff, in *SCF '20: Proc. 5th Annual ACM Symp. on Computational Fabrication*, ACM, New York **2020**, 1–11.
- [54] T. Cheng, D. Wood, B. Stolz, R. Mülhaupt, in *SCF '20: Proc. 5th Annual ACM Symp. on Computational Fabrication*, ACM, New York **2020**, 1–10.
- [55] Y. Tahouni, F. Krüger, S. Poppinga, D. Wood, M. Pfaff, J. Rühle, T. Speck, A. Menges, *Bioinspir. Biomim.* **2021**, 16, 5.
- [56] C. Zarna, S. Rodriguez-Fabià, A. T. Echtermeyer, G. Chinga-Carrasco, *Addit. Manuf.* **2022**, 59, 103166.
- [57] T. Cheng, M. Thielen, S. Poppinga, Y. Tahouni, D. Wood, T. Steinberg, A. Menges, T. Speck, *Adv. Sci.* **2021**, 8, 2100411.
- [58] A. Le Duigou, M. Castro, R. Bevan, N. Martin, *Mate. Des.* **2016**, 96, 106.
- [59] F. Krüger, R. Thierer, Y. Tahouni, R. Sachse, D. Wood, A. Menges, M. Bischoff, J. Rühle, *Biomimetics* **2021**, 6, 58.
- [60] M. C. Mulakkal, R. S. Trask, V. P. Ting, A. M. Seddon, *Mater. Des.* **2018**, 160, 108.

- [61] J. Lai, X. Ye, J. Liu, C. Wang, J. Li, X. Wang, M. Ma, M. Wang, *Mater. Des.* **2021**, 205, 1.
- [62] G. Qu, J. Huang, Z. Li, Y. Jiang, Y. Liu, K. Chen, Z. Xu, Y. Zhao, G. Gu, X. Wu, J. Ren, *Mater. Today Bio* **2022**, 16, 100363.
- [63] S. Poppinga, D. Correa, B. Bruchmann, A. Menges, T. Speck, *Integr. Compar. Biol.* **2020**, 60, 886.
- [64] M. Langhansl, J. Dörstein, P. Hornberger, C. Zollfrank, *Funct. Composite Mater.* **2021**, 2, 1.
- [65] E. Vazquez, B. Gürsoy, J. P. Duarte, *Int. J. Archit. Computing* **2019**, 18, 67.
- [66] E. Vazquez, B. Gürsoy, in *XXIV Int. Conf. of the Iberoamerican Society of Digital Graphics, SiGraDi 2020*, pp. 600–607.
- [67] D. K. Tomec, A. Straže, A. Haider, M. Kariž, *Polymers* **2021**, 13, 3209.
- [68] D. Correa, A. Menges, *Fused Filament Fabrication for Multi-Kinetic State Climate Responsive Aperture*, UCL Press, **2017**.
- [69] A. B. Baker, S. R. Bates, T. M. Llewellyn-Jones, L. P. Valori, M. P. Dicker, R. S. Trask, *Mater. Des.* **2019**, 163, 107544.
- [70] Z. Liu, C. He, C. Guo, F. Chen, B. Bhandari, M. Zhang, *Food Hydrocolloids* **2021**, 115, 106608.
- [71] J.-W. Su, X. Tao, H. Deng, C. Zhang, S. Jiang, Y. Lin, J. Lin, *Soft Matter* **2018**, 14, 765.
- [72] Z. Zhang, N. Corrigan, A. Bagheri, J. Jin, C. Boyer, *Angew. Chem. Int. Ed.* **2019**, 58, 17954.
- [73] J. J. Schwartz, A. J. Boydston, *Nat. Commun.* **2019**, 10, 1.
- [74] D. Raviv, W. Zhao, C. Mcknelly, A. Papadopoulou, A. Kadambi, B. Shi, S. Hirsch, D. Dikovskiy, M. Zyracki, C. Olguin, R. Raskar, S. Tibbits, *Sci. Rep.* **2014**, 4, 1.
- [75] O. Mesa, in *XXIV Int. Conf. of the Iberoamerican Society of Digital Graphics, 2020*, pp. 894–901.
- [76] Z. Zhao, X. Kuang, C. Yuan, H. J. Qi, D. Fang, *ACS Appl. Mater. Interfaces* **2018**, 10, 19932.
- [77] L. Hiendlmeier, T. F. Teshima, F. Zurita, H. Url, P. Rinklin, B. Wolfrum, *Macromol. Mater. Eng.* **2022**, 307, 2200306.
- [78] J. Ryu, M. Mohammadifar, M. Tahernia, H. i. Chun, Y. Gao, S. Choi, *Adv. Mater. Technol.* **2020**, 5, 1.
- [79] K. Kim, Y. Guo, J. Bae, S. Choi, H. Y. Song, S. Park, K. Hyun, S. K. Ahn, *Small* **2021**, 17, 2100910.
- [80] B. Yisong, C. Liu, Y. Li, J. Li, L. Qiao, J. Zhou, Y. Bai, *Mater. Horiz.* **2022**, 5, 311.
- [81] L. Ren, B. Li, Q. Liu, L. Ren, Z. Song, X. Zhou, P. Gao, *Front. Mater.* **2021**, 8, 1.
- [82] S. Olga Kuksenok, A. C. Balazs, O. Kuksenok, *Mater. Horiz.* **2016**, 3, 53.
- [83] X. Lu, C. P. Ambulo, S. Wang, L. K. Rivera-Tarazona, H. Kim, K. Searles, T. H. Ware, *Angew. Chem. Int. Ed.* **2021**, 60, 5536.
- [84] H. Deng, C. Zhang, K. Sattari, Y. Ling, J.-W. Su, Z. Yan, J. Lin, *ACS Appl. Mater. Interfaces* **2021**, 13, 12719.
- [85] A. Y. Lee, J. An, C. K. Chua, Y. Zhang, *Engineering* **2019**, 5, 1159.
- [86] S. Zeng, Y. Gao, Y. Feng, H. Zheng, H. Qiu, J. Tan, *Smart Mater. Struct.* **2019**, 28, 1.
- [87] G. Chabaud, M. Castro, C. Denoual, A. Le Duigou, *Addit. Manuf.* **2019**, 26, 94.
- [88] A. Regazzi, S. Corn, P. Ienny, J. C. Bénézet, A. Bergeret, *Ind. Crops Products* **2016**, 84, 358.
- [89] P. Li, L. Pan, D. Liu, Y. Tao, S. Q. Shi, *Materials* **2019**, 12, 2896.
- [90] C. Dingler, H. Müller, M. Wieland, D. Fauser, H. Steeb, S. Ludwigs, C. Dingler, H. Müller, M. Wieland, S. Ludwigs, D. Fauser, H. Steeb, *Adv. Mater.* **2021**, 33, 2007982.
- [91] Z. Jiang, P. Shen, M. Li Tan, Q. Yan, J. Viktorova, C. Cementon, X. Peng, P. Xiao, L. A. Connal, *Mate. Adv.* **2021**, 2, 5124.
- [92] M. Hua, D. Wu, S. Wu, Y. Ma, Y. Alsaïd, X. He, *ACS Appl. Mater. Interfaces* **2021**, 13, 12689.
- [93] D. Podstawczyk, M. Nizioł, P. Szymczyk-Ziółkowska, M. Fiedot-Toboła, D. Podstawczyk, M. Nizioł, P. Szymczyk-Ziółkowska, M. Fiedot-Toboła, *Adv. Funct. Mater.* **2021**, 31, 2009664.
- [94] H. Zhao, Y. Huang, F. Lv, L. Liu, Q. Gu, S. Wang, *Adv. Funct. Mater.* **2021**, 31, 2105544.
- [95] S. Naficy, R. Gately, R. Gorkin, H. Xin, G. M. Spinks, *Macromol. Mater. Eng.* **2017**, 302, 1600212.
- [96] K. Benyahia, H. Seriket, R. Prod'hon, S. Gomes, J.-C. André, H. J. Qi, F. Demoly, *Addit. Manuf.* **2022**, 58, 102993.
- [97] A. Le Duigou, V. Keryvin, J. Beaugrand, M. Pernes, F. Scarpa, M. Castro, *Composites Part A: Appl. Sci. Manuf.* **2019**, 116, 36.
- [98] Y. Yu, H. Liu, K. Qian, H. Yang, M. McGehee, J. Gu, D. Luo, L. Yao, Y. J. Zhang, *CAD Computer Aided Des.* **2020**, 122, 102817.
- [99] J. W. Boley, W. M. Van Rees, C. Lissandrello, M. N. Horenstein, R. L. Truby, A. Kotikian, J. A. Lewis, L. Mahadevan, *Proc. Natl. Acad. Sci. USA* **2019**, 116, 20856.
- [100] D. Stoof, K. Pickering, *Composites, Part B* **2018**, 135, 110.
- [101] E. Vazquez, B. Gürsoy, J. Duarte, in *24th Int. Conf. Assoc. Computer-Aided Architectural Design Research in Asia (CAADRIA) 2019*, pp. 391–400.
- [102] T. Y. Koh, A. Sutradhar, *Addit. Manuf.* **2022**, 56, 102866.
- [103] S. Zeng, Y. Feng, Y. Gao, Hao Zheng, J. Tan, *Bio-Des. Manuf.* **2022**, 5, 189.
- [104] H. Y. Jeong, E. Lee, S. Ha, N. Kim, Y. C. Jun, *Adv. Mater. Technol.* **2019**, 4, 3.
- [105] L. Kačergis, R. Mitkus, M. Sinapius, *Smart Mater. Struct.* **2019**, 28, 105042.
- [106] A. Y. Lee, A. Zhou, J. An, C. K. Chua, Y. Zhang, *Virtual Phys. Prototyping* **2020**, 15, 481.
- [107] M. O. Saed, C. P. Ambulo, H. Kim, R. De, V. Raval, K. Searles, D. A. Siddiqui, J. M. O. Cue, M. C. Stefan, M. R. Shankar, T. H. Ware, *Adv. Funct. Mater.* **2019**, 29, 3.
- [108] L.-Y. Zhou, J.-H. Ye, J.-Z. Fu, Q. Gao, Y. He, *ACS Appl. Mater. Interfaces* **2020**, 12, 12068.
- [109] J. Liu, O. Erol, A. Pantula, W. Liu, Z. Jiang, K. Kobayashi, D. Chatterjee, N. Hibino, L. H. Romer, S. H. Kang, T. D. Nguyen, D. H. Gracias, *Appl. Mater. Interfaces* **2019**, 11, 8492.
- [110] T. Uchida, H. Onoe, *Micromachines* **2019**, 10, 433.
- [111] B. Narupai, P. T. Smith, A. Nelson, B. Narupai, P. T. Smith, A. Nelson, *Adv. Funct. Mater.* **2021**, 31, 2011012.
- [112] X. Hu, Z. Ge, X. Wang, N. Jiao, S. Tung, L. Liu, *Composites, Part B* **2022**, 228, 109451.
- [113] M. N. I. Shiblee, K. Ahmed, M. Kawakami, H. Furukawa, *Adv. Mater. Technol.* **2019**, 4, 1900071.
- [114] D. M. Solis, A. Czekanski, *Soft Matter* **2022**, 18, 3422.
- [115] A. Nishiguchi, H. Zhang, S. Ren Schweizerhof, M. F. Schulte, A. Mourran, M. Mo, *ACS Appl. Mater. Interfaces* **2020**, 12, 12176.
- [116] Y. Li, W. Zheng, B. Li, J. Dong, G. Gao, Z. Jiang, *Colloids Surfaces A: Physicochem. Eng. Aspects* **2022**, 648, 129307.
- [117] B. Zou, C. Song, Z. He, J. Ju, *Extreme Mech. Lett.* **2022**, 54, 101779.
- [118] Z. Chen, D. Zhao, B. Liu, G. Nian, X. Li, J. Yin, S. Qu, W. Yang, Z. Chen, D. Zhao, B. Liu, G. Nian, S. Qu, W. Yang, X. Li, J. Yin, *Adv. Funct. Mater.* **2019**, 29, 1900971.
- [119] S. V. Hoa, D. I. Rosca, *Mater. Today Commun.* **2020**, 25, 101115.
- [120] S. V. Hoa, X. Cai, *Composite Struct.* **2020**, 238, 111883.
- [121] S. Van Hoa, *Adv. Manuf.: Polym. Compos. Sci.* **2017**, 3, 101.
- [122] S. V. Hoa, E. Fakhimi, *Compos. Struct.* **2022**, 292, 115704.
- [123] X. Peng, X. Kuang, D. J. Roach, Y. Wang, C. M. Hamel, C. Lu, H. J. Qi, *Additive Manufacturing* **2021**, 40, 101911.
- [124] A. Agkathidis, G. Varinlioglu, in *Advances in Product Design Engineering*, Springer, Cham **2022**, pp. 61–81, Ch. 3.
- [125] M. Bodaghi, A. R. Damanpack, W. H. Liao, *Smart Mater. Struct.* **2016**, 25, 105034.
- [126] D. Chen, Q. Liu, P. Geng, S. Tang, J. Zhang, S. Wen, Y. Zhou, C. Yan, Z. Han, Y. Shi, *Compos. Sci. Technol.* **2021**, 208, 108746.
- [127] M. Piedrahita-Bello, J. E. Angulo-Cervera, R. Courson, G. Molná, L. Malaquin, C. Thibault, B. Tondou, L. Salmon, A. Bousseksou, *J. Mater. Chem. C* **2020**, 8, 41.

- [128] C. Zhang, X. Lu, G. Fei, Z. Wang, H. Xia, Y. Zhao, *Appl. Mater. Interfaces* **2019**, *11*, 44774.
- [129] J. Guo, R. Zhang, L. Zhang, X. Cao, *ACS Macro Lett.* **2018**, *7*, 442.
- [130] D. Kokkinis, M. Schaffner, A. R. Studart, *Nat. Commun.* **2015**, *6*, 1.
- [131] S. Weng, X. Kuang, Q. Zhang, C. M. Hamel, D. J. Roach, N. Hu, H. J. Qi, *ACS Appl. Mater. Interfaces* **2021**, *13*, 12797.
- [132] C. M. Hamel, D. J. Roach, K. N. Long, F. Demoly, M. L. Dunn, H. J. Qi, *Smart Mater. Struct.* **2019**, *28*, 1.
- [133] C. Yuan, F. Wang, Q. Ge, *Extreme Mech. Lett.* **2021**, *42*, 101122.
- [134] K. K. Westbrook, H. J. Qi, *J. Intell. Material. Syst. Struct.* **2008**, *19*, 597.
- [135] Y. Mao, K. Yu, M. S. Isakov, J. Wu, M. L. Dunn, H. Jerry Qi, *Sci. Rep.* **2015**, *5*, 12.
- [136] Y. Liu, F. Zhang, J. Leng, L. Wang, C. Cotton, B. Sun, T. W. Chou, *Composites, Part B* **2019**, *179*, 107536.
- [137] T. van Manen, V. M. Dehabadi, M. C. Saldívar, M. J. Mirzaali, A. A. Zadpoor, *Commun. Mater.* **2022**, *3*, 1.
- [138] C. Y. Wu, J. R. Chen, C. K. Su, *Anal. Chim. Acta* **2022**, *1204*, 339733.
- [139] X. Sun, L. Yue, L. Yu, H. Shao, X. Peng, K. Zhou, F. Demoly, R. Zhao, H. J. Qi, *Adv. Funct. Mater.* **2022**, *32*, 10.
- [140] H. Liu, Z. Liu, G. Duan, J. Tan, *J. Intell. Mater. Syst. Struct.* **2022**, *33*, 1046.
- [141] A. Zolfagharian, A. Kaynak, S. Y. Khoo, A. Kouzani, *Sens. Actuators, A* **2018**, *274*, 231.
- [142] L. Huang, R. Jiang, J. Wu, J. Song, H. Bai, B. Li, Q. Zhao, T. Xie, *Adv. Mater.* **2017**, *29*, 7.
- [143] J. E. M. Teoh, J. An, C. K. Chua, M. Lv, V. Krishnasamy, Y. Liu, *Virtual Phys. Prototyping* **2017**, *12*, 61.
- [144] D. J. Roach, X. Sun, X. Peng, F. Demoly, K. Zhou, H. J. Qi, *Adv. Funct. Mater.* **2022**, *32*, 2203236.
- [145] Y.-D. Zhao, J.-H. Lai, M. Wang, *Nano LIFE* **2021**, *11*, 04.
- [146] Z. Zhao, H. J. Qi, D. Fang, *Soft Matter* **2019**, *15*, 1005.
- [147] Y. Zhang, H. Chen, S. Liu, L. Josien, G. Schrodi, A. Simon-Masseron, J. Lalevé, *Macromol. Mater. Eng.* **2021**, *306*, 6.
- [148] K. E. Mazur, A. Borucka, P. Kaczor, S. Gądek, R. Bogucki, D. Mirziewiński, S. Kuciel, *J. Polym. Environ.* **2022**, *30*, 2341.
- [149] D. Stooft, K. Pickering, Y. Zhang, *J. Compos. Sci.* **2017**, *1*, 8.
- [150] A. Zolfagharian, M. Denk, M. Bodaghi, A. Z. Kouzani, A. Kaynak, *Acta Mech. Solida Sin.* **2020**, *33*, 418.
- [151] S. Yamamura, E. Iwase, *Mater. Des.* **2021**, *203*, 109605.
- [152] Y. Yu, K. Qian, H. Yang, L. Yao, Y. J. Zhang, *J. Mater. Processing Technol.* **2022**, *302*, 117497.
- [153] G. Wang, Y. Tao, O. B. Capunaman, H. Yang, L. Yao, B. Capunaman, in *CHI, ACM*, **2019**, 1–12.
- [154] J. M. McCracken, B. M. Rauzan, J. C. Kjellman, H. Su, S. A. Rogers, R. G. Nuzzo, *Adv. Funct. Mater.* **2019**, *29*, 1806723.
- [155] B. Goo, C. H. Hong, K. Park, *Mater. Desi.* **2020**, *188*, 108485.
- [156] Y. Feng, W. Yan, H. Qiu, Z. Hong, S. Zeng, J. Xu, K. Cui, J. Tan, *Smart Mater. Struct.* **2022**, *31*, 1.
- [157] Y. Wang, X. Li, *Addit. Manuf.* **2022**, *58*, 102975.
- [158] Z. Siddiqui, J. Smay, A. Azoug, *Mechan. Mater.* **2022**, *170*, 1.
- [159] W. M. Van Rees, E. A. Matsumoto, A. S. Gladman, J. A. Lewis, L. Mahadevan, *Soft Matter* **2018**, *14*, 8771.
- [160] S. Wang, J. M. Lee, W. Y. Yeong, *Int. Bioprinting* **2015**, *1*, 3.
- [161] D. Deb, J. M. Jafferson, *Mater. Today: Proc.* **2021**, *46*, 1308.
- [162] L. P. Muthe, K. Pickering, C. Gauss, *Composites Part C: Open Access* **2022**, *8*, 100271.
- [163] C. Tze Seng, S. A. Yong, L. Eh Noum, S. A. Kumar, L. Sivanesan, L.-J. Yu, in *13th Int. Eng. Res. Conf.*, **2020**, 2233, 20086.
- [164] C. M. Vicente, J. Fernandes, L. Reis, A. M. De Deus, M. F. Vaz, M. Leite, *Fratt. Integrità Strutt.* **2019**, *13*, 748.
- [165] C. de Kergariou, H. Saidani-Scott, A. Perriman, F. Scarpa, A. Le Duigou, *Composites, Part A* **2022**, *155*, 1.
- [166] R. Matsuzaki, M. Ueda, M. Namiki, T. K. Jeong, H. Asahara, K. Horiguchi, T. Nakamura, A. Todoroki, Y. Hirano, *Sci. Rep.* **2016**, *6*, 1.
- [167] A. Zolfagharian, M. Denk, A. Z. Kouzani, M. Bodaghi, S. Nahavandi, A. Kaynak, *Int. J. Biol. Macromol.* **2020**, *6*, 260.
- [168] Y. S. Alshebly, M. Nafea, H. A. Almurib, M. Sultan Mohamed Ali, A. A. Mohd Faudzi, M. T. Tan, in *IEEE Int. Conf. Autom. Control Intell. Syst.*, IEEE, New York. **2021**, pp. 41–45.
- [169] A. R. Rajkumar, K. Shanmugam, *J. Mater. Res.* **2018**, *33*, 4362.
- [170] J. Fernandes, A. M. Deus, L. Reis, M. F. Vaz, M. Leite, in *International Conference on Progress in Additive Manufacturing*, Nanyang Technological University, Singapore **2018**, pp. 547–552.
- [171] M. S. Meiabadi, M. Moradi, M. Karamimoghdam, S. Ardabili, M. Bodaghi, M. Shokri, A. H. Mosavi, *Polymers* **2021**, *13*, 3219.
- [172] W. Helfrich, *J. Chem. Phys.* **1998**, *85*, 1085.
- [173] S. Turcaud, L. Guiducci, P. Fratzl, Y. J. Bréchet, J. W. Dunlop, *Int. J. Mater. Res.* **2011**, *102*, 607.
- [174] Y. Wang, W. Huang, Y. Wang, X. Mu, S. Ling, H. Yu, W. Chen, C. Guo, M. C. Watson, Y. Yu, L. D. Black, M. Li, F. G. Omenetto, C. Li, D. L. Kaplan, *Proc. Natl. Acad. Sci. USA* **2020**, *117*, 1.
- [175] H. Zhang, J. Chen, D. Yang, *Addit. Manuf.* **2021**, *38*, 101775.
- [176] S. Belhabib, S. Guessasma, *Int. J. Mech. Sci.* **2017**, *133*, 728.
- [177] W. Zhao, N. Li, L. Liu, J. Leng, Y. Liu, *Compos. Struct.* **2022**, *293*, 115669.
- [178] G. Sossou, F. Demoly, H. Belkebir, H. J. Qi, S. Gomes, G. Montavon, *Mater. Des.* **2019**, *181*, 108074.
- [179] C. Baley, Y. Perrot, F. Busnel, H. Guezencoc, P. Davies, *Mater. Lett.* **2006**, *60*, 2984.
- [180] J. Wollbrett-Blitz, S. Joannès, R. Bruant, C. Le Clerc, M. R. De La Osa, A. Bunsell, A. Marcellan, *J. Polym. Sci., Part B: Polym. Phys.* **2016**, *54*, 374.
- [181] H. Gonabadi, A. Yadav, S. J. Bull, *Int. J. Adv. Manuf. Technol.* **2020**, *111*, 695.
- [182] A. I. Cernencu, A. I. Dinu, I. C. Stancu, A. Lungu, H. Iovu, *Biotechnol. Bioeng.* **2022**, *119*, 762.
- [183] J. Li, Y. Durandet, X. Huang, G. Sun, D. Ruan, *J. Mater. Sci. Technol.* **2022**, *119*, 219.
- [184] A. Sayam, A. N. M. Masudur Rahman, M. Sakibur Rahman, S. Akter Smriti, F. Ahmed, M. Fogla Rabbi, M. Hossain, M. Omar Faruque, S. Akter Smriti sa, *Carbon Lett.* **2022**, *2022*, 1, 1.
- [185] V. Mishra, S. Negi, S. Kar, A. K. Sharma, Y. N. K. Rajbahadur, A. Kumar, *J. Thermoplast. Compos. Mater.* **2022**, *0*, 1.
- [186] A. Le Duigou, G. Chabaud, R. Matsuzaki, M. Castro, *Composites, Part B* **2020**, *203*, 108474.
- [187] S. Li, K. Wang, W. Zhu, Y. Peng, S. Ahzi, F. Chinesta, *Constr. Build. Mater.* **2022**, *340*, 127842.
- [188] L. Malagutti, V. Mazzanti, F. Mollica, *Rapid Prototyping J.* **2022**, *28*, 1834.
- [189] Y. Long, Z. Zhang, C. Yan, Z. Huang, K. Fu, Y. Li, *Compos. Commun.* **2022**, *35*, 101283.
- [190] I. P. Beckman, C. Lozano, E. Freeman, G. Riveros, M. Rahman, G. M. A. Khan, *Polymers* **2021**, *13*, 2233.
- [191] Z. Hou, X. Tian, Z. Zheng, J. Zhang, L. Zhe, D. Li, A. V. Malakhov, A. N. Polilov, *Composites, Part B* **2020**, *189*, 107893.
- [192] A. Todoroki, T. Oasada, Y. Mizutani, Y. Suzuki, M. Ueda, R. Matsuzaki, Y. Hirano, *Adv. Compos. Mater.* **2019**, *29*, 147.
- [193] D. R. Hetrick, S. Hamid, R. Saneii, C. E. Bakis, O. Ashour, *J. Reinf. Plast. Compos.* **2021**, *40*, 365.
- [194] J. Justo, L. Távara, L. García-Guzmán, F. París, *Compos. Struct.* **2018**, *185*, 537.
- [195] P. Bettini, G. Alitta, G. Sala, L. D. Landro, *J. Mater. Eng. Perform.* **2016**, *26*, 843.
- [196] L. G. Blok, M. L. Longana, H. Yu, B. K. Woods, *Addit. Manuf.* **2018**, *22*, 176.
- [197] M. Iragi, C. Pascual-Gonzalez, A. Esnaola, J. Aurrekoetxea, C. S. Lopes, L. Aretxabaleta, in *ECCM18-18th Eur. Conf. on Composite Materials ECCM*, Athens, Greece **2018**, pp. 1–8.

- [198] O. Andrés González-Estrada, A. Pertuz, J. Quiroga, *Key Eng. Mater.* **2018**, 774, 161.
- [199] C. Oztan, R. Karkkainen, M. Fittipaldi, G. Nygren, L. Roberson, M. Lane, E. Celik, *J. Compos. Mater.* **2019**, 53, 271.
- [200] S. H. R. Sanei, Z. Lash, J. Servey, F. Gardone, C. P. Nikhare, in *ASME Int. Mechanical. Eng. Congress and Exposition*, vol. 12, American Society of Mechanical Engineers, **2019**, 1–6.
- [201] K. Saeed, A. McIlhagger, E. Harkin-Jones, J. Kelly, E. Archer, *Compos. Struct.* **2021**, 259, 113226.
- [202] M. Iragi, C. Pascual-González, A. Esnaola, C. S. Lopes, L. Aretxabaleta, *Addit. Manuf.* **2019**, 30, 100884.
- [203] S. Terekhina, S. Egorov, T. Tarasova, I. Skornyakov, L. Guillaumat, M. L. Hattali, *Composites, Part A* **2022**, 153, 106725.
- [204] R. N. Yogeshvaran, B. G. Liu, F. Farukh, K. Kandam, *J. Mech.* **2020**, 36, 2.
- [205] A. Parmiggiani, M. Prato, M. Pizzorni, *Int. J. Adv. Des. Manuf. Technol.* **2021**, 114, 2085.
- [206] A. N. Dickson, J. N. Barry, K. A. McDonnell, D. P. Dowling, *Addit. Manuf.* **2017**, 16, 146.
- [207] A. Le Duigou, A. Barbé, E. Guillou, M. Castro, *Materials and Design* **2019**, 180, 1.
- [208] B. Akhoundi, A. H. Behraves, A. Bagheri Saed, *J. Reinf. Plast. Compos.* **2019**, 38, 99.
- [209] S. Kuschmitz, A. Schirp, J. Busse, H. Watschke, C. Schirp, T. Vietor, *Materials* **2021**, 14, 2332.
- [210] G. D. Goh, V. Dikshit, A. P. Nagalingam, G. L. Goh, S. Agarwala, S. L. Sing, J. Wei, W. Y. Yeong, *Mater. Des.* **2018**, 137, 79.
- [211] C. Yang, X. Tian, T. Liu, Y. Cao, D. Li, *Rapid Prototyping J.* **2017**, 23, 209.
- [212] L. Pyl, K. A. Kalteremidou, D. Van Hemelrijck, *Polym. Test.* **2018**, 71, 318.
- [213] J. M. Chacón, M. A. Caminero, P. J. Núñez, E. García-Plaza, I. García-Moreno, J. M. Reverte, *Compos. Sci. Technol.* **2019**, 181, 107688.
- [214] E. Giannakis, C. Koidis, P. Kyratsis, D. Tzetzis, *Int. J. Modern Manuf. Technol.* **2019**, XI, 69.
- [215] J. Naranjo Lozada, H. Ahuett-Garza, P. O. Castañón, W. M. H. Verbeeten, D. Sáiz González, *Addit. Manuf.* **2019**, 26, 227.
- [216] A. N. Sarvestani, N. Van De Werken, M. Tehrani, P. Khanbolouki, in *ASME International Mechanical Engineering Congress and Exposition*, vol. 72041, American Society of Mechanical Engineers, Salt Lake City, UT **2017**, pp. 1–6, <https://doi.org/10.1115/IMECE2017-72041>.
- [217] Q. He, H. Wang, K. Fu, L. Ye, *Compos. Sci. Technol.* **2020**, 191, 108077.
- [218] N. van de Werken, P. Koirala, J. Ghorbani, D. Doyle, M. Tehrani, *Addit. Manuf.* **2021**, 37, 101634.
- [219] N. van de Werken, J. Hurley, P. Khanbolouki, A. N. Sarvestani, A. Y. Tamijani, M. Tehrani, *Composites, Part B* **2019**, 160, 684.
- [220] Y. Long, Z. Zhang, K. Fu, Y. Li, *Composites, Part B* **2021**, 227, 109389.
- [221] N. Mosleh, A. M. Rezaoust, S. Dariushi, *Mater. Manuf. Processes* **2021**, 36, 409.
- [222] Y. Ming, Z. Xin, J. Zhang, Y. Duan, B. Wang, *Compos. Commun.* **2020**, 21, 100401.
- [223] H. Dou, Y. Cheng, W. Ye, D. Zhang, J. Li, Z. Miao, S. Rudykh, *Materials* **2020**, 13, 3850.
- [224] B. Chang, P. Parandoush, X. Li, S. Ruan, C. Shen, R. A. Behnagh, Y. Liu, D. Lin, *Polym. Compos.* **2020**, 41, 4706.
- [225] B. Chang, X. Li, P. Parandoush, S. Ruan, C. Shen, D. Lin, *Polym. Test.* **2020**, 88, 106563.
- [226] T. Liu, X. Tian, Y. Zhang, Y. Cao, D. Li, *Composites, Part A* **2020**, 130, 105770.
- [227] J. Y. Tey, W. O. Ding, W. H. Yeo, Y. J. King, L. H. Saw, *IOP Con. Ser.: Earth Environ. Sci.* **2020**, 463, 012091.
- [228] L. Li, W. Liu, L. Sun, *Compos. Sci. Technol.* **2022**, 227, 109618.
- [229] S. Rijckaert, L. Daelemans, L. Cardon, M. Boone, W. Van Paepegem, K. De Clerck, *Polymers* **2022**, 14, 298.
- [230] Z. Zhang, Y. Long, Z. Yang, K. Fu, Y. Li, *Composites, Part A* **2022**, 162, 107162.
- [231] N. W. Y. Omar, N. A. Shuaib, M. H. J. A. Hadi, A. I. Azmi, M. N. Misbah, *Materials* **2021**, 15, 190.
- [232] J. Yan, E. Demirci, A. Ganesan, A. Gleadall, *Addit. Manuf.* **2022**, 49, 102496.
- [233] A. Hendlmeier, a. Simon, Y. A. Wickramasingha, L. C. Henderson, *Polym. Compos.* **2021**, 42, 4728.
- [234] M. Mohammadzadeh, A. Gupta, I. Fidan, *J. Compos. Mater.* **2021**, 55, 3629.
- [235] P. A. Kumar Jain, S. Sattar, D. Mulqueen, D. Pedrazzoli, S. G. Kravchenko, O. G. Kravchenko, *Addit. Manuf.* **2022**, 57, 102599.
- [236] D. Thaler, N. Aliheidari, A. Ameli, *Smart Mater. Struct.* **2019**, 28, 084004.
- [237] M. Abshirini, M. Charara, Y. Liu, M. Saha, M. C. Altan, *Adv. Eng. Mater.* **2018**, 20, 1800425.
- [238] M. Petousis, N. Vidakis, N. Mountakis, V. Papadakis, S. Kanellopoulou, A. Gaganatsiou, N. Stefanoudakis, J. Kechagias, *Fibers* **2022**, 10, 52.
- [239] R. P. Rosa, G. Rosace, R. Arrigo, G. Malucelli, *Polymers* **2022**, Vol. 14, Page 1886 **2022**, 14, 1886.
- [240] M. Milosevic, D. Stooft, K. L. Pickering, *J. Compos. Sci.* **2017**, 1, 7.
- [241] H. Tanabi, *J. Thermoplast. Compos. Mater.* **2022**, 2022, 1.
- [242] C. Badouard, F. Traon, C. Denoual, C. Mayer-Laigle, G. Paës, A. Bourmaud, *Indus. Crops Products* **2019**, 135, 246.
- [243] A. R. Torrado Perez, D. A. Roberson, R. B. Wicker, *J. Failure Analysis Prevent.* **2014**, 14, 343.
- [244] M. Kariz, M. Sernek, M. Obućina, M. K. Kuzman, *Mater. Today Commun.* **2018**, 14, 135.
- [245] M. D. Zandi, R. Jerez-Mesa, J. Lluma-Fuentes, J. Jorba-Peiro, J. A. Travieso-Rodríguez, *Int. J. Adv. Des. Manuf. Technol.* **2020**, 108, 1725.
- [246] J. Andrzejewski, K. Grad, W. Wiśniewski, J. Szulc, *J. Compos. Sci.* **2021**, 5, 10.
- [247] T. C. Yang, C. H. Yeh, *Polymers* **2020**, 12, 1334.
- [248] K. H. Mohan, M. G. M. Benal, K. G. Pradeep, V. Tambrallimath, H. R. Geetha, T. M. Khan, A. A. Rajhi, M. A. A. Baig, *Polymers* **2022**, 14, 1182.
- [249] N. Maqsood, M. Rimašauskas, *Composites Part C* **2021**, 4, 100112.
- [250] Y. Huang, S. Lösche, G. Proust, *Composites Part C* **2021**, 5, 100140.
- [251] W. Yu, M. Li, W. Lei, Y. Pu, K. Sun, Y. Ma, *Molecules* **2022**, 27, 2985.
- [252] E. Shulga, R. Karamov, I. S. Sergeichev, S. D. Konev, L. I. Shurygina, I. S. Akhatov, S. D. Shandakov, A. G. Nasibulin, *Materials* **2020**, 13, 3442.
- [253] G. Sodeifian, S. Ghaseminejad, A. A. Yousefi, *Results Phys.* **2019**, 12, 205.
- [254] R. T. L. Ferreira, I. C. Amatte, T. A. Dutra, D. Bürger, *Composites, Part B* **2017**, 124, 88.
- [255] S. Guessasma, S. Belhabib, H. Nouri, *Polymers* **2019**, 11, 1778.
- [256] E. A. Papon, A. Haque, S. B. Mulani, *Composites, Part B* **2019**, 177, 107325.
- [257] F. Ning, W. Cong, Y. Hu, H. Wang, *J. Compos. Mater.* **2016**, 51, 451.
- [258] O. Guetta, D. Rittel, *J. Mech. Behav. Biomed. Mater.* **2021**, 124, 105857.
- [259] W. Zhao, Z. Shi, X. Chen, G. Yang, C. Lenardi, C. Liu, *Composites, Part B* **2015**, 76, 292.
- [260] B. C. Kikuchi, F. L. d. S. Bussamra, M. V. Donadon, R. T. L. Ferreira, R. d. C. M. Sales, *Polym. Compos.* **2020**, 41, 5227.
- [261] A. D. N. Celestine, V. Agrawal, B. Runnels, *Composites, Part B* **2020**, 207, 108369.
- [262] M. Péron, A. Céline, M. Castro, F. Jacquemin, A. Le Duigou, *Compos. Sci. Technol.* **2019**, 169, 7.

- [263] R. J. Zaldivar, T. D. Mclouth, G. L. Ferrelli, D. N. Patel, A. R. Hopkins, D. Witkin, *Addit. Manuf.* **2018**, *24*, 457.
- [264] T. May, B. Eslami, K. Fouladi, *Int. J. Adv. Des. Manuf. Technol.* **2022**, *118*, 2233.
- [265] M. Kariz, M. Sernek, M. Kitek Kuzman, *Wood Research* **2018**, *63*, 917.
- [266] Z. Kesentini, A. El Mahi, J.-L. Rebiere, R. El Guerjouna, M. Beyaoui, M. Haddar, *Polym. Polym. Compos.* **2022**, *30*, 1.
- [267] V. K. Balla, K. H. Kate, J. G. Dattatreya Tadimetri, J. Satyavolu, *J. Mater. Eng. Perform.* **2020**, *29*, 5582.
- [268] V. Chandran, J. Kalman, K. Fayazbakhsh, H. Bougherara, *J. Mech. Sci. Technol.* **2021**, *35*, 1977.
- [269] Y. Sun, Y. Wang, W. Mu, Z. Zheng, B. Yang, J. Wang, R. Zhang, K. Zhou, L. Chen, J. Ying, X. Liu, G. Xu, *J. Appl. Polym. Sci.* **2022**, *139*, 1.
- [270] A. Moetazedian, A. Gleadall, X. Han, V. V. Silberschmidt, *J. Mech. Behav. Biomed. Mater.* **2020**, *102*, 103510.
- [271] C. Lv, X. C. Sun, H. Xia, Y. H. Yu, G. Wang, X. W. Cao, S. X. Li, Y. S. Wang, Q. D. Chen, Y. D. Yu, H. B. Sun, *Sens. Actuators, B* **2018**, *259*, 736.
- [272] J. M. Lee, J. J. Pawlak, J. A. Heitmann, *Mater. Character.* **2010**, *61*, 507.
- [273] M. M. Lu, C. A. Fuentes, A. W. Van Vuure, *Composites, Part B* **2022**, *231*, 1.
- [274] H. Obeid, A. Clément, S. Fréour, F. Jacquemin, P. Casari, *Mech. Mater.* **2018**, *118*, 1.
- [275] Z. Zhang, X. Wang, *Acta Mech. Sol. Sin.* **2015**, *28*, 145.
- [276] N. Ayrlimis, M. Kariz, J. H. Kwon, Manja, K. Kuzman, *Int. J. Adv. Manuf. Technol.* **2019**, *102*, 2195.
- [277] K. Loos, V. M. Bruère, B. Demmel, Y. Ilmberger, A. Lion, M. Johlitz, *Polymers* **2021**, *13*, 4402.
- [278] T.-C. Yang, *Polymers* **2018**, *10*, 1.
- [279] P. B. Kreider, A. Cardew-Hall, S. Sommacal, A. Chadwick, S. Humbert, S. Nowotny, D. Nisbet, A. Tricoli, P. Compston, *Composites, Part A* **2021**, *145*, 1.
- [280] M. Vonk, N. A. M. Verschuur, R. H. J. Peerlings, M. G. D. Geers, J. P. M. Hoefnagels, *Cellulose* **2020**, *27*, 6777.
- [281] J. L. Faust, P. G. Kelly, B. D. Jones, J. D. Roy-Mayhew, *Polymers* **2021**, *13*, 3637.
- [282] M. Mehdikhani, L. Gorbatiikh, I. Verpoest, S. V. Lomov, *J. Compos. Mater.* **2019**, *53*, 1579.
- [283] V. Gager, A. Le Duigou, A. Bourmaud, F. Pierre, K. Behlouli, C. Baley, *Polym. Test.* **2019**, *78*, 105944.
- [284] S. M. Youssef, M. Soliman, M. A. Saleh, M. A. Mousa, M. Elsamanty, A. G. Radwan, *Micromachines* **2022**, *13*, 216.
- [285] A. Y. Al-Maharma, S. P. Patil, B. Markert, *Mater. Res. Express* **2020**, *7*, 122001.
- [286] C. Kergariou, A. L. Duigou, V. Popineau, V. Gager, A. Kervoelen, A. Perririau, H. Saidani-Scott, G. Allegri, T. H. Panzera, F. Scarpa, *Composites, Part A* **2021**, *141*, 106183.
- [287] z. Keleş, E. H. Anderson, J. Huynh, J. Gelb, J. Freund, A. Karakoç, *Sci. Rep.* **2018**, *8*, 1.
- [288] C. G. Schirmeister, T. Hees, E. H. Licht, R. Mülhaupt, *Addit. Manuf.* **2019**, *28*, 152.
- [289] E. A. Papon, A. Haque, *Addit. Manuf.* **2019**, *26*, 41.
- [290] S. Guessasma, S. Belhabib, A. Altin, *Polymers* **2020**, *12*, 1.
- [291] F. Akasheh, H. Aglan, *J. Elast. Plast.* **2018**, *51*, 698.
- [292] R. M. Erb, J. S. Sander, R. Grisch, A. R. Studart, *Nat. Commun.* **2013**, *4*, 1.
- [293] T. Cheng, D. Wood, L. Kiesewetter, E. Özdemir, K. Antorveza, A. Menges, *Bioinspir. Biomim.* **2021**, *16*, 55004.
- [294] R. C. Verpaalen, A. E. Souren, M. G. Debije, T. A. Engels, C. W. Bastiaansen, A. P. Schenning, *Soft Matter* **2020**, *16*, 2753.
- [295] E. Özdemir, L. Kiesewetter, K. Antorveza, T. Cheng, S. Leder, D. Wood, A. Menges, in *Proc. 2021 DigitalFUTURES*, Springer Singapore, Singapore **2022**, pp. 275–285.
- [296] L. Ren, Z. Li, Q. Liu, L. Ren, Q. Wu, B. Li, G. Li, Z. Song, X. Zhou, *Adv. Mater. Technol.* **2021**, *6*, 2001289.
- [297] W. Guo, M. Li, J. Zhou, *Smart Mater. Struct.* **2013**, *22*, 115028.
- [298] Z. Liu, H. Liu, G. Duan, J. Tan, *Math. Mech. Solids* **2020**, *25*, 348.
- [299] F. Connolly, C. J. Walsh, K. Bertoldi, *Proc. Natl. Acad. Sci. USA* **2017**, *114*, 51.
- [300] Y. Wei, P. Huang, Z. Li, P. Wang, X. Feng, *Smart Mater. Struct.* **2021**, *30*, 095002.
- [301] Y. Wang, X. Li, *Composites, Part B* **2021**, *219*, 108918.
- [302] J. Song, Y. Feng, Y. Wang, S. Zeng, Z. Hong, H. Qiu, J. Tan, *Appl. Math. Mechanics.* **2021**, *42*, 1619.
- [303] B. Jian, F. Demoly, Y. Zhang, S. Gomes, *Procedia CIRP* **2019**, *8*, 159.
- [304] J.-W. Su, D. Li, Y. Xie, T. Zhou, W. Gao, H. Deng, M. Xin, J. Lin, *Smart Mater. Struct.* **2020**, *30*, 015028.
- [305] S. Wu, C. M. Hamel, Q. Ze, F. Yang, H. J. Qi, R. Zhao, *Adv. Intell. Syst.* **2020**, *2*, 2000060.
- [306] Y. Wang, X. Li, *Composites, Part B* **2021**, *211*, 108644.
- [307] T. van Manen, S. Janbaz, K. M. Jansen, A. A. Zadpoor, *Commun. Mater.* **2021**, *2*, 1.
- [308] H. R. Safavi, A. Amiri, M. Baniassadi, A. Zolfagharian, M. Baghani, *Mech. Adv. Mater. Struct.* **2022**, *0*, 1.
- [309] P. Du, X. Lin, X. Zhang, *Sens. Actuators, A* **2010**, *163*, 240.
- [310] B. Shapiro, E. Smela, *J. Intell. Mater. Syst. Struct.* **2007**, *18*, 181.
- [311] M. Gigliotti, M. R. Wisnom, K. D. Potter, *Compos. Sci. Technol.* **2004**, *64*, 109.
- [312] K. G. Webber, D. P. Hopkinson, C. S. Lynch, *J. Intell. Mater. Syst. Struct.* **2006**, *17*, 29.
- [313] B. C. Kim, P. M. Weaver, K. Potter, *Compos. Struct.* **2015**, *129*, 256.
- [314] N. Boddeti, Y. Tang, K. Maute, D. W. Rosen, M. L. Dunn, *Sci. Rep.* **2020**, *10*, 1.
- [315] R. Guachi, F. Bini, M. Bici, F. Campana, F. Marinozzi, L. Guachi, *Comput. Methods Biomech. Biomed. Eng.: Imaging Vis.* **2019**, *8*, 219.
- [316] G. Sossou, F. Demoly, H. Belkebir, H. J. Qi, S. Gomes, G. Montavon, *Mater. Des.* **2019**, *175*, 107798.
- [317] F. Momeni, S. M. Mehdi Hassani, N. X. Liu, J. Ni, *Mater. Des.* **2017**, *122*, 42.
- [318] B. Jian, F. Demoly, Y. Zhang, H. J. Qi, J. C. André, S. Gomes, *Engineering* **2022**, *12*, 70.
- [319] W. Choi, D. Kim, S. Lee, Y. G. Lee, *J. Comput. Des. Eng.* **2021**, *8*, 1013.
- [320] T. H. Kwok, C. C. Wang, D. Deng, Y. Zhang, Y. Chen, *J. Mech. Des., Trans. ASME* **2015**, *137*, 11.
- [321] K. Maute, A. Tkachuk, J. Wu, H. J. Qi, Z. Ding, M. L. Dunn, *J. Mech. Des.* **2015**, *137*, 1.
- [322] Z. Zhang, G. X. Gu, *Advanced. Theory Simul.* **2020**, *3*, 2000031.
- [323] A. Zolfagharian, L. Durran, S. Gharaje, B. Rolfe, A. Kaynak, M. Bodaghi, *Sens. Actuators, A* **2021**, *328*, 112774.
- [324] K. Elgeneidy, N. Lohse, M. Jackson, *Mechatronics* **2018**, *50*, 234.
- [325] M. P. Bendsùe, O. Sigmund, *Arch. Appl. Mech.* **1999**, *69*, 635.
- [326] N. Fedon, P. M. Weaver, A. Pirrera, T. Macquart, *Compos. Struct.* **2021**, *259*, 113448.
- [327] D. W. Coit, A. E. Smith, D. M. Tate, *J. Comput.* **1995**, *8*, 1.
- [328] Y. Li, Y. Chen, in *2010 International Solid Freeform Fabrication Symposium*, University of Texas, Austin, TX **2010**, pp. 666–678.
- [329] Y. Chen, L. Ye, *Compos. Sci. Technol.* **2021**, *204*, 1.
- [330] Y. Chen, L. Ye, Y. X. Zhang, K. Fu, *Int. J. Mech. Sci.* **2021**, *206*, 1.
- [331] J. R. Kubalak, A. L. Wicks, C. B. Williams, M. Asme, *J. Mech. Des.* **2021**, *143*, 1.

- [332] A. Chandrasekhar, T. Kumar, K. Suresh, *Struct. Multidiscipl. Optim.* **2020**, 61, 77.
- [333] D. Ryan Seifert, A. Abbott, J. Baur, *Struct. Multidiscipl. Optim.* **2021**, 63, 2673.
- [334] M. Eckrich, P. A. Arrabiyeh, A. M. Dlugaj, D. May, *Compos. Struct.* **2022**, 289, 115488.
- [335] Z. Zhang, J. Shi, T. Yu, A. Santomauro, A. Gordon, J. Gou, D. Wu, *J. Compu. Inform. Sci. Eng.* **2020**, 20, 1.
- [336] A. W. Blom, M. M. Abdalla, Z. Gürdal, *Compos. Sci. Technol.* **2010**, 70, 564.
- [337] C. J. Brampton, K. C. Wu, H. A. Kim, *Struct. Multidiscipl. Optim.* **2015**, 52, 493.
- [338] V. S. Papapetrou, C. Patel, A. Y. Tamijani, *Composites, Part B* **2020**, 183, 107681.
- [339] H. Li, L. Gao, H. Li, X. Li, H. Tong, *Comput. Methods Appl. Mech. Eng.* **2021**, 377, 113668.
- [340] D. Kim, J. Lee, T. Nomura, E. M. Dede, J. Yoo, S. Min, *Comput. Methods Appl. Mech. Eng.* **2020**, 369, 113220.
- [341] Z. Yang, K. Fu, Z. Zhang, J. Zhang, Y. Li, *Compos. Sci. Technol.* **2022**, 230, 109727.
- [342] T. Wang, N. Li, G. Link, J. Jelonnek, J. Fleischer, J. Dittus, D. Kupzik, *Composites, Part A* **2021**, 140, 1.
- [343] Y. Huang, X. Tian, Z. Zheng, D. Li, A. V. Malakhov, A. N. Polilov, *Compos. Struct.* **2022**, 285, 115241.
- [344] R. Paz, E. Pei, M. Monzón, F. Ortega, L. Suárez, *Integr. Comput.-Aided Eng.* **2017**, 24, 225.
- [345] R. Paz, M. D. Monzón, A. N. Benítez, B. González, *Int. J. Comput. Integr. Manuf.* **2015**, 29, 462.
- [346] A. J. Taylor, R. Montayre, Z. Zhao, K. W. Kwok, Z. T. H. Tse, *Int. J. Comput. Assist. Radiol. Surg.* **2018**, 13, 1819.
- [347] G. Runge, M. Wiese, A. Raatz, in *2017 IEEE Int. Conf. on Robotics and Biomimetics*, Vol. 3, IEEE, New York, NY **2018**, pp. 385–392.
- [348] H. T. Kollmann, D. W. Abueidda, S. Koric, E. Guleryuz, N. A. Sobh, *Mater. Des.* **2020**, 196, 109098.
- [349] I. Sosnovik, I. Oseledets, *Russ. J. Num. Anal. Math. Model.* **2019**, 34, 215.
- [350] N. A. Kallioras, N. D. Lagaros, *Appl. Sci.* **2021**, 11, 12044.
- [351] F. Fernandez, W. S. Compel, J. P. Lewicki, D. A. Tortorelli, *Comput. Methods Appl. Mech. Eng.* **2019**, 353, 277.
- [352] A. Grant, B. Regez, S. Kocak, J. D. Huber, A. Mooers, *Results Mater.* **2021**, 12, 100227.
- [353] J. R. Kubalak, A. L. Wicks, C. B. Williams, *Proc. Manuf.* **2019**, 34, 754.
- [354] R. El-Dabaa, S. Abdelmohsen, Y. Mansour, in *Architecture and Urbanism: A Smart Outlook* (Eds: S. Kamel, H. Sabry, G. F. Hassan, M. Refat, A. Elshater, A. S. Abd Elrahman, D. K. Hassan, R. Rashed), Springer, Cham, Switzerland **2020**, pp. 73–82.
- [355] P. P. Parlevliet, H. E. Bersee, A. Beukers, *Composites, Part A* **2007**, 38, 651.
- [356] S. Pfeil, A. Mieting, R. Grün, K. Katzer, J. Mersch, C. Breitkopf, M. Zimmermann, G. Gerlach, *Actuators* **2021**, 10, 270.
- [357] M. Zarek, N. Mansour, S. Shapira, D. Cohn, *Macromol. Rapid Commun.* **2017**, 38, 1600628.
- [358] M. P. Chae, W. M. Rozen, R. T. Spychal, D. J. Hunter-Smith, *Gland Surg.* **2016**, 5, 212.
- [359] A. Blonder, E. Sharon, *Adv. Sci.* **2021**, 8, 2102171.



Charles de Kergariou is a Ph.D. student at the Bristol Composite Institute at the University of Bristol, working on 4D-printed natural fiber-based composite hygromorphs. His current research interests include natural fiber composites, 4D printing, mechanical characterization, and modeling. He obtained a double Master's degree in composite materials at Imperial College London and in engineering at École Nationale Supérieure d'Arts et Métiers de Cluny.



Frédéric Demoly is full professor and director of a CNRS department in the ICB Institute at the Belfort-Montbéliard University of Technology (UTBM). His current research focuses on computational intelligence-based design for assembly, multi-material additive manufacturing, and 4D printing. Frédéric DEMOLY is involved, as principal investigator, in several funded projects: PIA ISITE BFC 4D-META (2021) and HERMES (2018), Region BFC PAN (2019), EUR EIPHI LYRA (2020). More recently, he is laureate of a CNRS grant program (pre-maturation) on a hybrid 4D printing technology (GenIsis, 2021-2022) and a France 2030 targeted project on 4D printing involving multiple CNRS research units and CEA.



Adam Perriman is a full professor of Bioengineering at the University of Bristol, and director of the Bristol Centre for Bioprinting. He is internationally distinguished for his pioneering research on the construction of novel synthetic biomolecular systems, and his research interests span the fields of biophysics, synthetic biology, and tissue engineering. His contributions to this field of interdisciplinary science led to him being named a Wellcome Trust Frontiers Innovator in 2015, and in 2016, he was awarded the British Biophysical Society Young Investigator's Award and Medal. In 2019, he was named a UK Research and Innovation Future Leaders Fellow



Antoine Le Duigou is associate-professor at IRDL UMR CNRS 6027, Université de Bretagne Sud (UBS). He is currently supervising a research group dedicated to biomimicry for innovative composites (www.bionics-group.com). His current research focuses on biologically inspired composite (bio)composite materials, Eco-design and 4D printing (hygro/thermomorphing). He published more than 80 articles and was awarded by AMAC (French Society of composites) for best young researcher in 2017 and by ESCM (European Society of Composite Material) in 2018. He is involved, as principal investigator, in several funded projects: ANR REDESIGN4D (2022), ESA projects, (2020 and 2022) DSTL/DGA (2020-2021) projects, PHC Sakura (2022).



Fabrizio Scarpa (Laurea, PhD, FRAeS) is professor of smart materials and structures at the University of Bristol, and Materials Theme Leader at the Bristol Composites Institute. Professor Scarpa has developed metamaterials, nanomaterials, smart, and biobased natural fiber-based composites for more than 2 decades. His collaborative work with industrial stakeholders has also generated patents in the field of auxetics, multifunctional and energy absorption materials. Professor Scarpa is holder of an ERC Advanced Grant in Natural Neuractive Mechanical Metamaterials (NEUROMETA) and principal investigator in UK, EU, Dstl, and ONR Global projects related to smart biobased mechanical metamaterials.